FROM YEAST TO ANIMALS: A SMALL MOLECULE RESTORES IRON MOBILIZATION, ABSORPTION AND HEMOGLOBINIZATION

BY

ANNA MAY SANTAMARIA

DISSERTATION

Submitted in partial fulfillment of the requirements
for the degree of Doctor of Philosophy in Biochemistry
in the Graduate College of the
University of Illinois at Urbana-Champaign, 2019

Urbana, Illinois

Doctoral Committee:

Professor Martin D. Burke, Chair
Professor Wilfred A. van der Donk
Professor Robert B. Gennis
Professor Susan A. Martinis

ABSTRACT

In the classic paradigm of pharmacology, small molecules bind to and modulate dysfunctional or overactive proteins. However, in cases where a protein is missing, this strategy is no longer viable. Disorders of iron metabolism are the most prevalent genetic diseases worldwide and currently, there are more than 25 different human hereditary diseases associated with loss of iron transporter function and therefore aberrant iron transport, homeostasis and/or metabolism. Given all of the advantageous features that make small molecules effective therapeutics, we questioned whether small molecules could autonomously replicate the functions of deficient iron-transporting proteins and thereby restore physiology in human disease relevant models. As the remaining endogenous networks of transporters and regulators in the cell remain active, we hypothesized that a build-up of labile iron would occur upstream of membranes missing a protein transporter. We therefore hypothesized that a small molecule mimic may be able to restore physiology by facilitating the movement of iron in a site- and direction-selective manner down the established gradient. In this vein, we discovered that a small molecule natural product from the bark of Cypress trees, hinokitiol, could leverage built-up iron gradients to restore the movement of iron into, within, and/or out of cells, and restore physiology to the system. Hinokitiol promotes the movement of iron in cells deficient in Fet3Ftr1, DMT1, Mfrn1, or FPN1 to restore growth in Fet3Ftr1 yeast, transepithelial iron transport across DMT1-deficient gut epithelia, hemoglobinization in DMT1- and Mfrn1-deficient erythroid progenitors, and iron release from FPN1-deficient gut epithelia and reticuloendothelial macrophages. To test the hypothesis that deficiencies of iron transporters lead to a build-up of labile iron upstream of protein-deficient membranes, we chose to study DMT1-deficient mouse erythroleukemia (MEL) cells. We observed increased endosomal iron and reduced cytosolic and mitochondrial iron in

DMT1-deficient MEL cells, using spatiotemporal imaging with organelle-specific, iron-sensitive fluorescent dyes. When treated with hinokitiol, these endosomal iron gradients were released and a subsequent increase in cytosolic and mitochondrial iron levels was observed. We were able to artificially manipulate the direction of hinokitiol mediated iron transport by first loading J774 Mouse Macrophages with iron, adding hinokitiol and watching release of iron, followed by addition of a large excess of iron to the extracellular media. Upon addition of the extracellular iron, the direction reversed from exporting iron out of the cell to importing iron into the cell, further demonstrating hinokitiol's ability to facilitate the movement of iron down an established gradient. We provide evidence for collaboration between hinokitiol and endogenous IRE- and Hif2α-mediated regulatory networks, with levels of ferritin, IRP2, TfR2, and FPN1 responding to changes in the dynamic iron status upon hinokitiol treatment. Administration of hinokitiol via oral gavage promotes gut iron absorption in DMT1-deficient Belgrade (b/b) rats and FPN1-deficient flatiron (ffe/+) mice. Chronic injection of hinokitiol decreases liver non-heme iron and increases hematocrit in flatiron mice and hinokitiol treatment also restores hemoglobinization and reverses anemia in DMT1- and Mfrn1-deficient zebrafish embryos. I was further able to demonstrate that hinokitiol at concentrations orders of magnitude higher than efficacious doses mainly cause loss of efficacy by sequestering intracellular iron. Thus, a small molecule restores site- and direction-selective iron transport in cells deficient in three distinct iron-transport proteins, and promotes gut iron absorption and/or peripheral hemoglobinization in corresponding animal models. Mechanistic studies support the role of ion gradients that build up in cases of missing iron transporters, enabling hinokitiol to restore site- and direction-selective transmembrane iron transport. Furthermore, endogenous protein-based homeostatic mechanisms interface with this small molecule to promote iron-related physiological processes without

disrupting other cellular processes. Collectively, these results suggest that small molecules that partially mimic the function of missing protein transporters of iron, and possibly other ions, may have untapped potential in the treatment of diseases resulting from a deficiency of ion transporting proteins.

To My Family, Friends and The BSB

For Your Love, Support and Unwavering Belief in Me.

ACKNOWLEDGEMENTS

Obtaining a PhD is not a trivial undertaking and is not performed in a bubble. I have been fortunate to have the support, guidance and encouragement of a group of amazing scientists, friends, and family, and to them I am forever grateful. First and foremost, I would like to thank my advisor, Professor Marty Burke. I am so glad I chose your lab, despite one of the most awkward and ridiculous handshakes I have ever experienced in my life after your orientation talk, and swearing off organic chemistry forever during my sophomore year of undergrad. Thank you for all of the encouragement and for pushing me to be the rigorous, outspoken, and confident scientist I am today. Thank you for being willing to laugh at all of the lab's ridiculous antics and yourself as well as providing a constant source of comic relief. The lab may joke about your constant use of Marty-isms but there is nothing like hearing a heartfelt "Strong Work!" in subgroup after the assay you have been fighting with finally works. I hope that you and the lab are ready to roll, listen to your gut, and dive into the literature, towards tremendous success, building the plane as you fly it, with broad brushstrokes and laser beam focus, taking shots on goal and are able to draw a circle around a full court blitz, to really move the needle on your rock star science. In all seriousness Marty, thank you.

I would also like to thank my committee: Dr. Wilfred Wilfred A. van der Donk, Dr. Robert B Gennis, Dr. Susan A. Martinis for all of your support, insightful comments and rigorous scientific discussion. I always looked forward to the opportunity to have you all in the same room to comment on my science and welcomed your critiques, criticisms and suggestions. Thank you to Jeff Goldberg, Sherry Unkraut, and Cara Day for their invaluable help in navigating smoothly through the various stages of my PhD and their consistent and unflappable friendly and kind attitudes.

Thank you to the Burke group for being welcoming and inclusive since day one. I will miss our Game of Thrones watch parties, our impromptu fancy lunches, and the friends I have made over my last 6 years in the group. A special thank you to the Molecular Prosthetics Subgroup for supporting me when I first attempted chemistry, and for your insightful comments, suggestions and push back. Your passion for scientific rigor and drive to solve important, high impacting problems has served as a constant source of inspiration to me. I want to thank my colleagues who are apart of Team Iron: Dr. Tony Grillo, Dr. Alex Cioffi, Andrew Blake, Stella Ekaputri, Kelsie Green, Jacob Neethling, Tejashri Venkatesh, Chris Nardone, James Fan, Dillon Svoboda, Angela Li, Jacob Anderson, and John Hong. This project was a massive undertaking and wouldn't have been possible without each and every one of you.

I want to thank Dr. Stephan Davis for being my an amazing mentor and teaching me a very large portion of the chemistry I know today; because of you I can proudly say that I made a few derivatives of amphotericin B, and no longer see synthetic organic chemistry as something that is beyond my capabilities. Thank you for being the most patient organic chemist and not laughing too hard at my many blunders. Alex Cioffi, thank you for keeping me sane when things got flipped-turned upside down. I will always look back on our jam sessions in the BSL2 hood with fondness. Katrina Muraglia even though you hated me when I first joined the lab, I am glad you changed your mind and that we became such good friends, even after the "ANNA LIKES DOGS" incident. Rajeev Chorghade, thank you for being an amazing friend and for letting me bounce my experimental designs off of you constantly; also for being one of the most level headed and logical people in lab. Hannah Haley we've been through a lot together and I am so glad I had you as a sanity check all throughout my time in the group. I will miss yelling "heyyyy gurl" down the hall literally every time I see you. Melanie Trobe, I will miss bonding with you

over baking and exchanging baked goods in lab on a regular basis. I want to thank Anuj Khandelwal for being such a force for good in the lab. Thank you for staying up all night with me to finish that grant and for being such a positive and encouraging person. I remember when I first told you that I wanted to go into academia and complete a postdoc at the NIH but I wasn't sure if I could do it; you told me I could and would do it if I put my mind to it. I think about you often and miss your infectious positivity.

Last but definitely not least I would like to thank my friends and family. My road to this moment has been a winding one with both personal and professional setbacks but none of you ever wavered in your support of me. I couldn't have done it without you and I hope I've made you proud.

I also would like to acknowledge the University of Illinois at Urbana-Champaign, the National Institutes of Health, Howard Hughes Medical Institute, the Biochemistry Department, and Professor Martin Burke for funding.

Table of Contents

LIST OF ABBREVIATIONS

a.u.	absorption units
abs	Absorbance
b/b	Belgrade rat
C2DeOHino	C2-deoxy hinokitiol
Caco-2	Caucasian colon adenocarcinoma-2 Cells
Calcein green-AM	Calcein green acetoxymethyl ester
cdy/cdy	Chardonnay zebrafish
DFO	Desferoxamine
DFP	Deferiprone
DMSO	Dimethyl sulfoxide
DMT1	Divalent Transporter 1
ELISA	Enzyme linked immunosorbent assay
FACS	Fluorescence activated cell sorting
ffe/+	Flatiron mice
FPN1	Ferroportin
frs/frs	Frescotti zebrafish
FTH1	Ferritin heavy chain
FTL1	Ferritin light chain
GFP	Green fluorescent protein
HIF1α	Hypoxia inducible factor 1 Alpha
HIF2α	Hypoxia inducible factor 2 Alpha
Hino	Hinokitiol
hpf	hours post fertilization
hpi	hours post induction
ICP-MS	Inductively coupled plasma mass spectrometry
IRE	Iron response element
IRP1	Iron response protein 1
IRP2	Iron response protein 2
Ka	Association constant
Kd	Dissociation constant
MEL	Murine erythroleukemia
Mfrn1	Mitoferrin
MIC	Minimum inhibitory concentration
miRNA	Micro RNA
mRNA	Messenger RNA
NS	Not significant
PBS	Phosphate Buffered Saline
PCBP1	Poly(rC) binding protein 1
PIH	Pyridoxal isonicotinoyl hydrazone
POPC	1-palmitoyl-2-oleoyl-sn-glycero-3-phosphocholine

qRT-PCR	Quantitative real time polymerase chain reaction
RBC	Red Blood Cell
ROS	Reactive Oxygen Species
RPA	rhodamine B-[(1,10-phenanthrolin- 5-yl)-aminocarbonyl]benzyl ester
rpm	revolutions per minute
SEM	Standard error of mean
shRNA	short hairpin RNA
SIH	Salicaldehyde isonicotinoyl hydrazone
TFR1	Transferrin Receptor1
Tg	Transgenic
TLC	Thin Layer Chromatography
UTR	Untranslated region
UV-vis	Ultriviolet-Visable
V-ATPase	Vacuolar ATPase
WB	Western Blot
wt	Wild type
YNB	Yeast nitrogen base
YPD	yeast peptone dextrose

CHAPTER 1

DISORDERS OF IRON HOMEOSTASIS AND MOLECULAR PROSTHETICS

1.1 INTRODUCTION

In the classic paradigm of pharmacology, small molecules bind to, and modulate existing malfunctioning proteins; however in cases where diseases are alternatively caused by a missing protein this strategy is no longer viable[1]. Despite significant progress in other treatment strategies such as gene therapy, and the biosynthesis and subsequent direct replacement of missing proteins such as insulin, there are still many challenges associated with both treatment strategies and therefore many diseases caused by missing or deficient proteins remain untreatable[2,3]. It is clear that, despite the progress of medicinal research, there remains a large unmet medical need for new strategies to treat diseases caused by protein deficiencies. We therefore set out to find a new and generalizable approach to treat these currently untreatable diseases and landed on an interesting proposal. Due to the advantages of using small molecules as drugs, it is intriguing to consider the use of small molecules with protein like functions to replace missing proteins and thus restore physiology to protein deficient organisms.

Malfunctioning protein ion channels and transporters are implicated in more than 200 diseases resulting from missing ion transporters or channels[4–7]. Examples include genetic disorders such as in cystic fibrosis, Bartter syndrome, Liddle syndrome, and microcytic anemia amongst others[5,7,8]. The Burke group has previously demonstrated the ability of amphotericin B (AmB), a small molecule with ion channel forming capabilities, to restore physiology in yeast missing TRK1 potassium transporters[9]. More recently, in parallel with my thesis work other members of the Burke group in collaboration with the Welsh group at the University of Iowa, have shown that this same small molecule anion channel, AmB, can also restore bicarbonate ion

transport and therefore pH, viscosity, and antimicrobial peptide activity in fully differentiated, primary, cystic fibrosis lung epithelia as well as pH in the trachea of a pig model of cystic fibrosis (manuscript accepted). I had the great and unique opportunity to work on a secondary project involving disorders of iron homeostasis caused by missing or deficient proteins. The following chapter covers the relevant background to my thesis work towards developing a small molecule, molecular prosthetic for the mobilization of iron and therefore the treatment of iron metabolic diseases.

1.2 DISORDERS OF IRON HOMEOSTASIS

Anemia represents a major public heath problem in both developing and developed countries with an absolutely staggering 1.62 billion people world wide affected[10]. To put that into perspective 1.62 billion corresponds to ~25% of the worlds total population. About 50% (~1 billion in total) cases of anemia are thought to be caused solely by iron deficiency (Iron Deficiency Anemia, IDA), with the highest prevalence occurring in preschool age children with an incidence of over 47%, and non-pregnant women which represent the group with the greatest number (468.4 million) of individuals affected[10–12]. The negative consequences associated with iron deficiency anemia on cognitive and physical development, and in some cases even mortality, in children have been well documented and represent a major cause for concern, both for human health as well as economic and social development in both developed and developing countries world wide[10,13–16].

While iron is an essential nutrient and required for many important functions such as oxygen transport, electron transfer, oxidation-reduction reactions and catalytic activity in metaloproteins, it can also be very toxic when it builds up in excess within the body[17,18]. Iron is a

necessary nutrient because it is good at catalyzing biological reactions and is therefore often a cofactor in enzymes because of its redox capabilities; however, these same capabilities also lead to its toxicity. When too much free iron overwhelms a biological system it can lead to Reactive Oxygen Species (ROS) toxicity caused by the formation of superoxide followed by the formation of a hydroxyl radical (OH•)[19–22]. Hydroxyl radicals lead to DNA and protein damage as well as lipid peroxidation, which can cause genetic mutation, necrosis and tissue damage[17,23–25]. Therefore even though iron deficiency is a world wide problem, iron uptake, utilization, and storage within biological systems is highly regulated by a complex system of iron sensing proteins in concert with transcriptional and translational regulation[17,26–31].

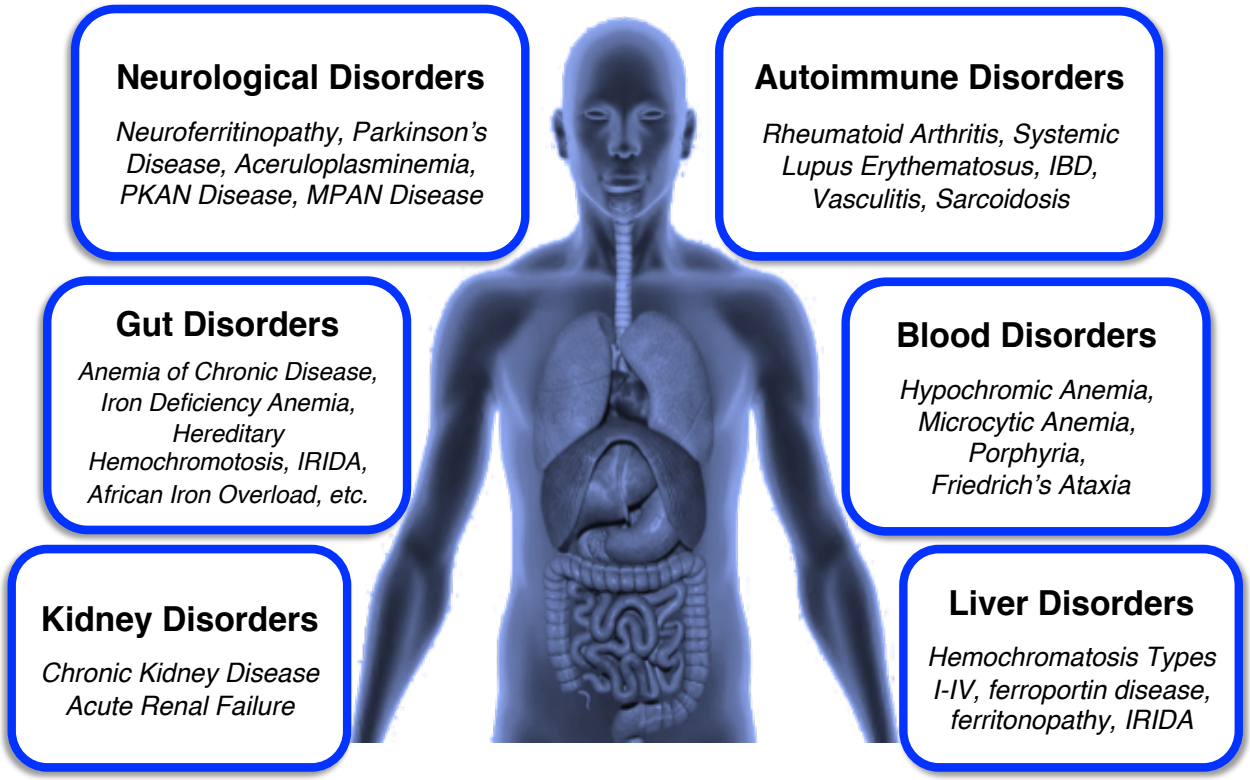

Figure 1.1 Examples of disorders of iron homeostasis and the affected organs or systems. Disregulation of iron absorption, utilization, recycling, and excretion can affect almost every system of the body, resulting in many different disorders of iron homeostasis affecting almost every system of the body.

In addition to its potential to cause toxicity, iron is at the forefront of host pathogen interactions[32]. Iron is a required nutrient for both pathogens and their hosts leading to a tug of war between pathogens, the microbiome and then host. This competition for resources leading to a molecular tug of war between pathogens, commensal microbe populations and the host; causes each group to balance sequestrating iron away from the other groups, while leaving enough labile, or free iron for their own utilization and storage[32]. Often, microbes biosynthesize siderophores to scavenge for iron in their environment, while hosts sequester iron away from pathogens by binding it with calprotectin in blood cells such as neutrophils, or storing it in the protein ferritin, or allowing it to circulate throughout the body bound to the protein transferrin; it is very rare for any iron to be free of any chelation agent within the body. This strategy is utilized to keep pathogens at bay and to minimize the toxicity mentioned above.

Because of iron's important role in biological systems, and the need for tight regulation of iron within the body, it makes sense that hundreds of diseases are associated with iron metabolism. Disorders of iron metabolism are the most common genetic deficiencies world wide and because iron is such an integral metal ion for many biological processes, iron overload and deficiency can affect almost every system and process of the body (**Figure 1.1**)[29,33–35]. Currently, there are more than 25 known hereditary diseases caused by deficiencies in iron regulation and homeostasis (**Table 1.1**), with additional disorders caused by acquired loss of protein function due to chronic illness, inflammation and other environmental factors.

DISEASES OF DEFECTIVE IRON ABSORPTION		
Mendelian Disease	**Gene Affected**	**Sites of aberrant iron levels**
Hypochromic, Microcytic Anemia	DMT1	Decreased iron absorption; decreased iron in enterocytes; increased iron in endosomes; increased hepatic iron
Erythropoietic Protoporphyria	Mfrn1	Predicted decrease of iron in mitochondrial matrix; predicted increase of iron in intermembrane space
Ferroportin Disease	FPN1	Increased iron in enterocytes; increased iron in Kupffer cells
Iron Refractory Iron Deficiency Anemia	TMPRSS6	Increased iron in enterocytes; increased iron in Kupffer cells
Hemochromatosis	DcytB	Predicted decrease of iron absorption
Inflammatory Bowel Disease	Multiple	Increased iron in enterocytes; increased iron in Kupffer cells
Rheumatoid Arthritis	HLA	Increased iron in enterocytes; increased iron in Kupffer cells
DISEASES OF IRON-RELATED PROTEINS ASSOCIATED WITH ABERRANT TISSUE IRON LEVELS		
Mendelian Disease	**Gene Affected**	**Sites of aberrant iron levels**
Hemochromatosos Type 1-3	HFE3, HFE2, HAMP, TfR2	Increased iron absorption; increased hepatic and cardiac iron
Friedreich's Ataxia	Frataxin	Increased iron in the mitochondria
Erytrhopoietic Protoporphyria	Ferrochelatase	Increased iron in the mitochondria
Aceruloplasminemia	Ceruloplasmin	Increased iron in hepatocytes, brain, and pancreas
Neuroferritinopathy	FTL1	Increased iron in basal ganglia of brain
Congenital Hypochromic Anemia	STEAP3	Predicted increase of endosomal iron; increased hepatic iron
FTH1-Related Iron Overload	FTH1	Increased iron in liver and spleen; increased serum iron
Hepatic Iron-Overload Insulin-Resistance Syndrome	HFE	Increased FPN1; increased iron in hepatocytes
SECONDARY DISORDERS ASSOCIATED WITH ABERRANT TISSUE IRON LEVELS		
Mendelian Disease	**Gene Affected**	**Sites of aberrant iron levels**
Wilson's Disease	ATP7B	Increased iron in liver
Menkes Disease	ATP7A	Increased iron in liver; increased iron deposition in the brain
Familial Porphyria Cutanea Tarda	UROD	Increased iron absorption; increased hepatic iron
Beta-thalassemia	HBB	Increased iron in liver and pancreas
Sideroblastic Anemia	Glutaredoxin-5	Increased iron in the mitochondria
X-Linked Sideroblastic Anemia with Ataxia	ABC7	Increased iron in the mitochondria
Huntington's Disease	HTT	Increased iron in basal ganglia of brain
MPAN Disease	c19orf12	Increased iron deposition in the brain
PKAN Disease	PANK2	Increased iron deposition in the brain
Kufor-Rakeb Syndrome	ATPC13A2	Increased iron deposition in the brain
PLAN Disease	PLA2G6	Increased iron deposition in the brain
BPAN Disease	WDR45	Increased iron deposition in the brain
Woodhouse-Sakati Syndrome	DCAF17	Increased iron deposition in the brain
Amyotrophic Lateral Sclerosis	SOD1	Iron deposition in the motor cortex of the brain
Congenital Dyserythropoietic Anemia Type I-IV	CDAN1, SEC23B KIF23, KLF1	Increased serum iron
Congenital Sideroblastic Anemia	SLC25A38	Increased serum iron; increased iron in cytoplasm
X-Linked Sideroblastic Anemia	Alas2	Increased iron in liver, heart, pancreas, and brain
Sickle Cell Disease	HBB	Increased liver and serum iron
Myelodysplastic Syndrome	Multiple	Increased liver and serum iron

Table 1.1 Disorders of iron absorption, homeostasis, and metabolism. Non-inclusive list of hereditary diseases associated with defective iron absorption, homeostasis, and metabolism. metabolism. These diseases can broadly be separated into three categories: (**i**) Diseases of defective iron absorption, (**ii**) Diseases of iron-related proteins associated with aberrant tissue iron levels, and (**iii**) Secondary disorders associated with aberrant tissue iron levels.

Unfortunately, because these disorders are caused by a deficiency of a specific protein, instead of an overactive or malfunctioning protein that is still physically present within the system, there is no protein target for a small molecule to bind to and modulate as expected in traditional pharmacological techniques. Therefore, many of these diseases have few treatment options. For example, Ferroportin Disease is caused by a dominant-negative mutation in ferroportin, a protein found both on the basolateral membrane of gut enterocytes as well as in macrophages (**Figure 1.2**). When ferroportin is not functioning properly patients have both anemia (due to lack of adequate iron absorption in the gut) as well as liver iron overload (due to reduced iron recycling in liver macrophages). The only treatment currently available for these patients is phlebotomy, or bloodletting, to reduce the liver iron burden to prevent cirrhosis. In some cases this leads to a worsening of the anemia they are already enduring.

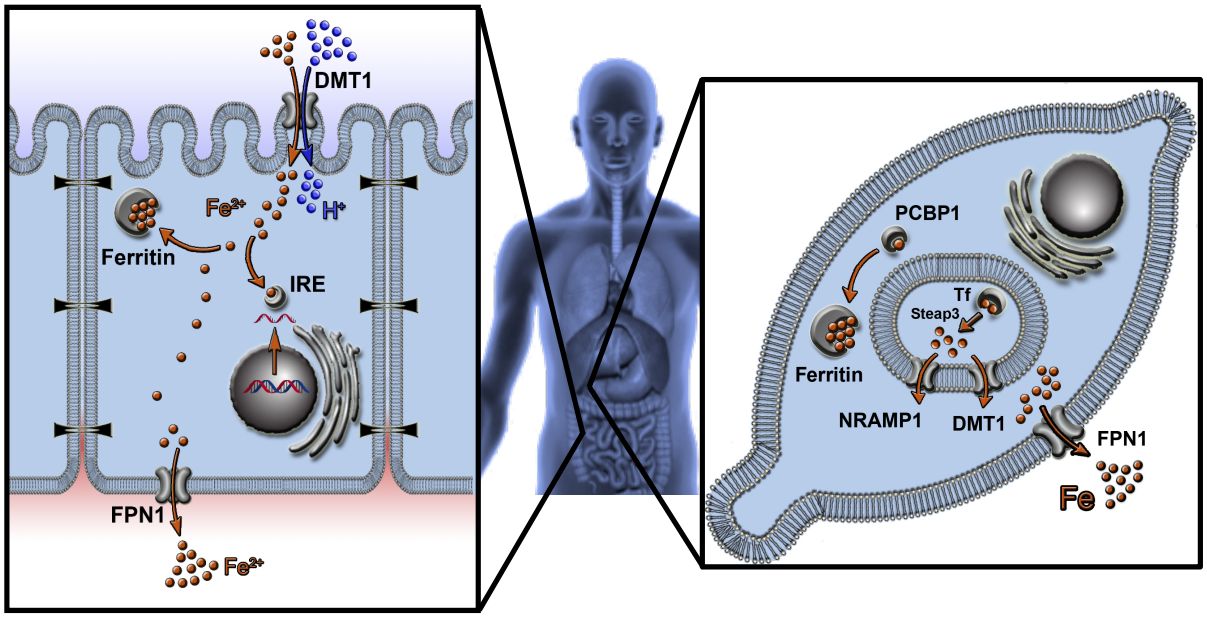

Figure 1.2 Ferroportin is important in both gut iron absorption and iron recycling in the liver. Ferroportin exists on the basolateral side of gut enterocytes and allows ferrous iron to flow into the blood where it is oxidized to ferric iron so that it can be bound by transferrin and circulated throughout the body. Ferroportin is also present on the cellular membrane of liver macrophages, called Kupffer cells, where it allows the iron released from damaged blood cells to be recycled and put back into circulation via transferrin.

1.3 IRON HOMEOSTASIS AND METABOLISM IN THE BODY

Iron is efficiently recycled in the body and therefore moves in a cycle (**Figure 1.3**). Typically only 1 to 1.5 mg of iron needs to be absorbed from the diet per day in order to replace the iron lost and keep the iron stores in the body sufficient for normal physiology[36]. Non-heme iron is absorbed from the diet by gut enterocytes through Divalent Metal Transporter 1 (DMT1, also known as NRAMP2, DCT1, or SLC11A2)[37], and secreted into the blood by Ferroportin (FPN1, also known as IREG1, MTP1, or SLC40A1)[38] where it is bound by transferrin[29] (**Figure 1.3 A**). Transferrin then circulates iron throughout the body with the vast majority of transferrin iron concentrating in bone marrow where reticulocytes phagocytose the transferrin, strip it of

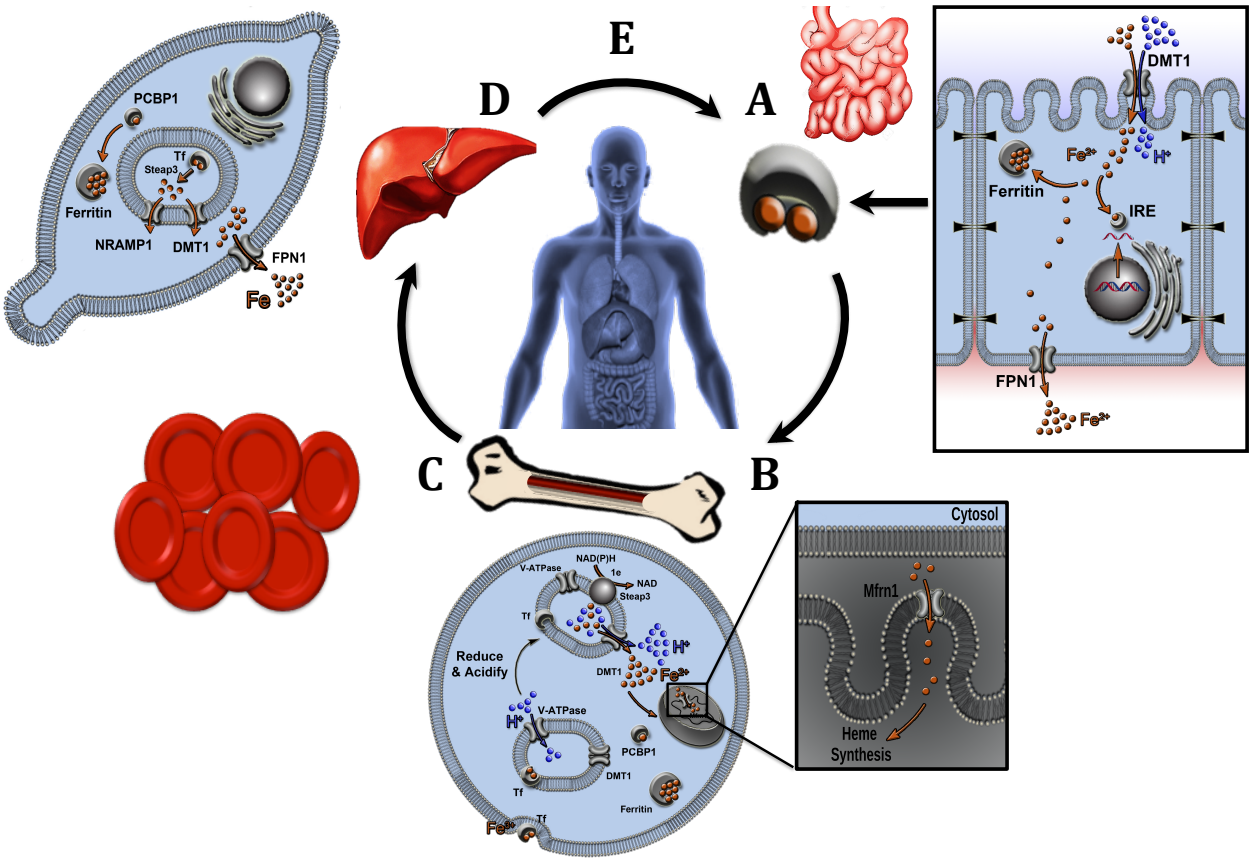

Figure 1.3 The Iron Cycle within the human body. A) Iron absorption by gut enterocytes, and iron circulation in the blood by transferrin. **B)** Hemoglobinization of reticulocytes causes **C)** red blood cell maturation. **D)** Iron recycling from damaged red blood cells by liver macrophages. **E)** Recycled iron is bound by transferrin and the cycle continues.

iron and then pump the iron through DMT1 into the cytosol and eventually the mitochondria[39]. Once the iron is in the intermembrane space between the outer mitochorial membrane and the inner membrane Mitoferrin (MFRN1, also known as SLC25A37)[40,41] moves the iron into the mitochondrial matrix where heme synthesis occurs[42,43](**Figure 1.3 B**). Once the hemoglobinization process has started the reticulocytes begin the differentiation process[28,30] into mature red blood cells, which circulate throughout the body delivering oxygen from the lungs to other tissues and organs (**Figure 1.3 C**). When red blood cells become damaged they are recycled by special macrophages in the liver called Kupffer cells. Kupffer cells phagocytose the damaged red blood cells strip the iron from heme and secrete it into the blood stream via FPN1[44–47] (**Figure 1.3 D**) where transferrin once again binds it and the cycle continues (**Figure 1.3 E)**[48,49].

1.4 THE PROSPECT OF MOLECULAR PROSTHETICS

The idea that an imperfect small molecule with protein-like function could mimic a missing protein, and allow for restoration of physiology in a diseased system, is a highly intriguing prospect. Small molecules have many advantages compared to other molecules such as oligonucleotides, proteins and peptides, which has lead them to be hugely successful as pharmaceuticals. This domination of the pharmaceutical industry is due to many factors including their naturally occurring diversity in nature and the potential to derivatize, their ease of delivery and bioavailability, their non-immunogenic nature, and the relative ease and cost effectiveness of their production and storage. That being said, proteins are large, complex structures that are, in most cases, highly regulated and very specialized for the specific function they perform. This raises the valid and logical question of how a small molecule, that is not as

complex, specific or specialized as the missing protein, could possibly replicate the function of that protein well enough in the system to allow for restoration of physiology. The answer to that question comes from nature itself.

Living systems are inherently robust, meaning that they have built in redundancy which allows them to adapt to environmental changes, genetic variation and injury[50–54]. This redundancy gives organisms more function than they need in order to survive so that if some of that function is lost they are still able to survive (**Figure 1.4 Left**). In fact, humans on average are missing about 20 proteins yet display no disease phenotype[55]. It is therefore, actually the rarer case in which a single missing or defective protein causes an organism to drop below the threshold needed to maintain physiology (**Figure 1.4 Middle**). With this in mind we

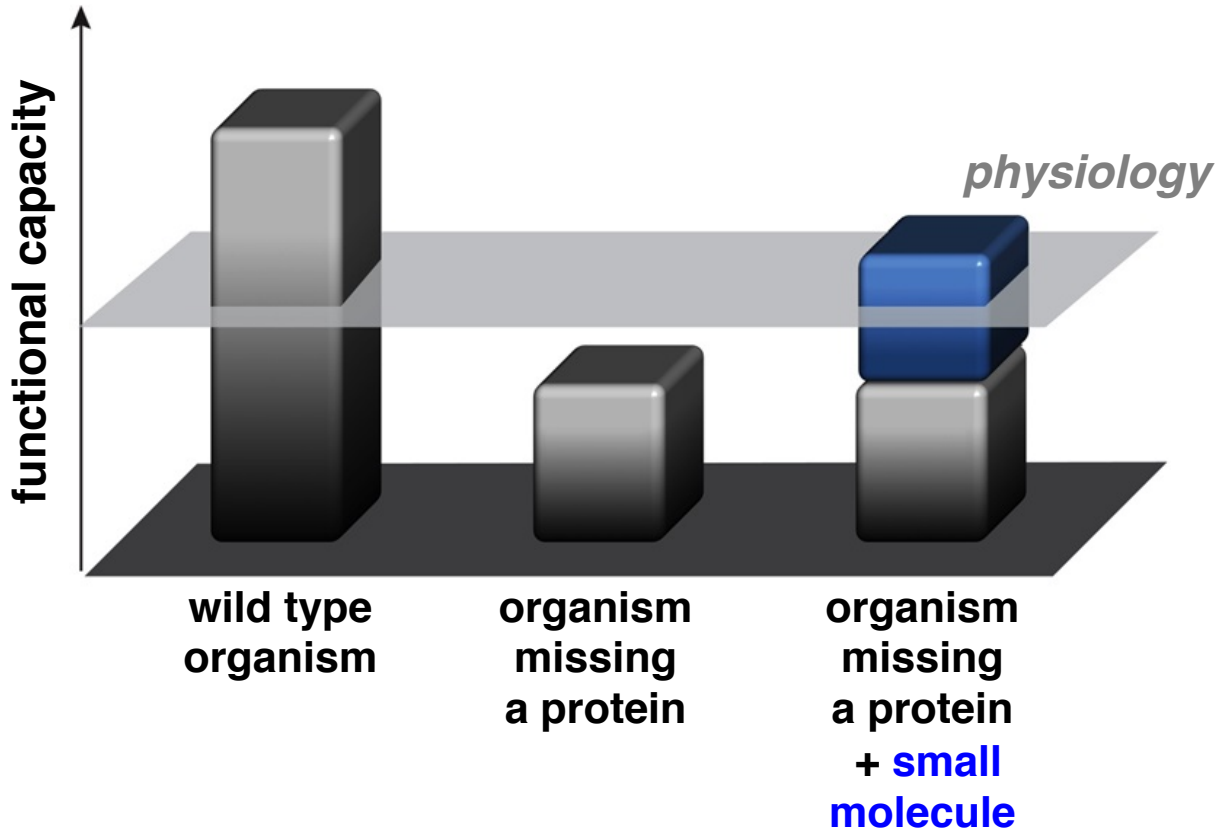

Figure 1.4 The prospect of molecular prosthetics. The robustness of living systems suggests that small molecules that only partially mimic the function of missing proteins could be capable of restoring physiology.

hypothesized that a small molecule, despite being an imperfect mimic, could collaborate with the endogenous system and perform enough function in order to bring an organism up past that threshold and therefore allow for restoration of physiology to the organism (**Figure 1.4 Right**).

1.5 MOLECULAR PROSTHETICS IN DISORDERS OF IRON HOMEOSTASIS

Disorders of iron homeostasis caused by missing proteins make good candidates for a molecular prosthetic treatment approach because the active ion pumps and passive ion channels upstream and downstream of the affected protein remain functional, and in some cases are even upregulated in order to compensate for the missing protein (**Figure 1.5**). The net movement of ions created within the organism essentially primes the system to allow for the site and direction selective flow of iron as well as other ions (**Figure 1.5 Left**). However in some cases the barrier of the missing protein cannot be surmounted and a disease phenotype is observed (**Figure 1.5 Middle)**. We hypothesized that because all of the other pumps and channels remain active, a site-specific iron gradient would accumulate upstream of the missing protein. Therefore if we could find a small molecule to not only bind that excess iron, but also mobilize it to release the gradient in a site- and direction- specific manner we could restore physiology downstream of the missing protein and treat the disease phenotype (**Figure 1.5 Right**). This approach is attractive because one could imagine it working in many different cases where iron is unable to move into, within or out of cells (**Figure 1.6**), representing a new generalizable approach to treating disorders caused by lack of iron mobilization and potentially other ions as well.

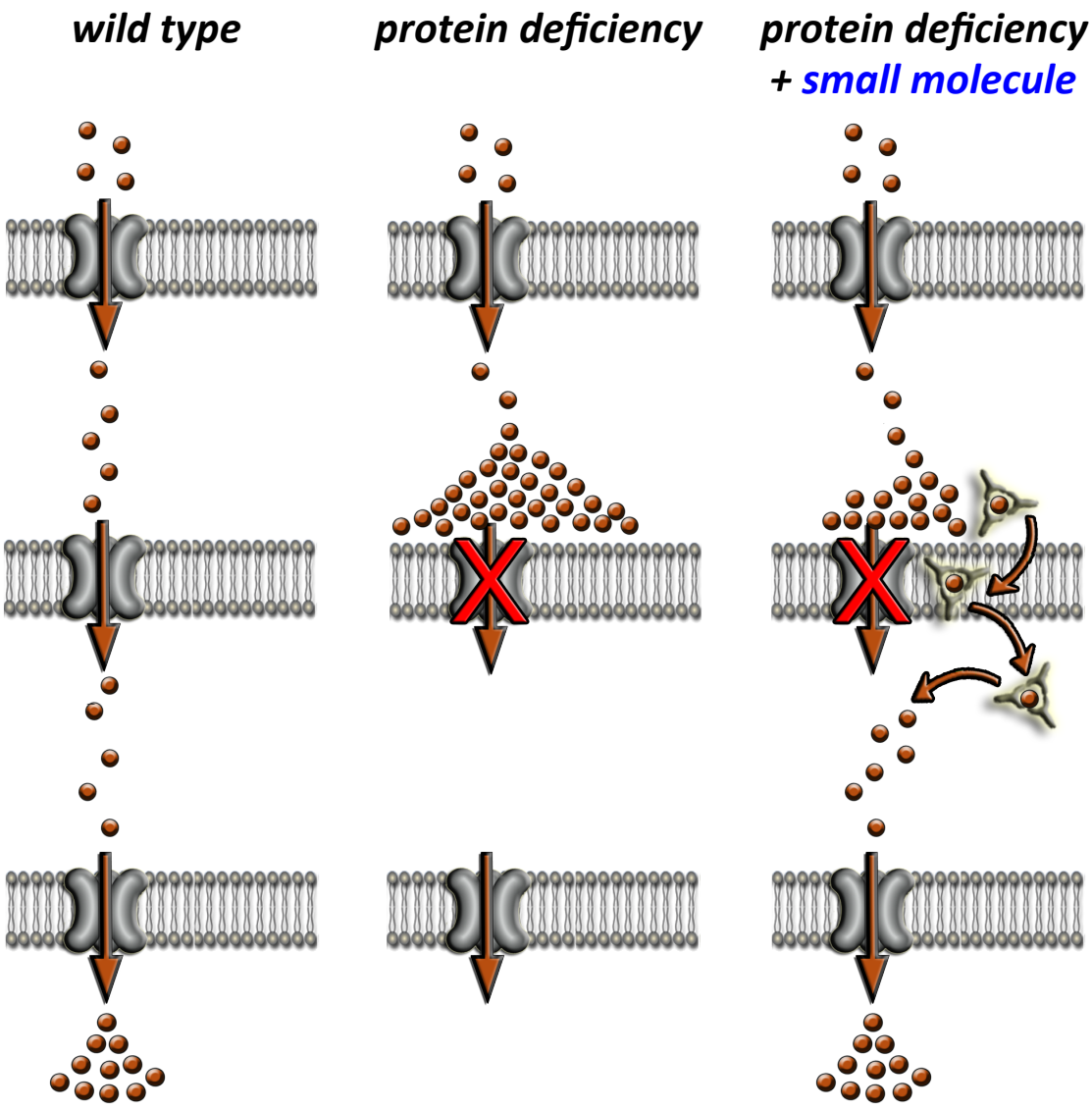

Figure 1.5 Build up of iron in protein transporter deficient systems. A) Iron flows through a wild type system. **B)** Iron gradients build upstream of a missing iron transporter. **C)** A small molecule binds and transports iron that has accumulated upstream of a missing an iron transporter.

I consequently chose three different iron transporting proteins to study that represent a deficit in the movement of iron into cells, divalent metal transporter 1, DMT-1 (**Figure 1.6 A**); within cells mitoferrin MFRN1 and DMT1 (**Figure 1.6 B**) ; and out of cells ferroportin FPN1 (**Figure 1.6 C**). I chose these proteins with the goal of learning whether a small molecule with protein-like function would be able to restore physiology via the site- and direction-selective movement of iron in systems missing integral iron transporting proteins, and how the iron regulatory system would respond to an exogenous iron delivery mechanism.

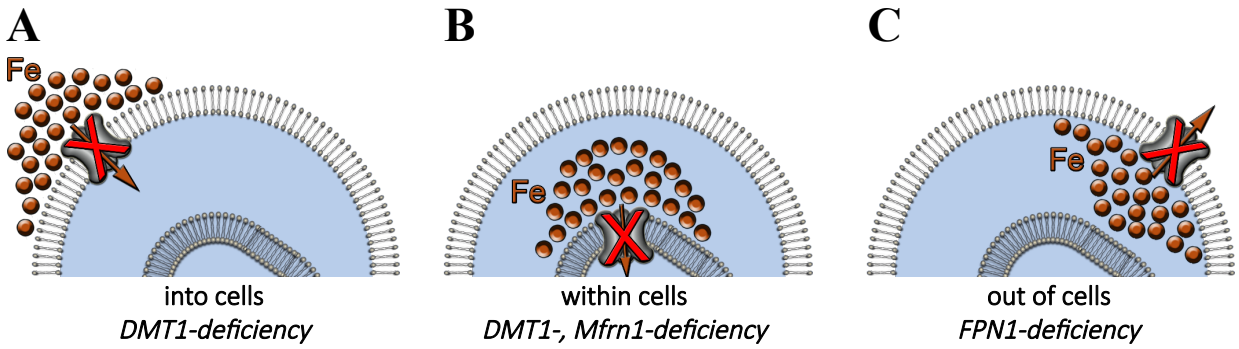

Figure 1.6 Iron is unable to move into (A) within (B) and out of (C) cells missing iron transporters creating site-specific iron gradients.

1.6 DISCOVERY OF A SMALL MOLECULE IRON TRANSPORTER

In order to find a molecule that could not only bind iron but also transport it across cellular membranes my colleagues Anthony Grillo and Alexander Cioffi performed a directed screen of iron binding molecules. In order to efficiently screen a number of different candidates they used a modified functional complemen-tation experiment[9], in which candidate compounds known or predicted to bind iron were tested for their capacity to restore growth to a strain of Saccharomyces cerevisiae missing the iron-transporting complex FetFtr1 (fet3Δftr1Δ, **Figure**

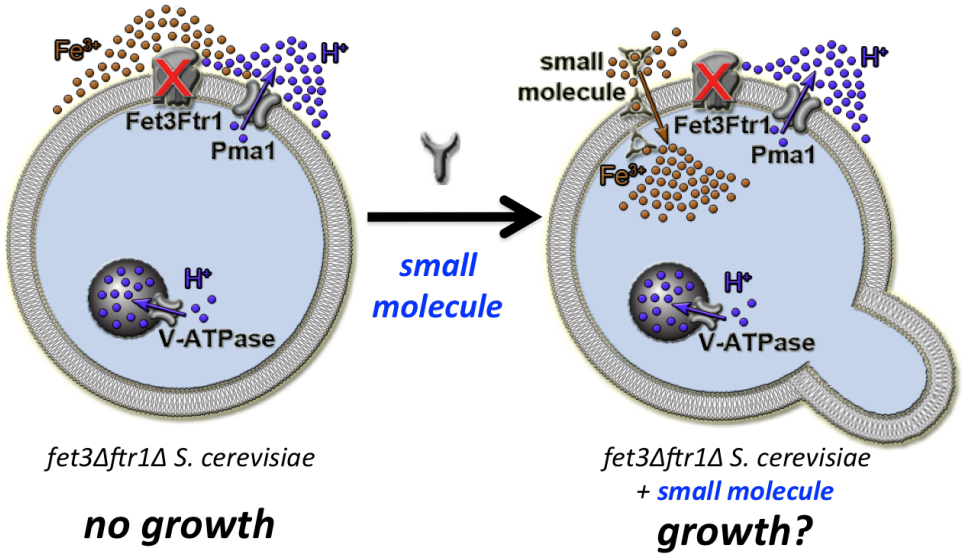

Figure 1.7 Schematic of the fet3Δftr1Δ yeast used in the modified functional complementation assay. The mutated fet3Δftr1Δ yeast are unable to grow under normal laboratory conditions (left). Small molecule mediated rescue of growth in fet3Δftr1Δ yeast (right).

1.7)[56]. The assay is run by streaking a lawn of yeast on agar plates that do not allow the fet3Δftr1Δ yeast to grow, a disc impregnated with vehicle or compound is then placed on the plate where it diffuses outward in a circular fashion. We hypothesized that if the compound was able to bind iron, as well as tranpost it across the membrane and then allow the yeast cell to utilize the iron we would be able to see the yeast grow in a very distinctive "bullseye" pattern. The pattern is created by a zone of inhibition (due to high, toxic concentrations), followed by the zone of functional complementation, (due to intermediate, efficacious concentrations) followed by no growth due to insufficient concentrations for functional complementation.

The small molecule natural product hinokitiol (Hino, b-thujaplicin; **Figure 1.8 A**) was highly effective at restoring growth to the fet3Δftr1Δ yeast (**Figure 1.8 B**). Hinokitiol is a known metal chelator, that has been studied for its antifungal[57], antimicrobial[58] and anticancer[59,60] activity. Hinokitiol was originally isolated by Japanese chemist Tetsuo Nozoe in 1935 from the

essential oils of the *Chamaecyparis taiwanensis*, or Taiwan Hinoki tree[61]. While hinokitiol is found at very low concentrations in the Hinoki tree it is abundant in the bark of many species of trees including *Thuja plicata* Donn, (The Western Red Cedar) and *Cupressus lusitanica* (Mexican Cypress)[62] with reports of up to 0.04% of the bark's biomass being comprised of hinokitiol.

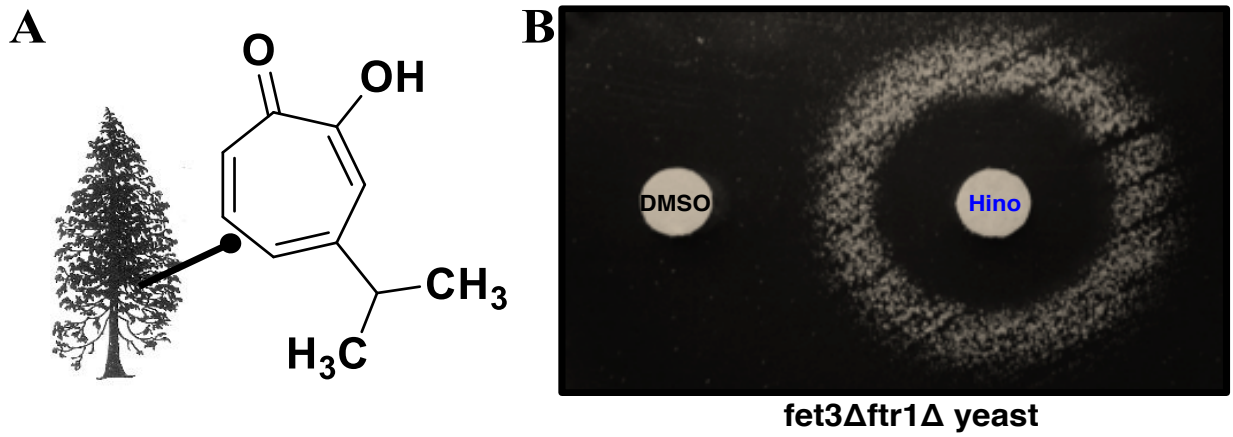

Figure 1.8 Hinokitiol restores growth in fet3Δftr1Δ yeast. A) Structure of the small molecule hinokitiol (Hino). **B**) Growth of fet3Δftr1Δ yeast cells was restored by disc diffusion with hinokitiol (Hino) on low-iron synthetic dextrose (SD) agar plate containing 10 μM $FeCl_3$.

With this exciting preliminary result in hand, I set out to characterize the rescue phenomena Anthony Grillo and Alexander Cioffi observed in the fet3Δftr1Δ yeast, expand the scope to mammalian cell lines and animals and explore the mechanisms that allowed for this imperfect small molecule to restore physiology. The Screen mentioned above as well as portions of chapters to follow have been adapted from: Grillo, A. S.; SantaMaria A. M.; Kafina M. D.; Cioffi A.G.; Huston N. C.; Han M.; Seo Y. A.; Yien YY3, Nardone C.; Menon A. V.; Fan J.; Svoboda D. C.; Anderson J. B.; Hong J.D.; Nicolau B. G.; Subedi K.; Gewirth A. A.; Wessling-Resnick M.; Kim J.; Paw B. H.; Burke M. D. "Restored iron transport by a small molecule

promotes absorption and hemoglobinization in animals" *Science.* **2017**, *356*, 608-616. Reprinted with permission from AAAS."

1.7 METHODS

Materials

Wild type (DEY1457) and isogenic fet3Δftr1Δ *S. cerevisiae* were obtained from D. Kosman[56] Yeast were maintained on standard YPD media containing 10 g/L yeast extract, 20 g/L peptone, and 20 g/L dextrose without (liquid media) or with (solid media) 20 g/L agar. Unless otherwise indicated, growth-restoration assays in yeast used a low iron SD media consisting of 1.91 g/L iron-free YNB-FeCl3 (ForMedium CYN 1201), 0.79 g/L Complete Supplement Mixture (Sunrise Science Products 1001-010), 5 g/L ammonium sulfate (Sigma A4418), 20 g/L dextrose, 10 μM FeCl3 (Sigma 451649, maintained in a glove box), and 10 μM hinokitiol (β-Thujaplicin, Sigma 469521) in 50 mM MES/Tris buffer at pH=7.0 without (liquid media) or with (solid media) 20 g/L agar. Dextrose and FeCl3 were added after autoclave sterilization from a filter-sterilized 40% w/v dextrose solution in water and from a freshly prepared 10 mM FeCl3 stock in sterile water, respectively.

Phenotypic screen of growth rescue in fet3Δftr1Δ yeast with small molecules

Growth rescue in yeast was performed, similar to previously reported[9], on low iron SD-agar plates containing 50 mM MES/Tris buffer at pH=7.0, 2% agar, and 10 μM $FeCl_3$. Yeast were grown overnight in YPD media and diluted to an OD600 = 0.1 in low iron SD media and streaked onto the low iron SD-agar plates. Stock solutions of candidate compounds (≥10 mM in DMSO) were impregnated onto filter paper discs and placed onto the streaked agar plates. Images were taken 48-72 hours after inoculation and incubation at 30 °C.

1.8 REFERENCES

1. *Basic and Clinical Pharmacology*. *Callaloo* **13**, (McGraw Hill, 2012).
2. Aiuti, A. *et al.* Gene Therapy for Immunodeficiency Due to Adenosine Deaminase Deficiency. *N. Engl. J. Med.* **360**, 447–458 (2009).
3. Dunbar, C. E. *et al.* Gene therapy comes of age. *Science (80-.).* **359**, eaan4672 (2018).
4. Imbrici, P. *et al.* Therapeutic approaches to genetic ion channelopathies and perspectives in drug discovery. *Front. Pharmacol.* **7**, 1–28 (2016).
5. Kim, J. Channelopathies. *Korean J. Pediatr.* **57**, 1–18 (2014).
6. Hubner, C. A. Ion channel diseases. *Hum. Mol. Genet.* **11**, 2435–2445 (2002).
7. Dworakowska, B. & Dołowy, K. Ion channels-related diseases. *Acta Biochim. Pol.* **47**, 685–703 (2000).
8. Garrick, M. D. *et al.* DMT1: A mammalian transporter for multiple metals. *BioMetals* **16**, 41–54 (2003).
9. Cioffi, A. G., Hou, J., Grillo, A. S., Diaz, K. A. & Burke, M. D. Restored physiology in protein-deficient yeast by a small molecule channel. *J. Am. Chem. Soc.* **137**, 10096–10099 (2015).
10. WHO. *Worldwide prevalence of anaemia 1993–2005*. (Geneva: World Health Organization, 2005).
11. WHO. Focusing on anaemia: Towards an intergrated approch for effective anaemia control. Joint Statement by WHO and UNICEF. (2004).
12. WHO. The Global Prevalence of Anemia in 2011. *Public Health Nutrition* (Geneva: World Health Organization, 2015).

13. Kretchmer, N., Beard, J. L. & Carlson, S. The role of nutrition in the development of normal cognition. *Am. J. Clin. Nutr.* **63**, 997S–1001S (1996).

14. Schmidt, A. T., Ladwig, E. K., Wobken, J. D., Grove, W. M. & Georgieff, M. K. Delayed alternation performance in rats following recovery from early iron deficiency. *Physiol. Behav.* **101**, 503–508 (2010).

15. Georgieff, M. K. Long-term brain and behavioral consequences of early iron deficiency. *Nutr. Rev.* **69**, S43–S48 (2011).

16. Brabin, B. J., Premji, Z. & Verhoeff, F. An Analysis of Anemia and Child Mortality. *J. Nutr.* **131**, 636S–648S (2001).

17. Papanikolaou, G. & Pantopoulos, K. Iron metabolism and toxicity. *Toxicol. Appl. Pharmacol.* **202**, 199–211 (2005).

18. Cherayil, B. J. Iron and immunity: Immunological consequences of iron deficiency and overload. *Arch. Immunol. Ther. Exp. (Warsz).* **58**, 407–415 (2010).

19. Bresgen, N. & Eckl, P. M. Oxidative stress and the homeodynamics of iron metabolism. *Biomolecules* **5**, 808–847 (2015).

20. Steinbicker, A. U. & Muckenthaler, M. U. Out of balance-systemic iron homeostasis in iron-related disorders. *Nutrients* **5**, 3034–3061 (2013).

21. Mackenzie, E. L., Iwasaki, K. & Tsuji, Y. Intracellular Iron Transport and Storage: From Molecular Mechanisms to Health Implications. *Antioxid. Redox Signal.* **10**, 997–1030 (2008).

22. Kakhlon, O. & Cabantchik, Z. I. The labile iron pool: Characterization, measurement, and participation in cellular processes. *Free Radic. Biol. Med.* **33**, 1037–1046 (2002).

23. Aisen, P., Enns, C. & Wessling-Resnick, M. Chemistry and biology of eukaryotic iron metabolism. *Int. J. Biochem. Cell Biol.* **33**, 940–959 (2001).

24. Pietrangelo, A. Hereditary Hemochromatosis — A New Look at an Old Disease. *N. Engl. J. Med.* **350**, 2383–2397 (2004).

25. Haley, H. M. S. *et al.* Peridinin Is an Exceptionally Potent and Membrane-Embedded Inhibitor of Bilayer Lipid Peroxidation. *J. Am. Chem. Soc.* **140**, 15227–15240 (2018).

26. Muckenthaler, M. U., Galy, B. & Hentze, M. W. Systemic Iron Homeostasis and the Iron-Responsive Element/Iron-Regulatory Protein (IRE/IRP) Regulatory Network. *Annu. Rev. Nutr.* **28**, 197–213 (2008).

27. Hentze, M. W., Muckenthaler, M. U., Galy, B. & Camaschella, C. Two to Tango: Regulation of Mammalian Iron Metabolism. *Cell* **142**, 24–38 (2010).

28. Hentze, M. W., Muckenthaler, M. U. & Andrews, N. C. Balancing Acts: Molecular Control of Mammalian Iron Metabolism. *Cell* **117**, 285–297 (2004).

29. Andrews, N. C. Iron homeostasis: Insights from genetics and animal models. *Nat. Rev. Genet.* **1**, 208–217 (2000).

30. Andrews, N. C. & Andrews, N. C. Forging a field : the golden age of iron biology ASH 50th anniversary review Forging a field : the golden age of iron biology. *Blood* **112**, 219–230 (2009).

31. Morgan, E. H. & Oates, P. S. Mechanisms and regulation of intestinal iron absorption. *Blood Cells. Mol. Dis.* **29**, 384–399 (2002).

32. Nairz, M., Haschka, D., Demetz, E. & Weiss, G. Iron at the interface of immunity and infection. *Front. Pharmacol.* **5 JUL**, 1–11 (2014).

33. Anderson, G. J. Ironing Out Disease: Inherited Disorders of Iron Homeostasis. *IUBMB Life.* **51**, 11–17 (2001).

34. Andrews, N. Disorders of Iron Metabolism. *N. Engl. J. Med.* **341**, 1986–1995 (1999).

35. Brissot, P., Bardou-Jacquet, E., Jouanolle, A. M. & Loréal, O. Iron disorders of genetic origin: A changing world. *Trends Mol. Med.* **17**, 707–713 (2011).

36. Saito, H., Sargent, T., Parker, H. G. & Lawrence, J. H. Whole-body Iron Loss In Normal Man Measured with a Gamma Spectrometer'. *J. Nucl. Med.* **5**, 571–580 (1964).

37. Andrews, N. C. The iron transporter DMT1. *Int. J. Biochem. Cell Biol.* **31**, 991–4 (1999).

38. Zoller, H., Theurl, I., Koch, R., Kaser, A. & Weiss, G. Mechanisms of iron mediated regulation of the duodenal iron transporters divalent metal transporter 1 and ferroportin 1. *Blood Cells. Mol. Dis.* **29**, 488–497 (2002).

39. Canonne-Hergaux, F., Zhang, A. S., Ponka, P. & Gros, P. Characterization of the iron transporter DMT1 (NRAMP2/DCT1) in red blood cells of normal and anemic mk/mk mice. *Blood* **98**, 3823–3830 (2001).

40. Shaw, G. C. *et al.* Mitoferrin is essential for erythroid iron assimilation. *Nature* **440**, 96–100 (2006).

41. Chung, J. *et al.* Iron regulatory protein-1 protects against mitoferrin-1-deficient porphyria. *J. Biol. Chem.* **289**, 7835–7843 (2014).

42. Friend, C., Scher, W., Holland, J. G. & Sato, T. Hemoglobin synthesis in murine virus-induced leukemic cells in vitro: stimulation of erythroid differentiation by dimethyl sulfoxide. *Proc. Natl. Acad. Sci. U. S. A.* **68**, 378–82 (1971).

43. Levi, S. & Rovida, E. The role of iron in mitochondrial function. *Biochim. Biophys. Acta - Gen. Subj.* **1790**, 629–636 (2009).

44. Donovan, A. *et al.* Positional cloning of zebrafish ferroportin1 identifies a conserved vertebrate iron exporter. *Nature* **403**, 776–781 (2000).

45. Sabelli, M. *et al.* Human macrophage ferroportin biology and the basis for the ferroportin disease. *Hepatology* **65**, 1512–1525 (2017).

46. Garrick, M. D. & Garrick, L. M. Cellular iron transport. *Biochim. Biophys. Acta - Gen. Subj.* **1790**, 309–325 (2009).

47. Korolnek, T. & Hamza, I. Macrophages and iron trafficking at the birth and death of red cells. *Blood* **125**, 2893–2897 (2015).

48. Garrick, M. D. Human iron transporters. *Genes Nutr.* **6**, 45–54 (2011).

49. Lane, D. J. R. *et al.* Cellular iron uptake, trafficking and metabolism: Key molecules and mechanisms and their roles in disease. *Biochim. Biophys. Acta - Mol. Cell Res.* **1853**, 1130–1144 (2015).

50. Félix, M. A. & Barkoulas, M. Pervasive robustness in biological systems. *Nat. Rev. Genet.* **16**, 483–496 (2015).

51. Hsiao, T. L. & Vitkup, D. Role of duplicate genes in robustness against deleterious human mutations. *PLoS Genet.* **4**, (2008).

52. Rg Stelling, J., Sauer, U., Szallasi, Z., Doyle, F. J. & Doyle, J. Robustness of Cellular Functions. *Cell* **118**, 675–685 (2004).

53. S.H., F. & E.E., S. Clues from the resilient. *Science (80-.).* **344**, 970–972 (2014).

54. Hartman IV, J. L., Garvik, B. & Hartwell, L. Cell Biology: Principles for the buffering of genetic variation. *Science* **291**, 1001–1004 (2001).

55. MacArthur, D., Balasubramanian, S. & Frankish, A. A Systematic Survey of Loss-of-Function Variants in Human Protein-Coding Genes. *Science (80-.).* **335**, 1–14 (2012).

56. Kwok, E. Y., Severance, S. & Kosman, D. J. Evidence for iron channeling in the Fet3p-Ftr1p high-affinity iron uptake complex in the yeast plasma membrane. *Biochemistry* **45**, 6317–6327 (2006).

57. Morita, Y. *et al.* Biological activity of α-Thujaplicin, the isomer of hinokitiol. *Biol. Pharm. Bull.* **27**, 899–902 (2004).

58. Shih, Y. H. *et al.* Evaluation physical characteristics and comparison antimicrobial and anti-inflammation potentials of dental root canal sealers containing hinokitiol in vitro. *PLoS One* **9**, (2014).

59. Shih, Y. H. *et al.* In vitro antimicrobial and anticancer potential of hinokitiol against oral pathogens and oral cancer cell lines. *Microbiol. Res.* **168**, 254–262 (2013).

60. Huang, C. H. *et al.* Hinokitiol exerts anticancer activity through downregulation of MMPs 9/2 and enhancement of catalase and SOD enzymes: In vivo augmentation of lung histoarchitecture. *Molecules* **20**, 17720–17734 (2015).

61. Nozoe, T. Über die farbstoffe im holzteile des "hinoki" -baumes. I. Hinokitin und hinokitiol. (Vorläufige Mitteilung). *Bull. Chem. Soc. Jpn.* **11**, 295–298 (1936).

62. Chedgy, R. J., Daniels, C. R., Kadla, J. & Breuil, C. Screening fungi tolerant to Western red cedar (Thuja plicata Donn) extractives. *Holzforschung* **61**, 190–194 (2007).

CHAPTER 2

HINOKITIOL RESTORES PHYSIOLOGY IN CELLS AND ANIMALS

2.1 INTRODUCTION

In this chapter, I will explore hinokitiol's basic biophysical properties, from lipophilicy and metal selectivity, to iron binding and transport. I also probe hinokitiol's ability to restore physiology in multiple protein iron transporter deficient mammalian cells lines and animals. These studies provide phenomenological evidence for the first time, that an imperfect, small molecule can replace a missing protein in an animal and thereby restore normal physiology.

Portions of the work presented in this chapter were preformed with aid from my colleagues Dr. Anthony Grillo, Dr. Alexander Cioffi, and Dr. Bruno Nicolau our undergrads Dillon Svoboda, Chris Nardone, James Fan, John Hong, Jake Anderson, and Tejashri Venkatesh and my high school student Angela Li. Animal studies were performed with our collaborators Archita Menon and Murui Han from Jonghan Kim's Lab at Northeastern University (Belgrade Rat), Young Ah Seo and Marianne Wessling-Resnick at Harvard Medical School (Flatiron Mice), as well as Dr. Yvette Yien, Nick Huston, and Martin Kafina from Barry Paw's Lab at Harvard Medical School (Zebrafish). Portions of this chapter have been adapted from Grillo, A. S.; SantaMaria A. M.; Kafina M. D.; Cioffi A.G.; Huston N. C.; Han M.; Seo Y. A.; Yien Y.Y.; Nardone C.; Menon A. V.; Fan J.; Svoboda D. C.; Anderson J. B.; Hong J.D.; Nicolau B. G.; Subedi K.; Gewirth A. A.; Wessling-Resnick M.; Kim J.; Paw B. H.; Burke M. D. "Restored iron transport by a small molecule promotes absorption and hemoglobinization in animals" *Science.* **2017**, *356*, 608-616. Reprinted with permission from AAAS.

2.2 CHARACTERIZATION OF HINOKITIOL IRON BINDING AND TRANSPORT

In order to probe the mechanism which allows for hinokitiol to rescue the growth phenotype in iron deficient yeast we first wanted to understand its basic biophysical properties. Specifically, we hypothesized that hinokitiol mediated growth is due to its ability to transport iron through cell membranes into the cytoplasm where the iron is released and therefore available for necessary cellular processes. However, with only the results of the disc diffusion assay in hand it was possible that hinokitiol was allowing for growth due to another, unexpected, off-target effect.

We found that hinokitiol binds iron as evident by a shift in its UV spectrum upon titration with iron (**Figure 2.1 A**) and that hinokitiol is able to bind iron that is weakly associated with common iron chelating small molecules found abundantly in cells (**Figure 2.1 B**). The alpha-hydroxy ketone in hinokitiol is thought to be an essential part of its iron binding motif, therefore we synthetically removed a single oxygen atom at the C2 position by hydrogenolysis (**Figure 2.1 C**). This two-step synthesis yielded C2-deoxy hinokitiol or C2deOHino a derivative that is unable to bind iron, as evident by the lack of shift seen in its UV spectra upon titration with iron (**Figure 2.1 D**). Hinokitiol is able to mobilize ferrous (**Figure 2.1 E**) and ferric (**Figure 2.1 F**) iron from model liposomes while C2deOHino, Deferirone[1], a clinically approved iron chelator and pyridoxal isonicotinoyl hydrazone (PIH)[2], an iron chelator from the literature shown to mobilize cellular iron, were all unable to do so (**Figure 2.1 E and F**). These data coupled with the results of the yeast screen lead us to choose hinokitiol as the primary candidate for further study in the pursuit of finding a small molecule Molecular Prosthetic to replace missing iron transporters.

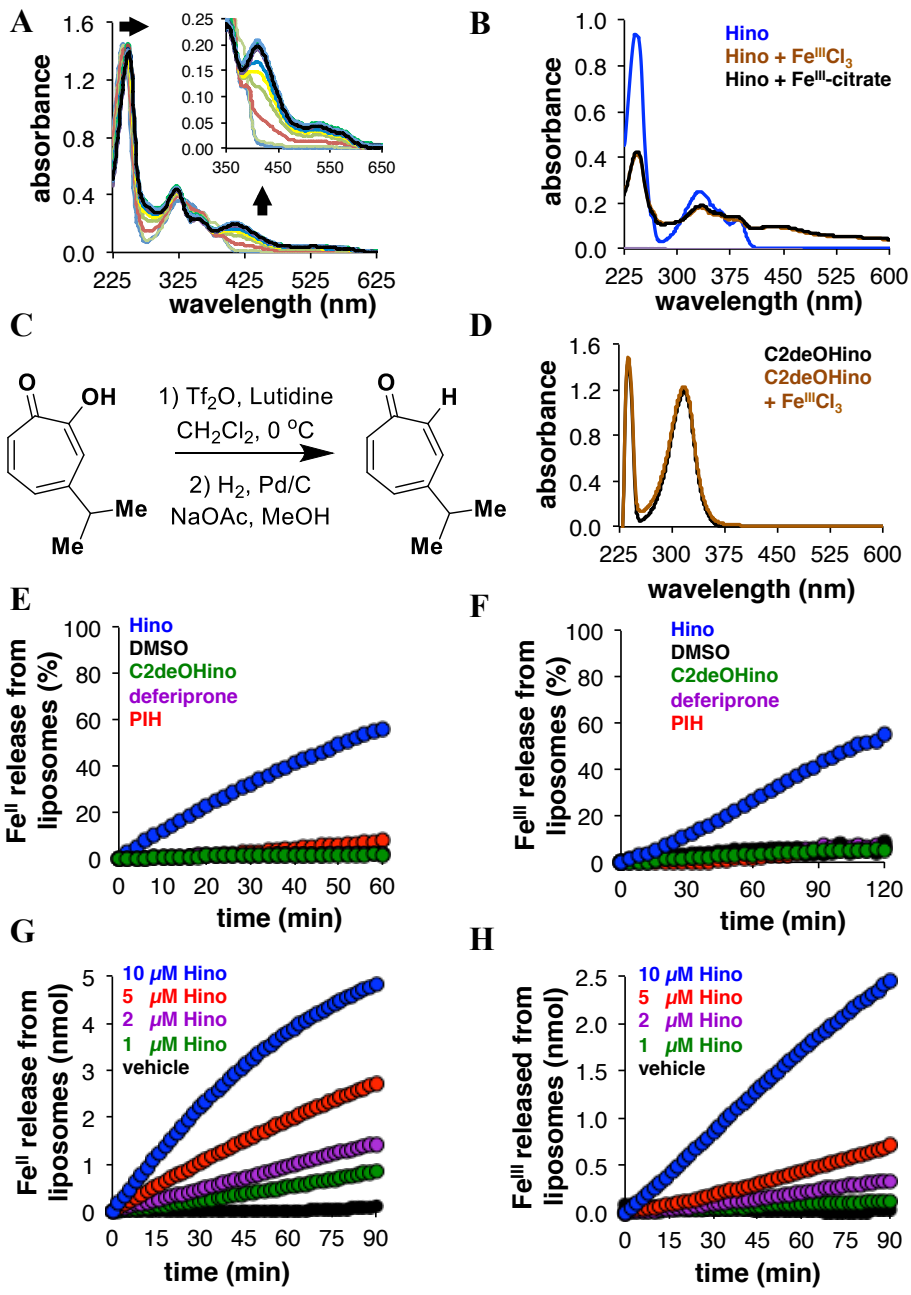

Figure 2.1 Hinokitiol binds and transports iron. (**A**) UV-vis titration study of hinokitiol with increasing $FeCl_3$ indicates that hinokitiol binds iron. Arrows indicate changes in the UV spectrum with increasing iron from 0:1 Fe:Hino (light blue line with least absorbance at 420 nm) to 6:1 Fe:Hino (black line). (**B**) Hinokitiol binds iron (III) using a source of ionic iron (III) and iron (III) weakly bound to small molecules. (**C**) The transport inactive derivative, C2-deoxy hinokitiol (C2deOHino), was synthesized on multi-gram scale in two steps from hinokitiol. (**D**) C2deOHino does not bind iron. (**E** and **F**) In contrast to deferiprone, PIH and C2deOHino, hinokitiol autonomously promotes the efflux of (**E**) ferrous and (**D**) ferric iron from model POPC liposomes (**G, H**) in a dose dependent maner (n = 3).

2.3 CHARACTERIZATION OF HINOKITIOL IRON TRANSPORT IN YEAST

Based on the efflux data as well as the initial screen mentioned in chapter one, a striking trend arose when the compounds that restore transport iron across lipid membranes as well as growth were compared to those that are unable to do so. In the screening assay deferiprone[1],

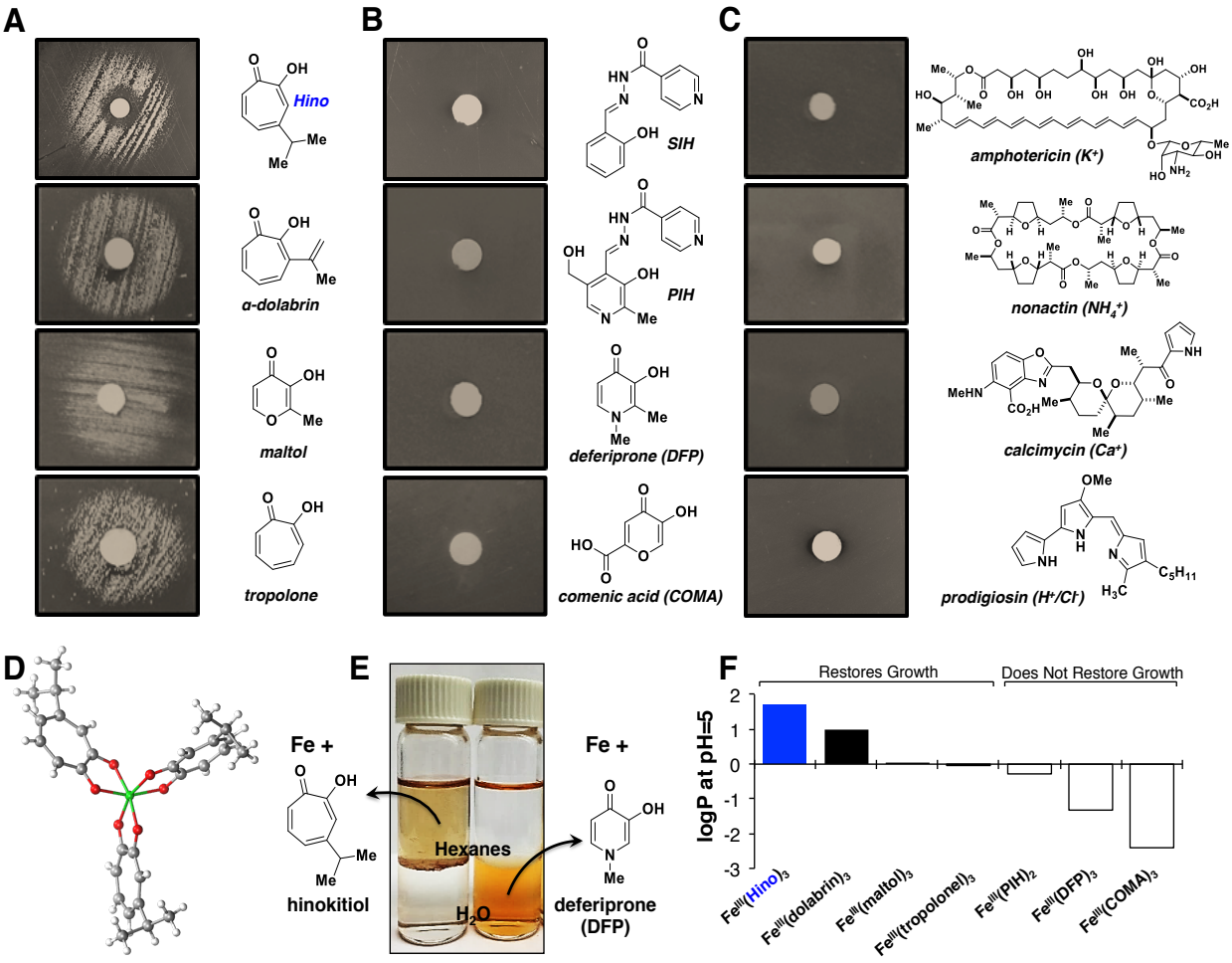

Figure 2.2 Small molecule-mediated growth is general to lipophilic carriers. A) Hinokitiol and other lipophilic α-hydroxy ketones restore growth to fet3Δftr1Δ yeast streaked onto low iron SDagar plates containing 10 μM FeCl3 while **B**) other, more hydrophilic iron chelators and **C**) small molecule transporters of other ions do not restore growth under identical conditions. **D**) X-ray crystal structure of a C1-symmetric Fe(Hino)3 complex. **E**) In contrast to water soluble chelators, such as deferiprone, the hinokitiol-iron complex partitions into nonpolar solvents. **F**) Octanol/water partition coefficients of the iron complexes of other iron chelators that do or do not restore growth to fet3Δftr1Δ yeast.

(PIH)[2], and salicylaldehyde isonicotinoyl hydrozone (SIH)[3,4] were unable to promote growth of the fet3Δftr1Δ yeast (**Figure 2.2 B**) while hinokitiol, tropolone and maltol were able to vigorously promote growth (**Figure 2.2 A**). We discovered that in general, chelators which form lipophilic iron complexes were efficacious (**Figure 2.2 A, E, F**), while more hydrophilic iron chelator complexes (**Figure 2.2 B, E, F**) or other non-iron binding transporters (**Figure 2.2 C)** were not. We hypothesized that in the case of hinokitiol, the isopropyl groups form a lipophilic cage around a hydrophilic ferric-iron binding core, allowing for the Fe:Hino complex to pass through lipid membrane and Anthony Grillo was able to obtain a high resolution crystal structure of $Fe(Hino)_3$ which supports this hypothesis (**Figure 2.2 D**). The Fe:Hino complex is so lipophilic compared to deferiprone that you can readily see the difference by eye (**Figure 2.2 E**) and quantitatively (**Figure 2.2 F**) in partitioning experiments. Interestingly when my high school student, Angela Li, and I synthesized more lipophilic derivatives of deferiprone, they were able to restore yeast growth (**Figure 2.3**). This further supports the hypothesis that lipophilicity is a key contributing factor that determines whether an iron binding small molecule is able to restore growth in iron deficient yeast.

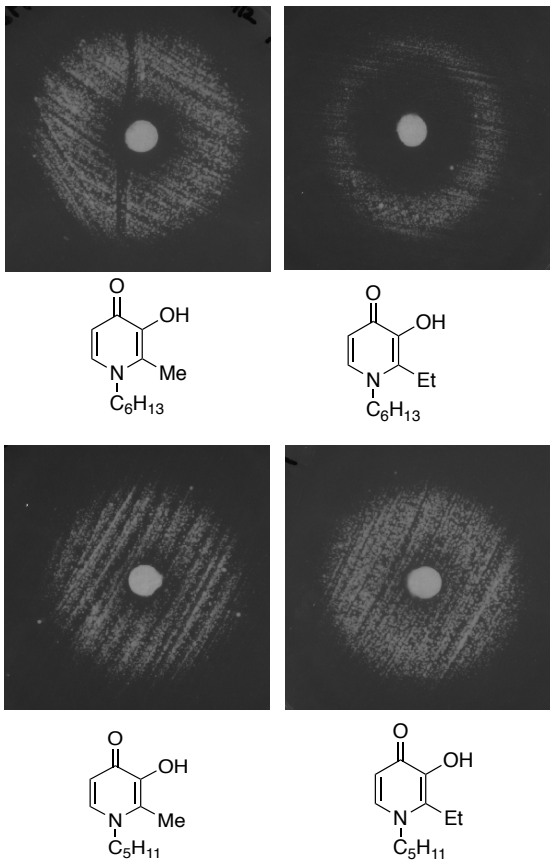

Figure 2.3 Lipophilic derivatives of deferiprone are able to recue iron deficient yeast growth. Disc diffusion assays performed under identical conditions to those in figure 2.2 with lipophilic derivatives of deferiprone.

Continuing to explore the rescue phenomena in yeast we found that hinokitiol allows the yeast to grow as vigorously as wild type (**Figure 2.4 A**), was independent of the yeast siderophore proteins Arn1-4[5] (**Figure 2.4 B**) , and was sustainable on non-fermentable glycerol media (**Figure 2.4 C**). Of special importance is the ability of hinokitiol to restore growth in yeast without their siderophore proteins present. There are currently no known equivalent siderophore scavenging proteins in humans and therefore a siderophore protein mediated rescue of yeast growth would not have been translatable to human health and therefore of less interest for future study.

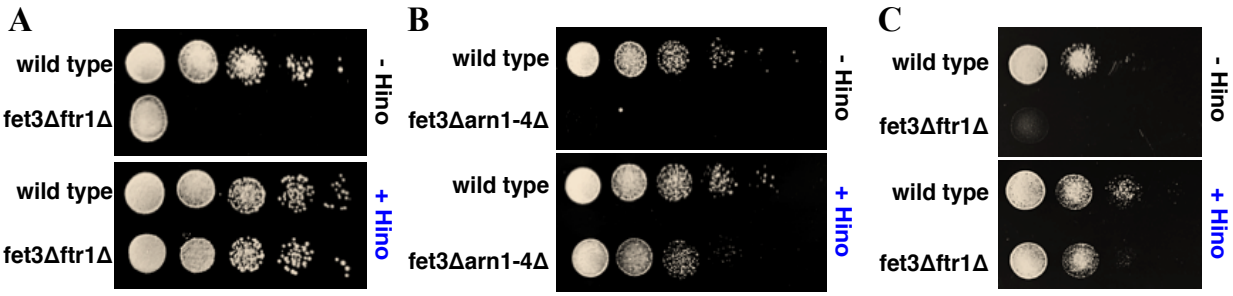

Figure 2.4 Hinokitiol restores growth to fet3Δftr1Δ yeast robustly, independently of siderophore proteins and on both fermentable and non-fermentable media. **A**) In the absence of hinokitiol, reduced fet3Δftr1Δ yeast cell growth was observed on low-iron SD agar plates containing 10 μM FeCl3 by serial 10-fold dilution plating [from OD600 (optical density at 600 nm) = 1.0]. Under identical conditions, but in the presence of 10 μM hinokitiol, restored cell growth was observed on the same low-iron SD agar plates. **B**) Hinokitiol (10 μM) also restores growth to iron-deficient yeast missing all known siderophore protein transporters (fet3Δarn1-4Δ) on low iron SD-agar plates containing 10 μM FeCl3. **C**) 10-fold serial dilution plating (from OD600 = 1.0) of iron-deficient yeast (fet3Δftr1Δ) on low iron SG-agar plates containing 10 μM FeCl3 in the absence or presence of hinokitiol (10 μM).

To further demonstrate that the growth we were observing in the fet3Δftr1Δ yeast treated with hinokitiol was in fact iron dependent, my colleagues Anthony Grillo and Alexander Cioffi were able to show that hinokitiol causes an influx of ^{55}Fe in the fet3Δftr1Δ yeast that is similar to that of the wild type (**Figure 2.5 A**). We then demonstrated that the hinokitiol mediated restoration of growth is vigorous and gets up to wild type levels (**Figure 2.5 B**) occurs over a

range of concentrations up to ~62 μM hinokitiol (**Figure 2.5 C**), has a similar doubling time to wild type yeast (**Figure 2.5 D, E**) and is iron concentration dependent (**Figure 2.5 F**). C2deOHino, which is unable to bind or transport iron (**Figure 2.1 C-F**), is also unable to restore iron influx (**Figure 2.5 A**) or restore yeast growth at any concentration tested (**Figure 2.5 C**), further demonstrating that hinokitiol rescue is due to iron mobilization.

In order to probe the sustainability of hinokitiol mediated rescue I treated fet3Δftr1Δ hinokitiol and switched the cultures back and forth between solid and liquid low iron SD media repeatedly and checked growth quantitatively in the liquid growth stage by OD_{600} after 48 hours of incubation. I found that Hinokitiol mediated growth is sustainable for over 110 days (**Figure 2.5 G**), and if at any point during the experiment hinokitiol was removed from the assay the fet3Δftr1Δ yeast were unable to grow. This loss of growth upon denying hinokitiol to the fet3Δftr1Δ yeast is important because it indicates that the long-term sustained growth was not due to genetic drift and loss of phenotype, but actually a function of hinokitiol rescue.

With the validation of our negative probe, C2DeOHino, and all of the biophysical, phenomenological and mechanistic data in hand we were even more confident that hinokitiol's unique properties made it a promising lead compound toward developing a small molecule iron transporter to treat diseases of iron homeostasis. We therefore chose three mammalian proteins for further study, Divalent Metal Transporter 1, Ferroportin, and Mitoferrin.

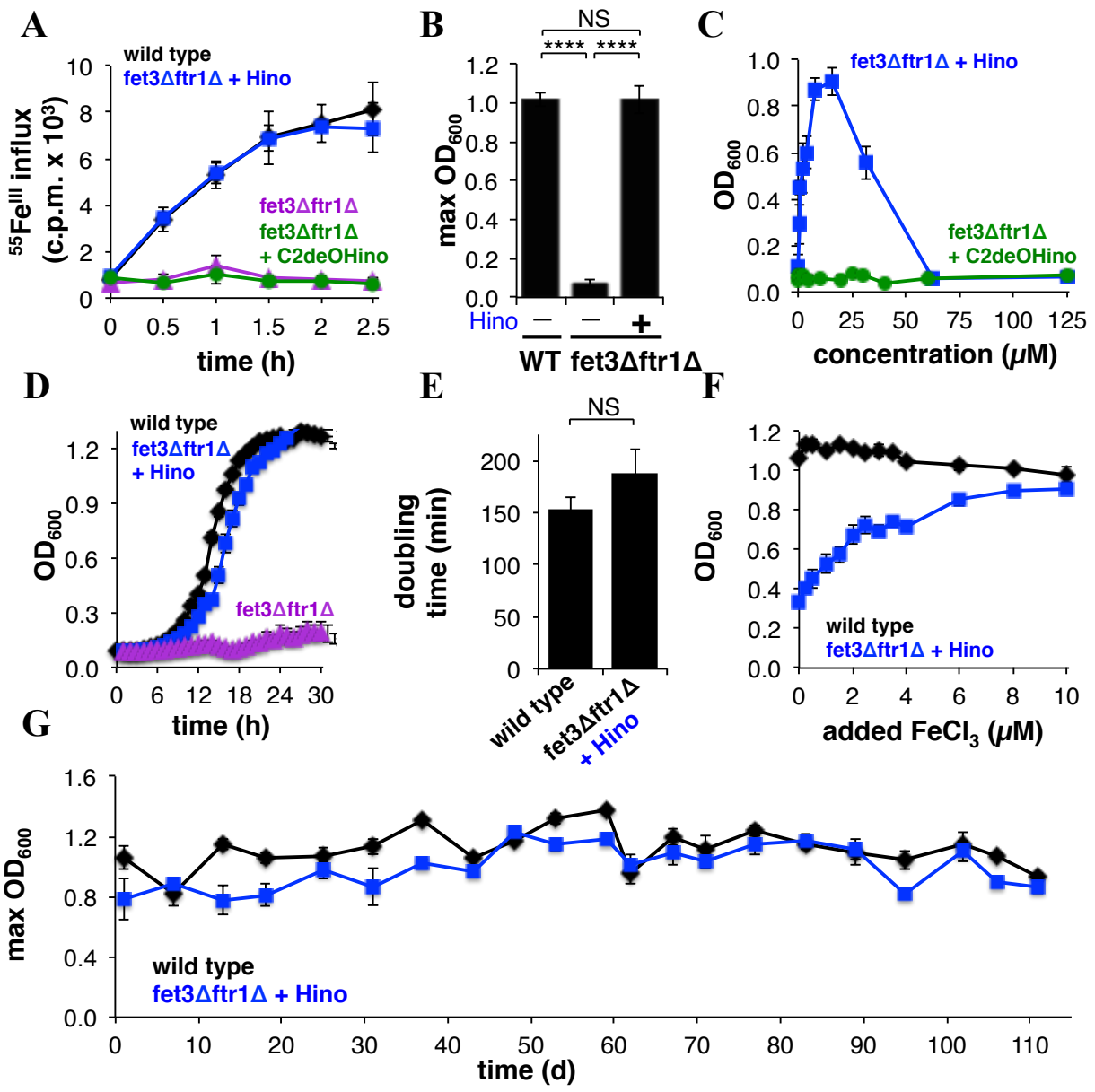

Figure 2.5 Hinokitiol causes the influx of iron into yeast cells and causes robust restoration of growth. **A**) Hinokitiol increased ^{55}Fe influx into fet3Δftr1Δ yeast, whereas C2deOHino did not (n = 3). **B**) Yeast cell growth in liquid SDmedia containing 10 μM FeCl3 in the absence or presence of 10 μM hinokitiol (n = 3). NS, not significant; ****P ≤ 0.0001. **C**) Hinokitiol restored growth of fet3Δftr1Δ yeast, whereas C2deOHino did not (n = 3). **D and E**) Hinokitiol treated fet3Δftr1Δ yeast have similar growth kinetics and doubling time compared to wild type. **F**) Hinokitiol-promoted growth restoration of fet3Δftr1Δ yeast is dependent on iron levels in the media (n=3). **G**) Growth restoration to fet3Δftr1Δ yeast can be sustained for >100 days with continued reliance on hinokitiol (n= 8).

2.4 HINOKITIOL RESTORES IRON MOBILIZATION INTO CELLS

Divalent Metal Transporter 1 (DMT1) is the sole non-heme iron transporter present in the apical, microvillus membrane of gut enterocytes (**Figure 2.6 left**) [6,7] and is therefore the main gateway through which iron from the diet is absorbed. In humans, DMT1 mutations cause an extremely rare form of microcytic anemia that does not respond to iron supplementation orally or intravenously due to the peripheral function of DMT1 in red blood cell progenitors[7–14](**Figure 2.6 right**). These patients present with severe anemia, high reticulocyte count and occasionally iron overload[15].

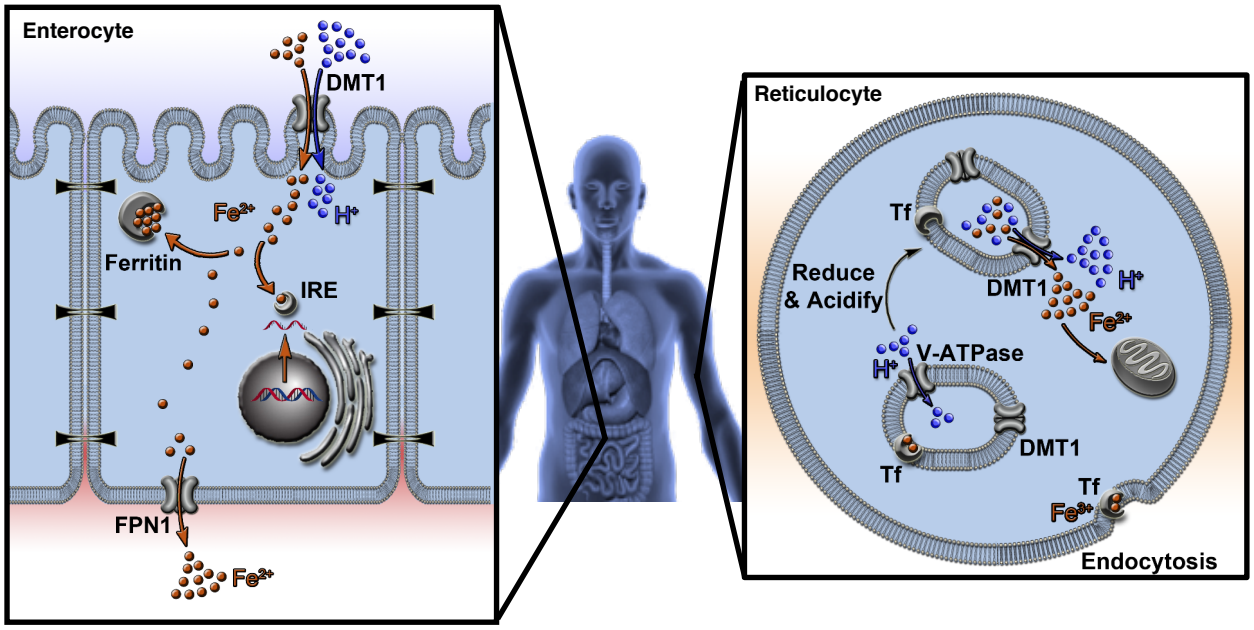

Figure 2.6 DMT1 is found in both gut enterocytes (left) and red blood cell progenitors (right) where it allows for the absorption of iron and hemoglobinization respectively to occur.

DMT1 mutations only contribute to 5-10 cases of microcytic anemia world wide, it is considered an extremely a rare disease and therefore there remain few treatment options for patients. Chelation therapy has been attempted in order to reduce the liver iron burden in patients

with hepatic iron overload, however it is often ineffective and occasionally actively harmful to the patient's health. Chelators were found to be ineffective at removing iron from the liver or led to a drop in hemoglobin level that was deemed unsafe and the treatment regimen was thus was interrupted (G. Tchernia C. Beaumont, unpublished data, 2007)[16]. With these challenges in mind we asked whether hinokitiol could promote iron mobilization into cells and therefore restore down stream physiology in a DMT1 deficient system.

We first studied iron uptake and transepithelial transport in fully differentiated DMT1-deficient Caco-2 gut epithelia monolayers (**Figure 2.7 A**). In order to make a stable knockdown of DMT1 in the Caco-2 cells we utilized stable short hairpin RNA (shRNA) transfection[17,18] and selected the clones with the greatest, and most consistent knock down of iron ^{55}Fe transport (**Figure 2.7 D**). We then characterized DMT1 expression via mRNA expression (**Figure 2.7 B**) and protein quantification (**Figure 2.7 C**) via quantitative PCR (qPCR) and western blot respectively. Control Clone A was found to have the highest ^{55}Fe transport and shDMT1 Clone 4A was found to have the most diminished ^{55}Fe transport and so both were chosen for further study in order to give the greatest delta that hinokitiol would have to overcome. Importantly in the presence of hinokitiol we do not observe an increase in DMT1 protein production, therefore any effects we see in the shDMT1 membranes are not due to an off target increase in DMT1 protein expression induced by hinokitiol.

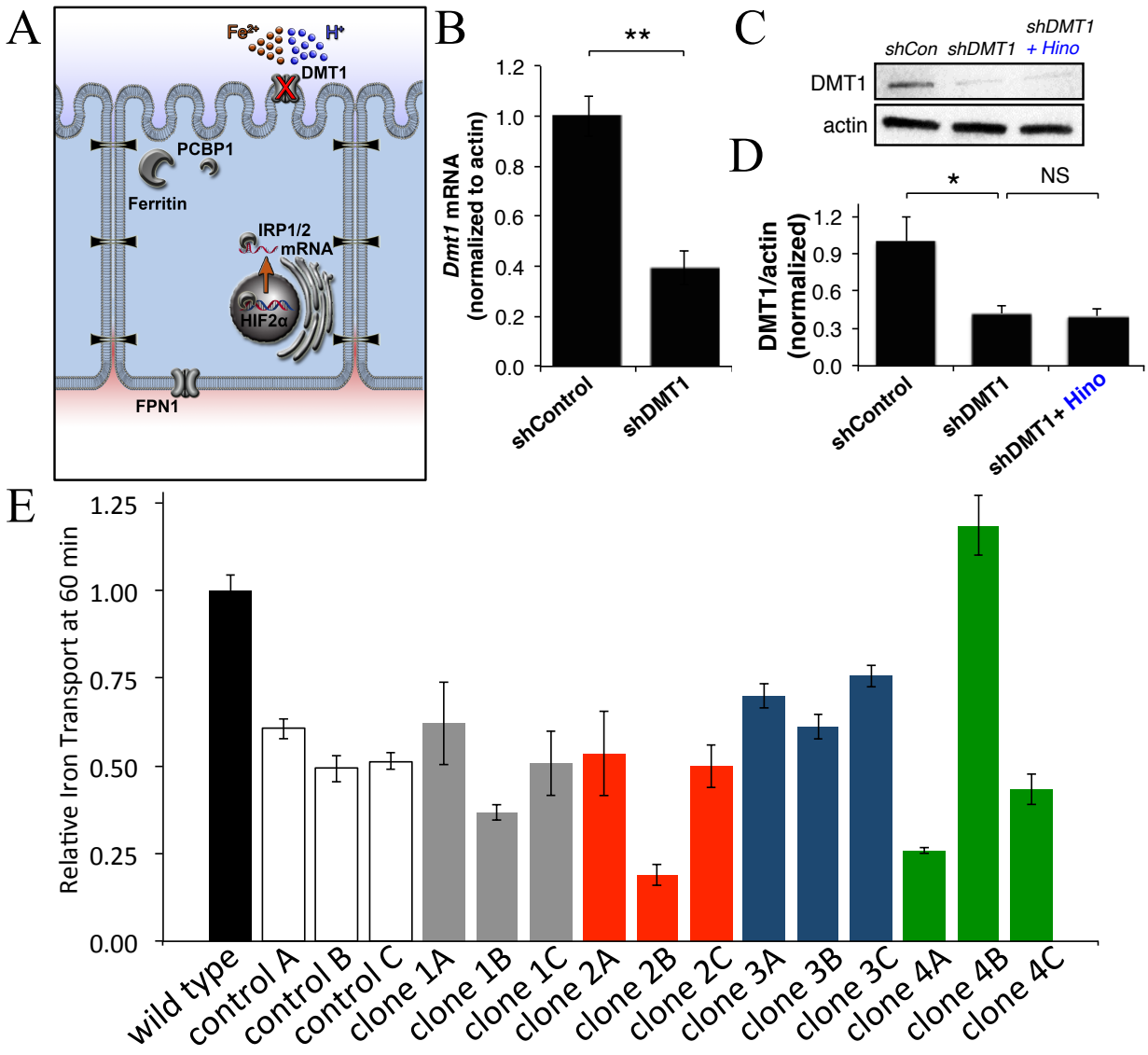

Figure 2.7 Characterization of shDMT1 Caco-2 cells. (**A**) DMT1-deficient gut epithelia exhibit reduced dietary iron absorption across the apical membrane resulting in decreased transport to the basolateral fluid. (**B**) Dmt1 mRNA levels, quantified via qRT-PCR, are reduced in shDMT1 Caco-2 monolayers as compared to the shControl cell monolayers. N = 9. (**C** and **D**) Quantitative densitometric analysis of western blots indicated decreased DMT1 protein levels in shDMT1 Caco-2 monolayers. Hinokitiol (500 nM) treatment did not induce DMT1 expression. N = 13-14. **E**) Iron-55 transport assay performed on shDMT1 clone membranes 14-21 days after seeding. Control Clone A and shDMT1 Clone 4A were the best control and knock down lines respectively at the 1 hour time point and were chosen for further study (N=3) .

Relative to wild-type controls, DMT1-deficient monolayers (**Figure 2.8 A**) showed reduced iron uptake into cells and reduced transepithelial iron transport to the basolateral fluid after apical addition of a trace amount (200 nM) of ^{55}FeCl3 (**Figure 2.8 B and C**). Apical addition of just 500 nM of hinokitiol restored uptake and transport to control levels (**Figure 2.8 B and C**) over 4 hours, a time frame commensurate with dwell times in the gut (**Figure 2.8 D**). The kinetics of hinokitiol mediated iron uptake and therefore transport observed over the 4 hour

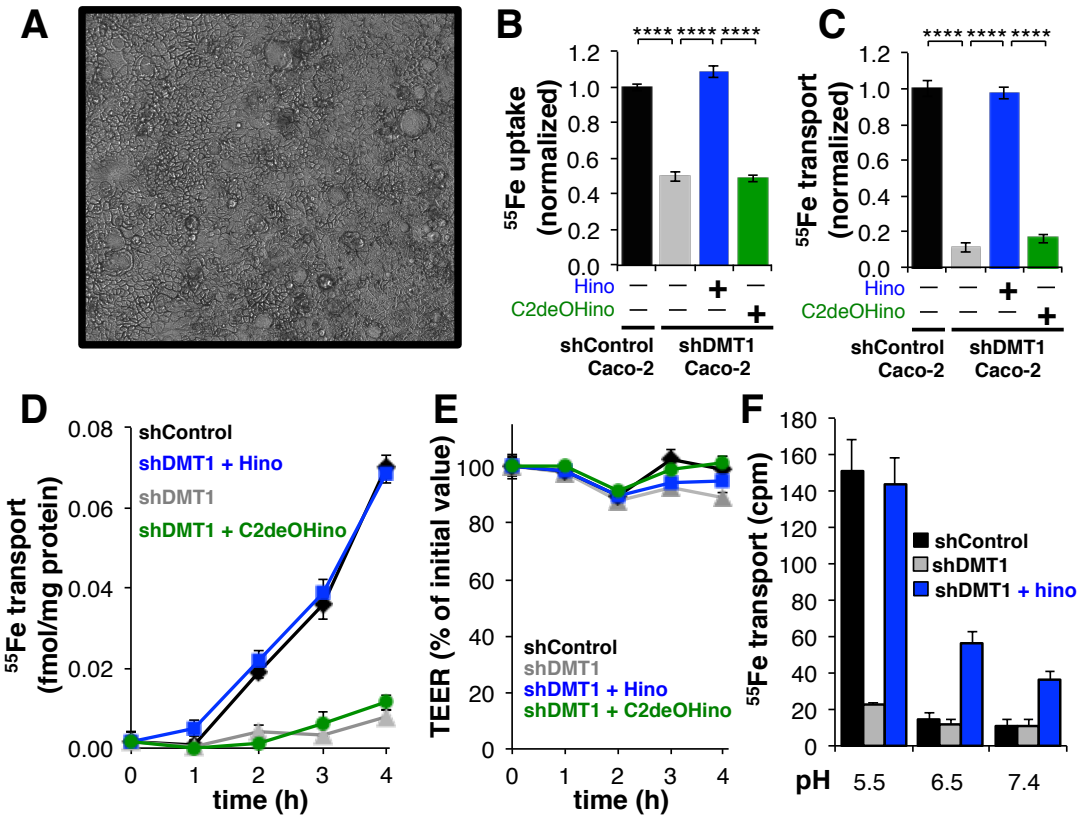

Figure 2.8 Hinokitiol Restores Iron uptake and therefore transport in DMT1 Deficient Caco-2 monolayers. (**A**) Bright field microscope image 40x ofshDMT1 Caco-2 monolayers. (**B**) ^{55}Fe uptake into DMT1-deficient (shDMT1) Caco-2 monolayers and (**C**) transepithelial transport (apical to basolateral) indicated that hinokitiol (500 nM) restored normal iron absorption (n = 3). shControl refers to Caco-2 monolayers that were transfected with a non-targeting control shRNA plasmid. (**D**) Hinokitiolpromoted ^{55}Fe transport occurs on time scales commensurate with dwell times in the gut (n = 3). (**E**) Transepithelial electrical resistance (TEER) values of Caco-2 monolayers treated with DMSO, hinokitiol (500 nM), or C2deOHino (500 nM) remain consistent over the course of the experiment. N = 3. (**F**) Hinokitiol (500 nM) promotes transport in shDMT1 Caco-2 monolayers at a range of pHs found throughout the duodenum. N = 3.

experiment tracked extremely well with the control membranes indicating that the system is working well with the exogenous transport of iron.

Importantly, hinokitiol did not disrupt monolayer integrity (**Figure 2.8 E**), indicating that the monolayers remained intact and any iron transport observed was trasnepithelial and not due to loss of tight junctions and therefore a simple "leak" of iron transcellularly between the cells within the membrane. Hinokitiol caused no observable toxicity as evident by a WST-8 assay (EC_{90} >100 μM), and did not affect basal DMT1 expression as evident by western blot quantification after 4 hours of hinokitiol treatment (**Figure 2.7 C and D**). Hinokitiol-mediated transport occurred across a wide range of pHs found in the gut throughout the duodenum and increased with decreasing pH (**Figure 2.8 F**). This further supports that this is a hinokitiol mediated phenomena because proteins have the opposite trend where more uptake and transport occur at higher pHs.

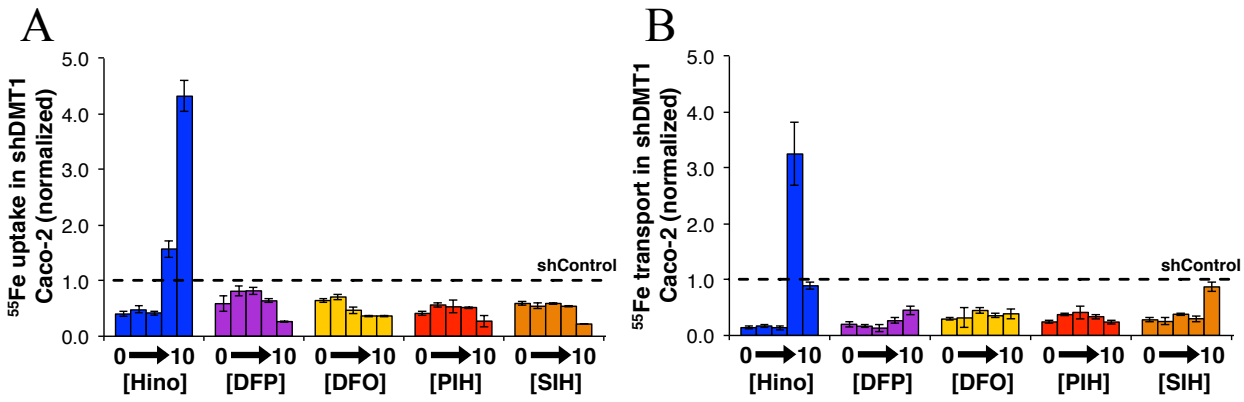

Figure 2.9 Hydrophilic iron chelators do not restore iron transport in Caco-2 monolayers. In contrast to hinokitiol, the iron chelators deferiprone, PIH, SIH, and deferoxamine do not simultaneously restore (**A**) uptake into or (**B**) transcellular transport across DMT1-deficient Caco-2 monolayers under identical conditions (pH = 5.5 apical, pH = 7.4 basolateral). Dotted line represents shControl levels. While a slight increase in transport was observed in SIH treated cells, reduced uptake was observed, consistent with paracellular, and not transcellular, iron transport. Concentrations used for each small molecule were 0, 0.01, 0.1, 1, and 10 μM. N = 3.

Whereas hinokitiol promoted uptake and transport over a wide range of concentrations, C2deOHino (**Figure 2.8 A, B**), and subtoxic concentrations of the iron chelators deferiprone, deferoxamine, PIH, and SIH did not promote either uptake or transport (**Figure 2.9 A and B**). High concentrations of these more hydrophilic iron chelators instead decreased iron uptake into DMT1-deficient monolayers (**Figure 2.9 A**) corroborating the negative results seen in DMT1 patients treated with the same chelators. These data demonstrate that hinokitiol is able to mobilize iron into cells and therefore restore iron uptake and transepithelial transport in a mammalian tissue culture system.

2.5 HINOKITIOL RESTORES MOBILIZATION OF IRON WITHIN CELLS

As stated in the previous section DMT1 is also very important peripherally to iron absorption in the gut, it is also necessary for hemoglobinization and differentiation of red blood cell progenitors (**Figure 2.6 B**)[9,19,20]. If DMT1 is missing, depleted, or hypomorphic, intracellular iron(II) efflux from endosomes of erythroid precursors is precluded, thus preventing hemoglobinization and differentiation in mature red blood cells (**Figure 2.10 A**)[21–23]. In order to study hinokitiol's ability to transport iron within DMT1 deficient cells, we made stable knockdown cell lines with shDMT1 in DS19 murine erythroleukemia (MEL) cells[24]. We quantified DMT1 expression via mRNA expression (**Figure 2.10 C**) and protein quantification (**Figure 2.10 B and D**) with quantitative PCR (qPCR) and western blot respectively. We then chose the shDMT1 clones with the best DMT1 knock down, shDMT1 Clone 1, 2 and 4, for further study in order to give the largest difference between the DMT1 deficient and the control line.

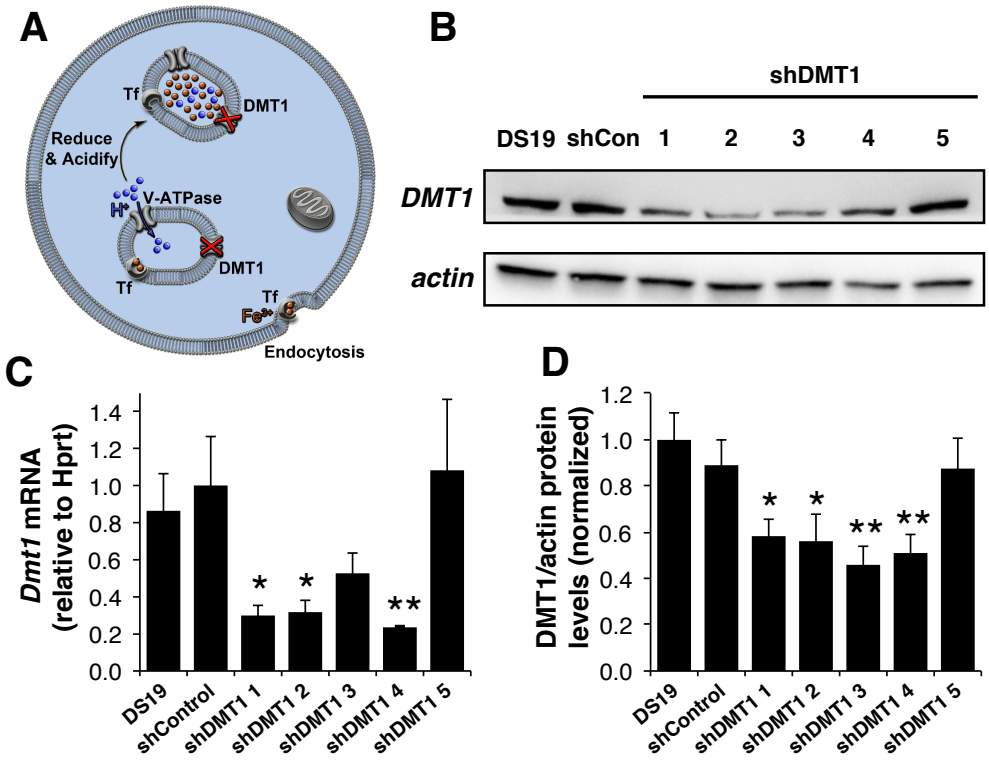

Figure 2.10 Characterization of shDMT1 MEL cells. (**A**) DMT1 deficiencies impair normal differentiation of red blood cell progenitors by precluding endosomal iron release to the cytosol for mitochondrial hemoglobinization. (**B**) Representative western blot image of DMT1 protein levels in differentiated MEL cells**.** (**C**) Dmt1 mRNA (N = 12-16) and (**D**) DMT1 protein levels are reduced in shDMT1 MEL cells (Clones 1, 2, and 4) relative to shControl after DMSO induction for terminal differentiation. N = 13.

We tested for dimethyl sulfoxide (DMSO)–induced differentiation and hemoglobinization in DS19 murine erythroleukemia (MEL) cells[24] and shRNA transfected DMT1-deficient MEL cells in the absence or presence of hinokitiol. shControl cells differentiated normally after 3 days as indicated by the characteristic pink color of hemoglobin in cell pellets (**Figure 2.11 A**). We were able to quantify the differentiation of each clone by staining with o-dianisidine (**Figure 2.11 C and D**). Dianisidine specifically stains hemoglobinized cells; when heme is present in a cell the iron in the heme along with H_2O_2 react and oxidize the dianisidine to form a dark brown color which in turn stains the cell. These cells are imaged and ImageJ is used to quantify the stained cells/frame. Reduced hemoglobinization

was observed in DMT1-deficient cells (**Figure 2.11 A-D**). Three days of hinokitiol treatment (1 mM) restored ^{55}Fe incorporation into heme (**Figure 2.11 D**), and hemoglobinization (**Figure 2.11 A-D**). The efficacious concentration of hinokitiol was over an order of magnitude higher than the dose found to be toxic (determined via WST-8, EC_{90} =24). C2deOHino had no effect (**Figure 2.11 C and D**) and, as expected, no differentiation or staining was observed in the absence of DMSO, with or without hinokitiol treatment. Collectively, these studies demonstrate that hinokitiol is able to move iron within cells and therefore allow for restoration of physiology, in this case restoration of hemoglobinization and differentiation.

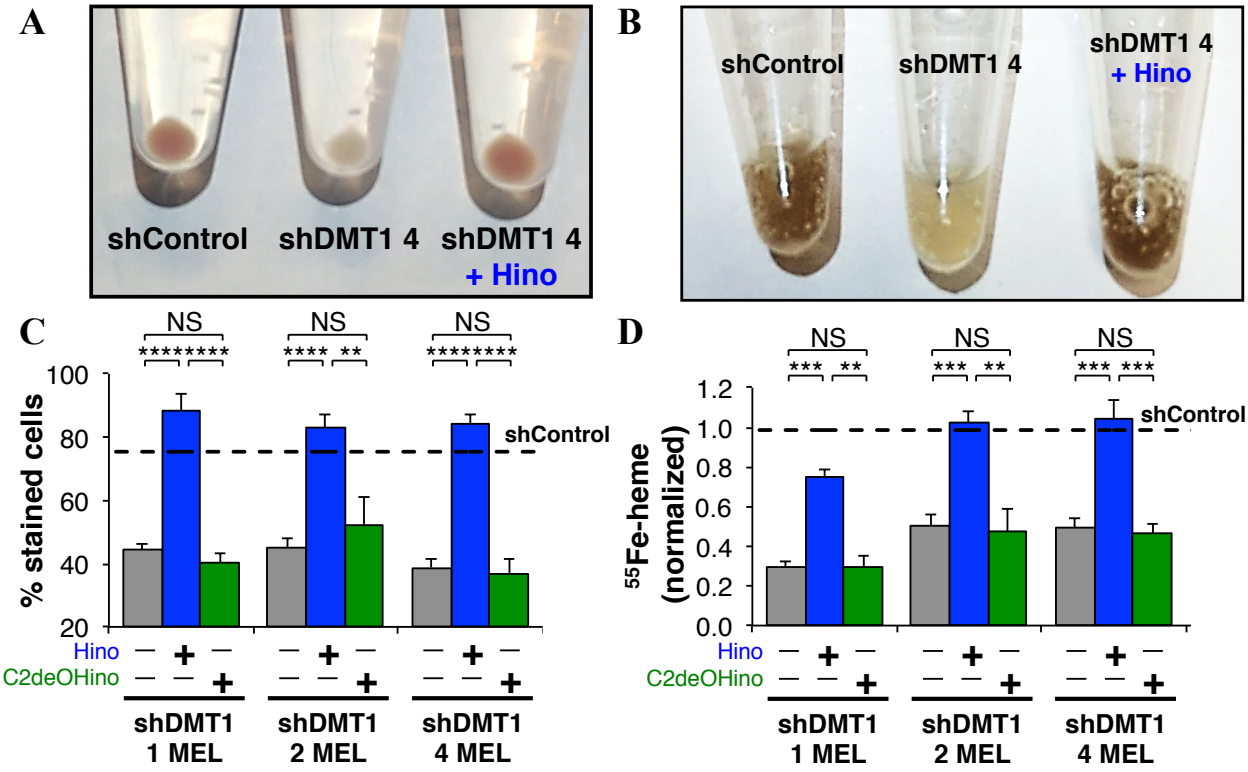

Figure 2.11 Hinokitiol Restores hemoglobinization in DMT1 Deficient MEL cells. (**A**) Cell pellets from shControl and hinokitiol-treated (1 μM) DMT1-deficient MEL cells appear pink, characteristic of hemoglobin, whereas DMT1-deficient cell pellets do not. (**B**) Hinokitiol (1 μM for three days) visually restores differentiation as evidenced by staining hemoglobinized cells brown with o-dianisidine. (**C**) ImageJ quantification of MEL cells stained brown with o-dianisidine (n= 6 -48). The dashed line represents shControl levels. (**D**) ^{55}Fe incorporation into heme in hinokitiol rescued DMT1-deficient MEL cells (n= 3-23). The dashed line represents shControl levels.

2.6 HINOKITIOL RESTORES MOBILIZATION OF IRON OUT OF CELLS

With evidence that hinokitiol is able to mobilize iron into and within cells we next probed its ability to mobilize iron out of cells. Ferroportin is an important iron exporter that is highly expressed in both the duodenum and liver macrophages and therefore involved in both iron absorption and iron recycling within the body (**Figure 1.6**) [20,25,26]. Hemochromatosis Type IV, or The ferroportin Disease, is caused by dominant negative mutations in FPN1 leading to iron overload and interestingly a concomitant anemia characterized by hypoferremia and liver macrophage iron loading[27]. The iron overload in the liver can lead to cirrhosis and therefore, as mentioned in chapter 1, the recommended treatment is phlebotomy[27,28]. The problem with this treatment is that some patients have a very low tolerance to phlebotomy due to the inherent low iron absorption and therefore the anemia that is characteristic of the disease. There are over 200 confirmed patients world wide with that number growing as the disease becomes more recognized.

In order to study the effect of FPN1 deficiency on iron efflux across the basolateral side of fully differentiated Caco-2 monoloayers (**Figure 2.12 A**), we utilized the small molecule inhibitor quercetin (**Figure 2.12 B**). Quercetin is a natural product found in many of the foods we consume including apples, onions, and tea[29]. It is the most abundant dietary flavonoid and makes up about 25% of the total flavonoid intake in an average diet which corresponds to 10-20 mgs/day[29]. In a study by Lusjek *et al* it was found that quercetin specifically upregulates a single miRNA (miR-17-3p) which interacts with interaction with the FPN1 3'UTR[29]. This interaction causes a decrease in FPN1 protein expression and leads to a FPN1 deficient state[29]. After treating fully differentiated Caco-2 monolayer with quercetin for 18 hours, the quercetin was removed and the FPN1 protein levels were checked via western blot to confirm satisfactory

knock down as compared to wild type (**Figure 2.12 C and D**).

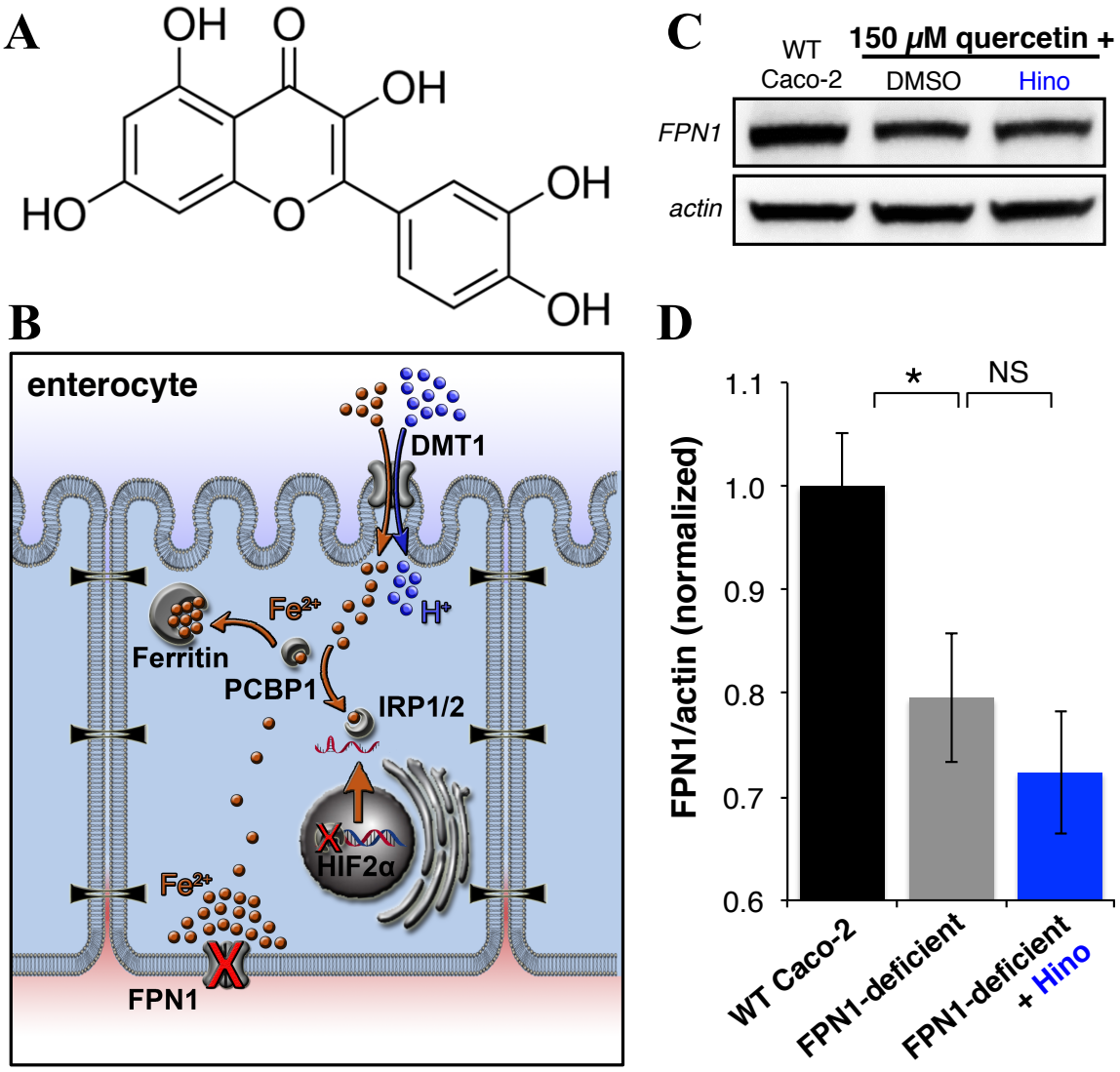

Figure 2.12 FPN1 knock down in Caco-2 monolayers by quercetin. (**A**) Quercetin, a flavonoid natural product that causes miRNA mediated knockdown of ferroportin. (**B**) FPN1 deficiencies prevent the proper release of iron from gut enterocytes leading to reduced transport to the basolateral fluid. (**C and D**) Quercetin incubation for eighteen hours knocks down FPN1 protein levels in Caco-2 cells; hinokitiol (1 μM) does not increase FPN1 levels. N = 8.

FPN1 deficiencies reduce iron efflux across the basolateral membrane of gut epithelia (**Figure 2.13 A**). Hinokitiol (1 μM) restored transepithelial iron transport in FPN1-deficient Caco-2 monolayers (**Figure 2.13 A**) over 4 hours, commensurate with dwell time in the gut

(**Figure 2.13 B).** Importantly iron uptake, which is ferroportin independent was not affected with hinokitiol treatment (**Figure 2.13 C**). Hinokitiol treatment after treatment after pretreatment with quercetin did not disrupt monolayer integrity (**Figure 2.13 D**).

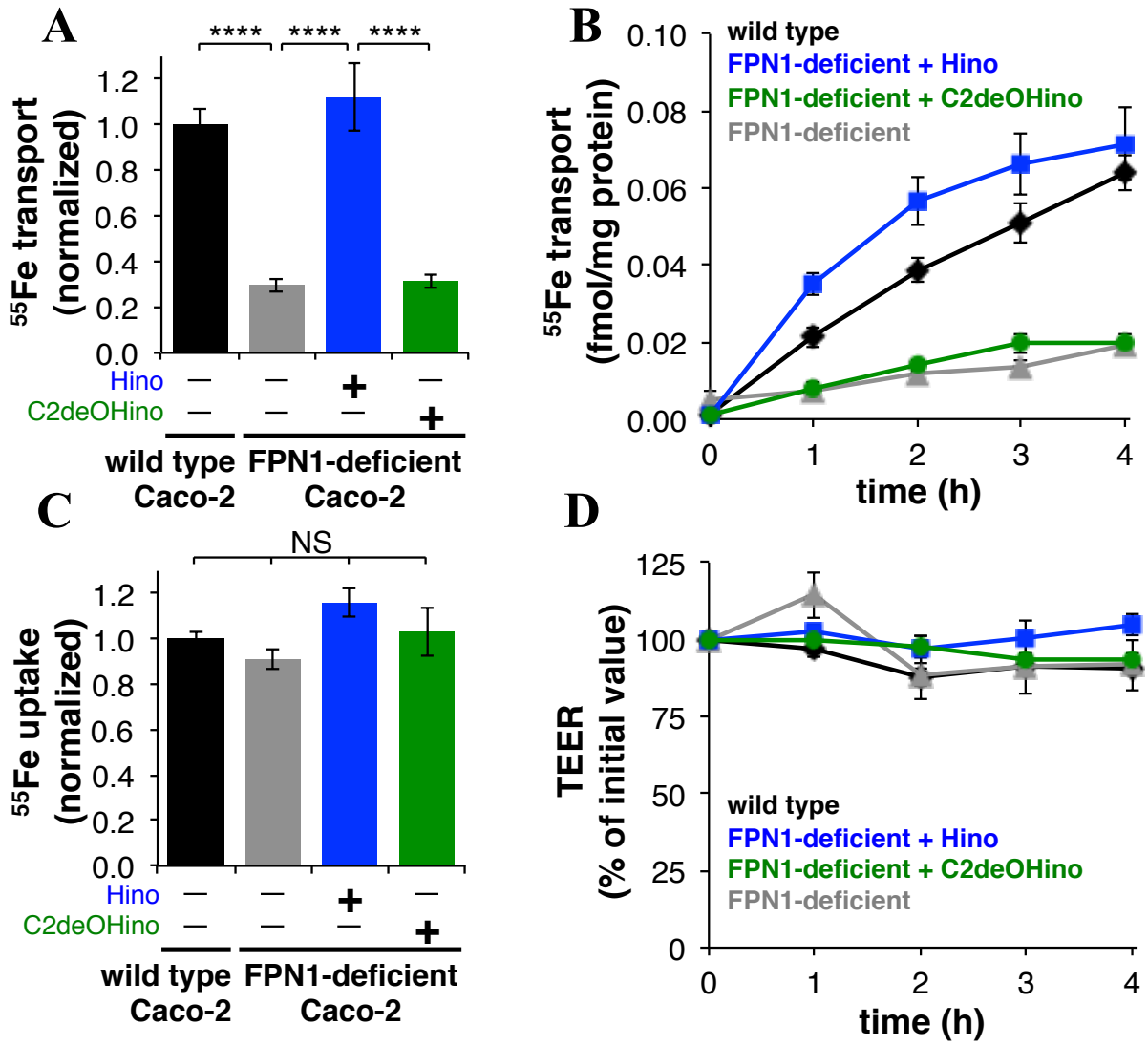

Figure 2.13 Hinokitiol restores iron transport in FPN1 deficient Caco-2 monolayers. (**A**) 1 μM Hinoktiol restores ^{55}Fe transepithelial transport across FPN1-deficient Caco-2 monolayers (**B**) over 4 hours (**C**) without affecting iron uptake (n = 12) or (**D**) disrupting monolayer integrity.

FPN1 is also important in iron recycling in liver macrophages called Kupffer cells (**Figure 1.6 right**). In order to recycle iron the Kupffer cells phagocytose senescent erythrocytes, digest them and then efflux the iron into the blood where it is bound by transferrin and circulated

through out the body (**Figure 1.3**)[30,31]. In order to make FPN1 deficient macrophages we treated them with the peptide hepcidin. Hepcidin is a small regulatory peptide, or hormone, that regulates iron absorption and recycling within the body[31–34]. When there is high iron in the blood hepcidin is upregulated and then binds to, and downregulates ferroportin in both the gut and liver (**Figure 2.14 A**). This stops the absorption of iron from the diet as well as iron recycling in the liver[31] in order to keep free, non-transferrin bound iron out of the blood. We therefore used hepcidin to make FPN1 deficient J774 mouse reticuloendothelial macrophages (**Figure 2.14 B**)[35] and quantified the FPN1 protein knockdown via western blot (**Figure 2.14 C and D**) .

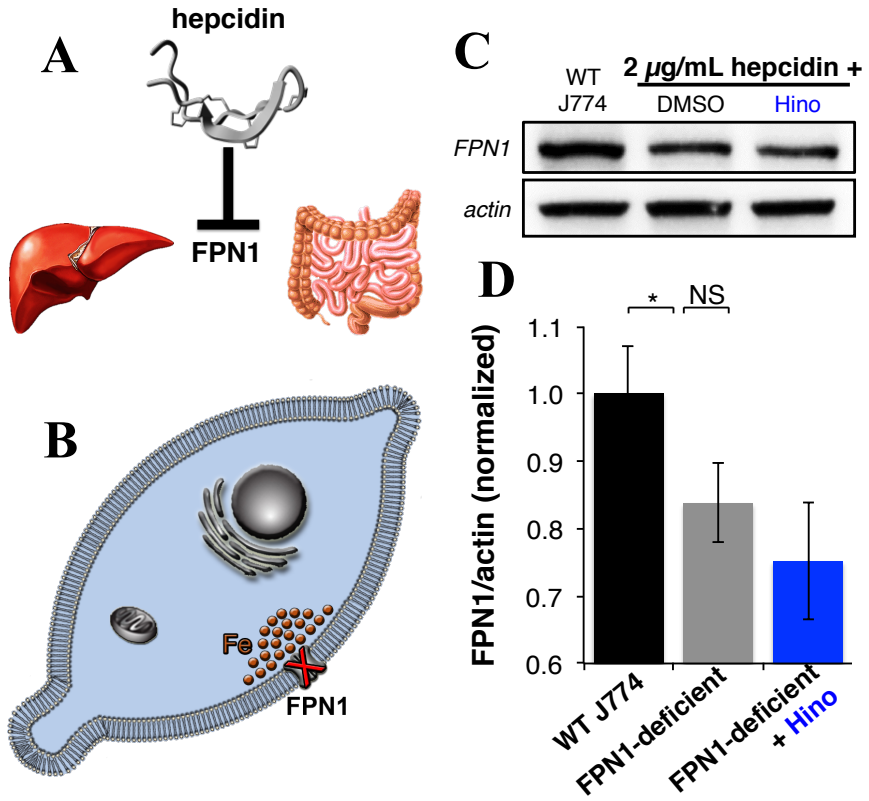

Figure 2.14 Characterization of hepcidin knock down of FPN1 in J774 Macrophages. (**A**) Hepcidin downregualtes FPN1 in both the liver and the gut. (**B**) FPN1 deficiencies preclude the release of labile iron from reticuloendothelial macrophages in the liver (**C and D**) Hepcidin reduces FPN1 levels in J774 macrophages; hinokitiol (5 μM) does not increase FPN1 levels. N = 20.

Hepcidin decreased the amount of iron efflux out of J774 macrophages (**Figure 2.15 A**). Hinokitiol was able to restore iron efflux back to wild type levels (**Figure 2.15 A**). The

restoration of efflux with hinokitiol was time dependent (**Figure 2.15 B**) as well as dose-dependent (**Figure 2.15 C**). The restored iron release from FPN1-deficient J774 macrophages was achieved without observable toxicity (EC_{90} >100, **Figure 2.15 D**).

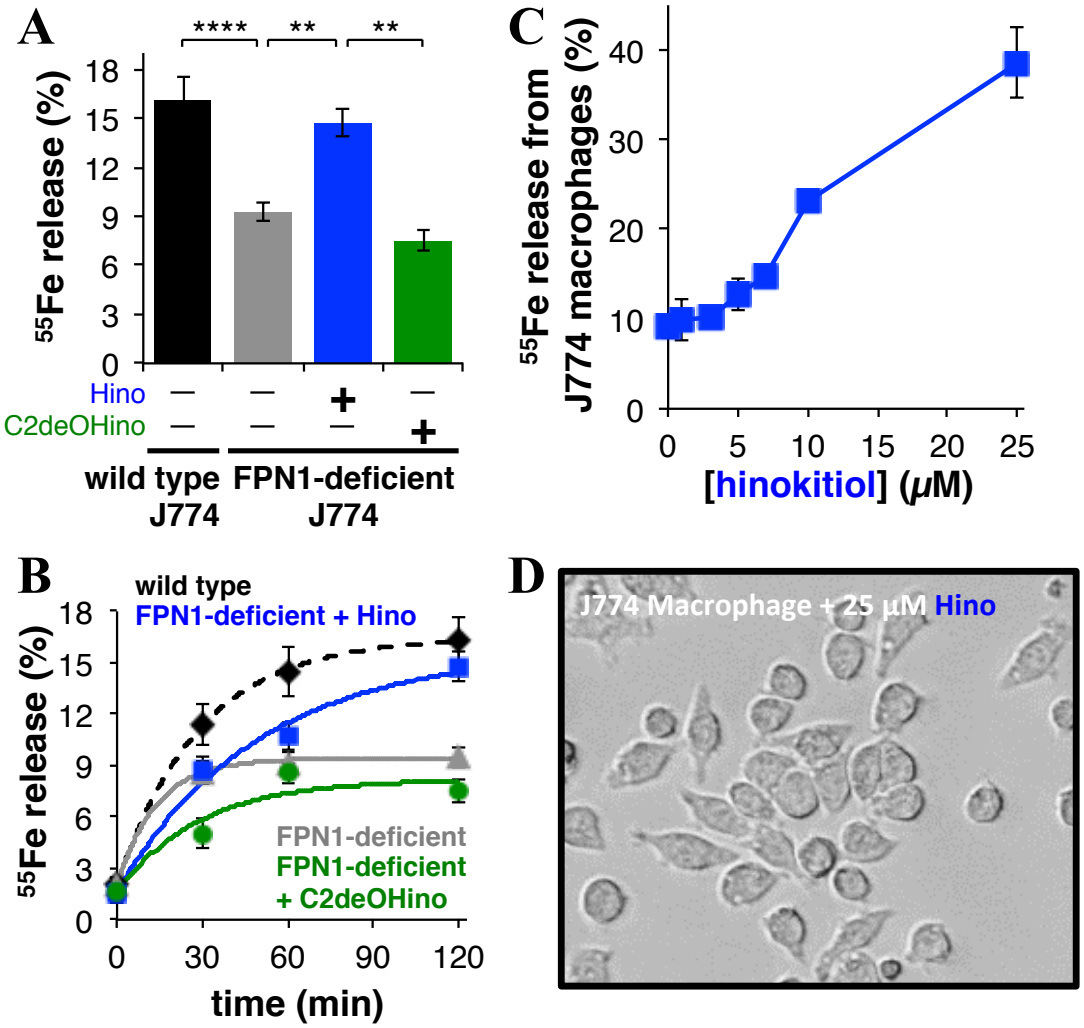

Figure 2.15 Hinokitiol restores iron efflux from FPN1 deficient Caco-2 monolayers and J774 Macrophages. (**A**) Hinokitiol (5 μM) promotes the release of 55Fe from hepcidin-treated FPN1- deficient J774 macrophages (t = 2 hours; n = 6 to 20). (**B**) Time-dependent release of 55Fe from wild-type J774 macrophages and FPN1-deficient J774 macrophages treated with DMSO, hinokitiol, or C2deOHino (n = 6 to 20). (**C**) Hinokitiol promotes iron release in FPN1-deficient J774 cells in a dose-dependent manner after 2 hours. N = 6-20. (**D**) 40x bright field microscopy picture of J774 cell incubated with 25 μM Hinokitiol for 2 hours do not show a morphology indicating toxicity.

2.7 HINOKITIOL RESTORES IRON MOBILIZATION AND THEREFORE PHYSIOLOGY IN MULTIPLE ANIMAL MODELS MISSING IRON TRANSPORTERS

With all of the promising data we collected in cellular systems we were thus encouraged to ask whether hinokitiol could restore gut iron absorption and hemoglobinization in animal models of these iron-transporter deficiencies. DMT1 deficiencies in duodenal enterocytes reduce rates of iron absorption in the gut by disrupting apical iron uptake into cells[21,22,30,36]. We therefore tested gut iron absorption in DMT1-deficient Belgrade (b/b) rats, the leading animal model of DMT1 deficiencey[37]. Homozygous Belgrade rats are much smaller than their littermates (**Figure 2.16** A) with a low survival rate and life expectancy,[37] along with low hemoglobin and hematocrit. They have a high reticulocyte count thought to be caused by immature reticulocytes being released by the marrow to compensate for the anemic phenotype[37].

We tested hinokitiol's ability to restore gut iron absorption upon administration of a single dose of ^{59}Fe and 1.5 mg of hinokitiol per kilogram of body weight via oral gavage. Higher doses of hinokitiol are reported to be nontoxic in rats subjected to chronic oral administration for 2 years[38]. Similar to the reduced iron absorption previously reported in *b/b* rats[37], a twofold reduction in ^{59}Fe absorption was observed in C2deOHino treated *b/b* rats relative to sibling controls (+/+ or *+/b*) (**Figure 2.16 B**). Treatment of b/b rats with hinokitiol increased 59Fe absorption back to control levels after 1 hour (**Figure 2.16 B and C**). There is a slight dip of ^{59}Fe concentration in the blood at 120 min in the hinokitiol treated rats (**Figure 2.16 C**), however that correlates with a concomitant increase in ^{59}Fe in the kidney and the femur (**Figure 2.16 D and E**). This is encouraging because after just one dose of hinokitiol we are starting to see the iron move into the tissues, indicating that not only is there an increase in iron absorption but that iron is bioavailable and potentially being used for red blood cell synthesis.

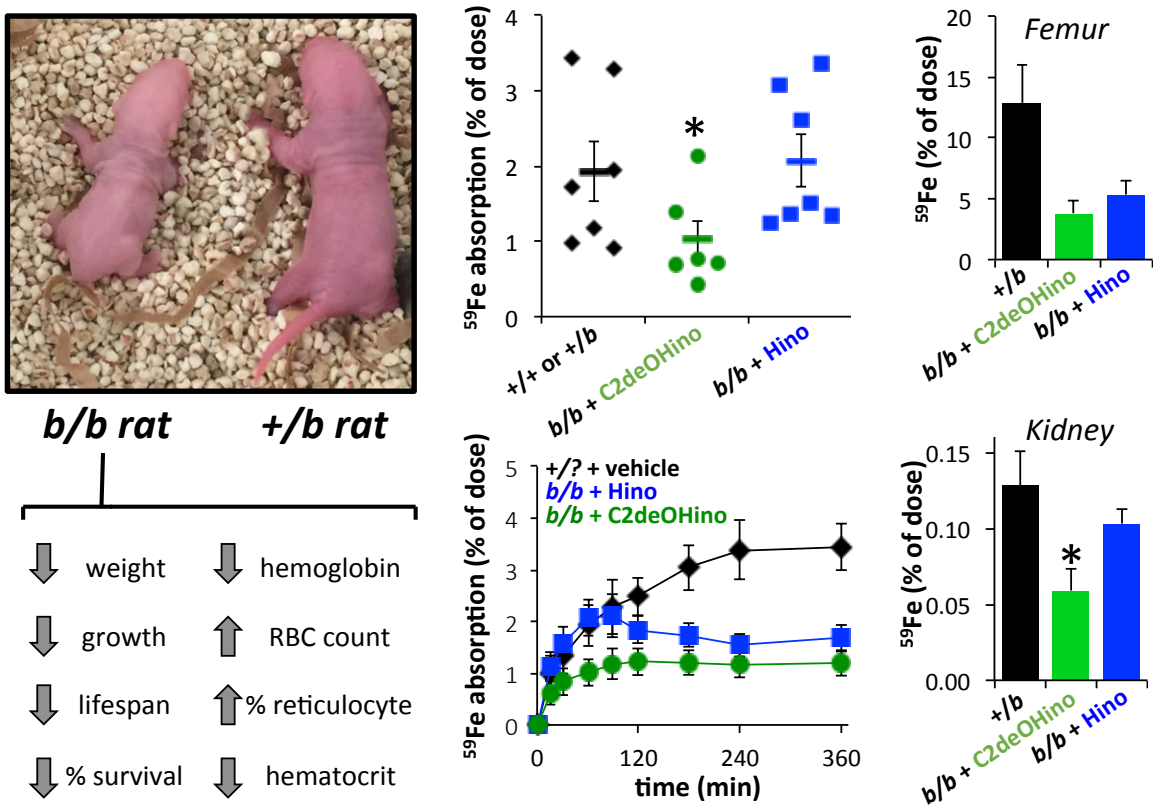

Figure 2.16 Hinokitiol restores iron absorption in the Belgrade rat (**A**) A difference between day old Belgrade rat littermates is already noticeable between the homozygous (*b/b*, left) and heterozygous (*b/+*, right). (**B**) Oral gavage of 1.5 mg/kg hinokitiol promotes the gut absorption of ^{59}Fe into DMT1-deficient Belgrade (b/b) rats. (**C**) Time-dependent gut iron absorption in Belgrade (*b/b*) and healthy (+/+ or +/*b*) rats treated with vehicle, hinokitiol or C2deOHino. (**D** and **E**) ^{59}Fe in (**D**) femur and (**E**) kidney after 4 hours in rats after oral gavage with vehicle, hinokitiol (1.5 mg/kg), or C2deOHino (1.5 mg/kg).

We next looked at the Flatiron mouse, the leading model of genetic FPN1 deficiencey and The Ferroportin Disease or Hemochromotosis Type IV. Flatiron mice have a dominant negative mutation in their FPN1 gene and therefore have reduced hematocrit and liver iron overload, similar to the phenotype seen in the clinic[39]. Similarly to the Belgrade rat we tested hinokitiol's ability to restore gut iron absorption upon administration of a single dose of ^{59}Fe and 1.5 mg of hinokitiol per kilogram of body weight via oral gavage. Consistent with our collaborators previous results[39,40] *ffe/+* mice also absorbed iron at low rates (**Figure 2.17 A**).

Hinokitiol increased ^{59}Fe absorption in *ffe*/+ mice after 1 and 2 hours (**Figure 2.17 A**). Hinokitiol reduced the liver non-heme iron burden in the Flatiron with chronic treatment (**Figure 2.17 B**). With increased iron absorption from the diet (**Figure 2.17 A**), coupled with the increased iron recycling in the liver (**Figure 2.17 B**) after chronic treatment we observed a concomitant restoration of hematocrit back to wild type levels (**Figure 2.17 C**)

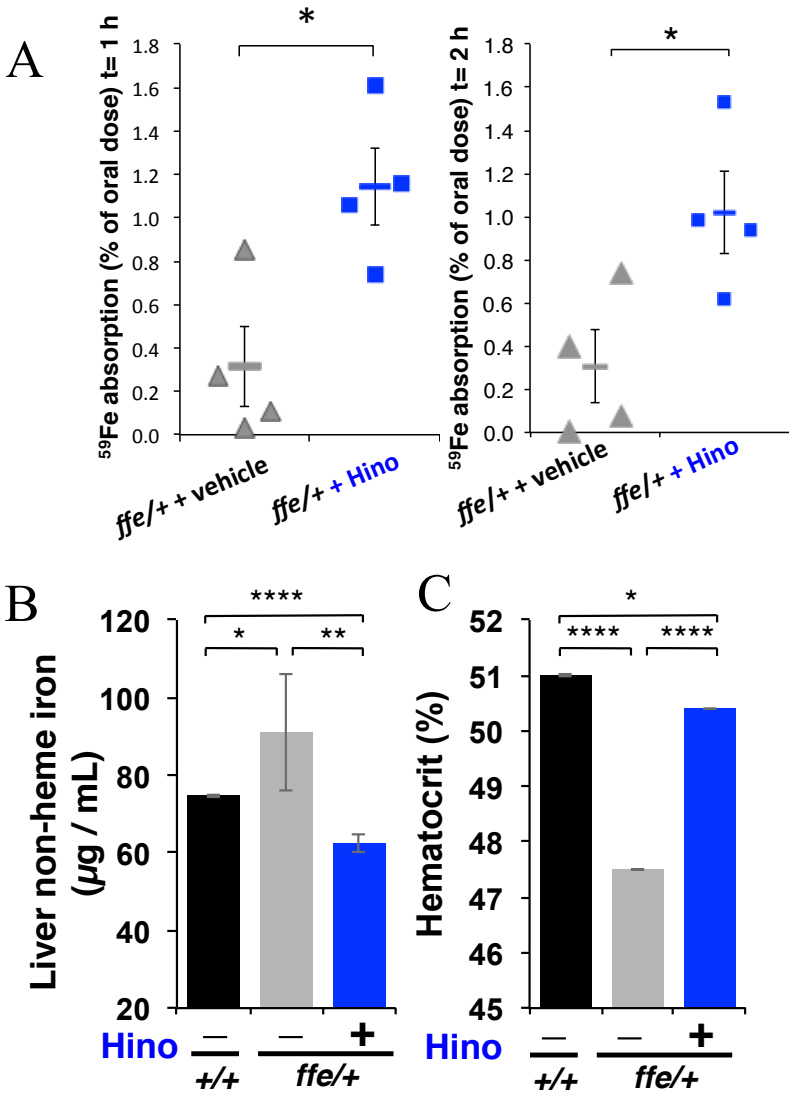

Figure 2.17 Hinoktiol restores iron absorption in FPN1 deficient flatiron mice. (**A**) Oral gavage of 1.5 mg/kg hinokitiol promotes the gut absorption of ^{59}Fe into FPN1-deficient flatiron (*ffe*/+) mice after 1 (**left**) and 2 hours (**right**) (n = 4-7). (**B and C**) Chronic IP injection of Hino (3 mg/kg) daily for 1 week causes a (**B**) release of iron from the liver and an (**C**) increase in hematocrit in flatiron mice (n= 4/group).

In the Belgrade rat we were able to show increased gut iron absorption however, due to the sickly nature of the rats we were unable to perform chronic studies. Instead of doing chronic studies in the rat we next moved onto zebrafish. *Danio rerio* is well established as a powerful model organism in the study of hematopoiesis[41]. We therefore used it to test whether chronic treatment with a small molecule iron transporter could restore hemoglobinization in both Dmt1 and Mfrn1 deficiencies[19,42]. We first performed morpholino-mediated transient knockdown of Dmt1 in a *Tg(globinLCR:eGFP*) zebrafish strain expressing green fluorescent protein (GFP)–tagged erythrocytes (**Figure 2.18 A bottom**)[43]. Injection of a designed antisense morpholino targeting the exon 4–intron 4 junction of premature *dmt1* mRNA reduced steady-state *dmt1* levels (**Figure 2.18 A top**) and decreased the number of GFP positive erythroid cells detected by fluorescence activated cell sorting (FACS) analysis (**Figure 2.18 B**). Addition of hinokitiol to the embryo media 24 hours post fertilization (hpf) and incubation for an additional 2 days promoted hemoglobinization in these DMT1-deficientmorphant zebrafish without observable toxicity, whereas C2deOHino had no effect (**Figure 2.18 B**). Using the same morpholino approach we looked at Mfrn1 and hemoglobinization in Mfrn1-deficient morphant *Tg(globinLCR:eGFP*) zebrafish)[42,43]. Our collaborators have previously shown restoration of hemoglobinization in Mfrn1-deficient zebrafish through ectopic expression of Mfrn1 protein with complementary RNA[42]. Forty-eight hours of hinokitiol treatment restored hemoglobinization and the number of GFP-positive erythrocytes in these morphants (**Figure 2.18 C**). We further tested whether hinokitiol could similarly restore hemoglobinization in genetically mutated chardonnay (cdyte216) zebrafish, which contain a nonsense mutation leading to truncated Dmt1 and thereby exhibit severe hypochromic, microcytic anemia[19]. A heterozygous cross of *+/cdy* fish (**Figure 2.18 D**) led to a Mendelian distribution of ~75% healthy (+/+ and *+/cdy*) and ~25% anemic

(*cdy/cdy*) embryos in each clutch after o-dianisidine staining 72 hpf (**Figure 2.18 E**). Hinokitiol treatment for 2 days increased the number of fish exhibiting high hemoglobin levels, whereas C2deOHino had no effect (**Figure 2.18 E**). Last, following a similar approach, we tested whether hinokitiol could restore hemoglobinization in genetically mutated frascati (frstq223) zebrafish, which contain a missense mutation leading to an inactive Mfrn1 mitochondrial protein and profound anemia during embryogenesis[42,44]. Hinokitiol treatment of embryos collected from a heterozygous cross of *+/frs* fish prevented the anemic phenotype (**Figure 2.18 F**). Genotyped (**Figure 2.18 G**) healthy larvae (+/+ and *+/frs*) exhibited brown staining with o-dianisidine, whereas untreated frs/frs fish did not (**Figure 2.18 G**). Hinokitiol treatment restored brown staining to *frs/frs* fish (**Figure 2.18 G**). As expected, hinokitiol did not affect sauternes (sautb223) zebrafish[45] deficient in the initial enzyme involved in porphyrin biosynthesis (Alas2) indicating the specificity of hinokitiol effects to defects in iron transport.

Collectively these studies represent the first time we have seen a small molecule mimic a protein in a whole animal and restore downstream physiology. We have shown that hinokitiol can move iron into, within and out of cells. The next, logical step was to discover how an imperfect small molecule was able to accomplish this. The next two chapters focus on the mechanistic underpinnings that allow hinokitiol to harness the gradients created by the missing iron transporters it is replacing, as well as how it interfaces with the endogenous regulatory system, allowing for hinokitiol mediated iron transport to be a regulated phenomena.

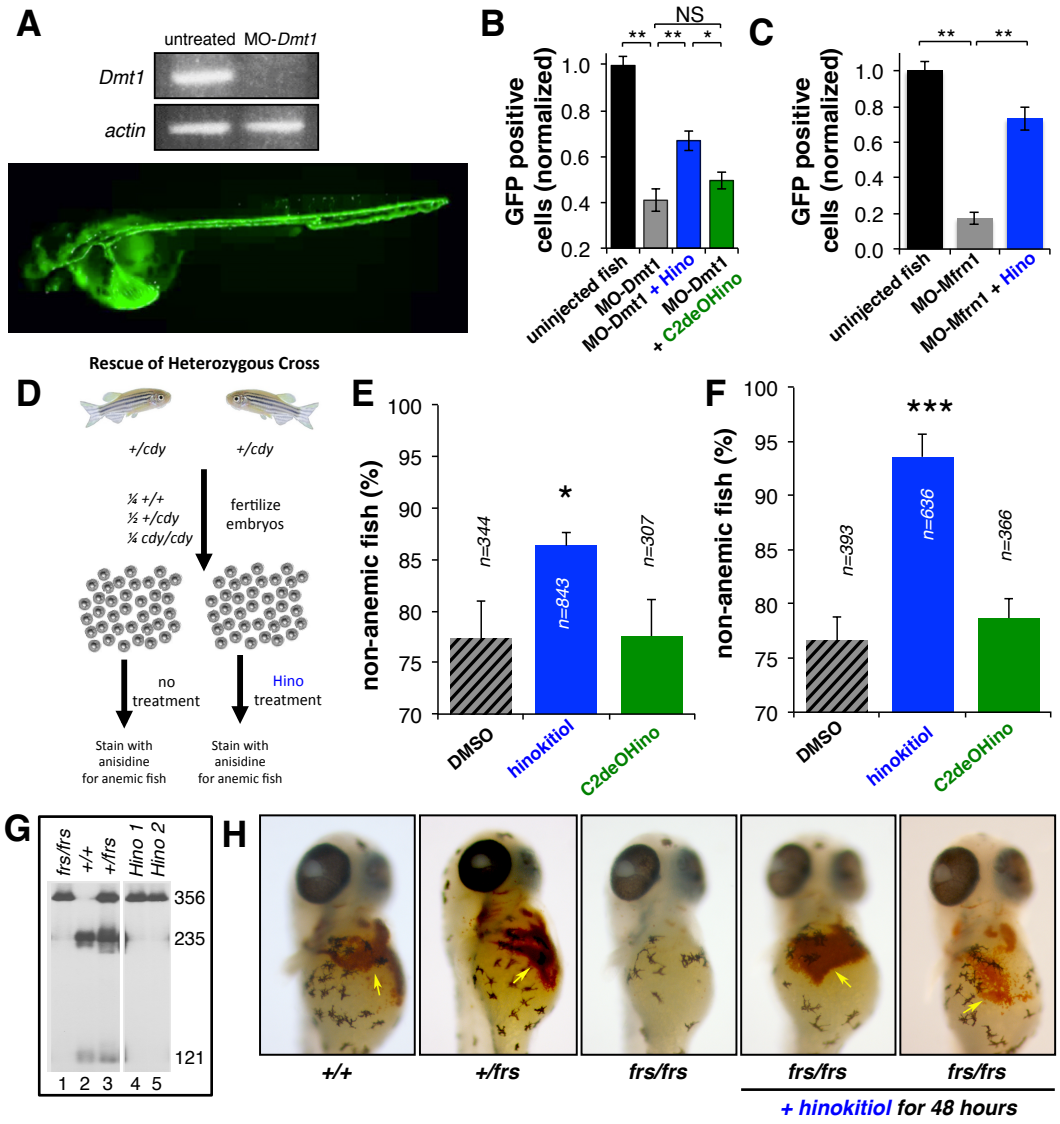

Figure 2.18 Hinokitiol Restores Hemoglobinization in Zebrafish. (**A**) Top: Morpholino-mediated knockdown of steady-state Dmt1 mRNA in Tg(globinLCR:eGFP) fish as determined by semi-quantitative RTPCR with β-actin as a loading control. Bottom: Image of a zebrafish with GFP-tagged erythrocytes (J. J. Ganis *et al.*, Dev. Biol 366. 185-194. 2012). (**B and C**) Hinokitiol treatment (1 μM) added to the embryo media (containing 10 μM iron citrate) at 24 hpf and incubation for an additional 48 hours increases the number of GFP-positive erythroids (detected by FACS analysis) in (**B**) Dmt1-deficient and (**C**) Mfrn1-deficient morphant zebrafish from a line of transgenic fish containing GFP tagged erythroids (n = 7 to 17). (**D**) Heterozygous cross of *cdy*/+ zebrafish yields 75% non-anemic fish 25% anemic fish due to mendelian genetics. (**E and F**) Hinokitiol decreases the number of anemic fish from a heterozygous cross of (**E**) +/cdy fish, and (**F**) *+/frs* fish as determined by o-dianisidine staining, whereas C2deOHino does not. (**G**) Embryos from a heterozygous cross of *+/frs* fish were genotyped by restriction enzyme digestion with BsrI restriction enzyme. Lanes 4 and 5 correspond to *frs/frs* fish treated with hinokitiol for 48 hours. (**H**) Hinokitiol-treated *frs/frs* fish stain brown with o-dianisidine, whereas anemic *frs/frs* fish do not, indicating increased hemoglobin levels after hinokitiol treatment.

2.8 METHODS

Materials

Wild type (DEY1457) and isogenic fet3Δftr1Δ *S. cerevisiae* were obtained from D. Kosman[46]. Wild type (YPH499) and isogenic fet3Δarn1-4Δ *S. cerevisiae* were obtained from C. Philpott[47]. Yeast were maintained on standard YPD media containing 10 g/L yeast extract, 20 g/L peptone, and 20 g/L dextrose without (liquid media) or with (solid media) 20 g/L agar. Unless otherwise indicated, growth-restoration assays in yeast used a low iron SD media consisting of 1.91 g/L iron-free YNB-$FeCl_3$ (ForMedium CYN 1201), 0.79 g/L Complete Supplement Mixture (Sunrise Science Products 1001-010), 5 g/L ammonium sulfate (Sigma A4418), 20 g/L dextrose, 10 μM $FeCl_3$ (Sigma 451649), and 10 μM hinokitiol (β-Thujaplicin, Sigma 469521) in 50 mM MES/Tris buffer at pH=7.0 without (liquid media) or with (solid media) 20 g/L agar. Dextrose, hinokitiol, and $FeCl_3$ were added after autoclave sterilization from a filter-sterilized 40% w/v dextrose solution in water, from a freshly prepared sterile 10 mM hinokitiol stock in DMSO, and from a freshly prepared 10 mM $FeCl_3$ stock in sterile water, respectively. Non-fermentable growth restoration used the same synthetic medium except for the use of 30 g/L glycerol instead of dextrose.

Human Caco-2 cells (HTB-37) and mouse macrophages (J774A.1) were obtained from ATCC and cultured with DMEM (Gibco 10313-021) containing 10% HI FBS (Gibco 16000-036), 4 mM glutamine (Lonza BE17-605E), 100 μg/mL PEN-STREP (Lonza DE17-602E), and 1% MEM NEAA (Fisher 11140-050). Transfected Caco-2 cell lines were maintained on this media containing 800 mg/L G418 (Santa Cruz sc-29065B). Friend mouse erythroleukemia cells (MEL, DS19 subclone) were obtained from Arthur Skoultchi (Albert Einstein College of Medicine, Bronx, NY) and cultured with DMEM containing 10% HI FBS, 2 mM glutamine, 100

μg/mL PEN-STREP, and 1% MEM NEAA. Transfected shControl and shDMT1 MEL cell lines were maintained on this media containing 1 g/L G418.

Caco-2 cells (passage 18-50) were grown in T75 flasks to ≥90% confluency before trypsinization with 0.25% trypsin-EDTA (Fisher 25200-056) and passaging at 10:1 dilution in Caco-2 media without (wild type) or with G418 (transfected). Monolayers were grown by seeding Caco-2 cells (passage 20-50) onto 0.4 μm PET cell culture inserts (Fisher 08-771) in 6-well companion plates (Fisher 08-771-24) at $2x10^5$ cells/well and allowed to fully differentiate for 21-28 days before experiments were performed with changing of media every 3-4 days.

MEL cells were grown in suspension in T25 flasks until ~$1x10^6$ cells/mL and re-seeding into a new T25 flask at $1x10^5$ cells/mL in MEL Complete media with or without G418. Every month of culturing, new backstocks of MEL cells were used.

J774 cells (passage 20-80) were grown in T25 flasks to ≥90% confluency before scraping and re-seeding at 5:1 dilution in J774 Complete media. Media was changed every 1-2 days.

Animals and animal care

The studies performed were in strict accordance with the guidance and recommendations outlined in the Guide for the Care and Use of Laboratory Animals of the National Institutes of Health.

The protocols used for studies in healthy (+/+) and *Flatiron* (*ffe*/+) mice were approved by the Harvard Medical Animal Care and Use Committee. Breeding, diets, and genotyping of *flatiron* mice were performed as previously described[39].

All zebrafish experiments were performed in accordance with the Institutional Animal Care and Use Committee regulations. The following wild type AB strains and zebrafish mutant strains were used: *frascati* (*frs*^{tq223})[42], *chardonnay* (*cdy*^{te216})[19], and *sauternes* (*sau*^{tb223})[45].

The protocols for studies in Belgrade (+/+, *+/b*, or *b/b*) rats were approved by the Division of Laboratory Animal Medicine (DLAM) and the Northeastern University-Institutional Animal Care and Use Committee (NU-IACUC). Breeders of heterozygous (*+/b*) and homozygous (*b/b*) Belgrade rats (Fischer F344 background) were kindly provided by Dr. Michael Garrick (SUNY Buffalo) and maintained on a 12:12-hr light/dark cycle and given water and facility chow *ad libitum*. Prior to ^{59}Fe gut iron absorption experiments, a variety of preliminary studies were performed on cohorts of Belgrade rats (ranging from 3-5 months old) during which the rats were treated with vehicle or various compounds for ≤ 15 weeks in iron-supplemented diet containing 500 mg/kg iron (TD.02385, Harlan Teklad, Madison, WI). All rats were allowed to be drug-free and continued to receive iron-supplemented diet for at least one week before ^{59}Fe gut absorption experiments were performed.

Statistics

All data depicts the means or weighted mean ± SEM with a minimum of 3 biological replicates unless otherwise noted. Statistical analysis represents P values obtained from student t-test or one- or two-way analysis of variance (ANOVA) with post-hoc TUKEY test where appropriate. NS, not significant; * $P < 0.05$; ** $P \leq 0.01$; *** $P \leq 0.001$; **** $P \leq 0.0001$ unless otherwise noted.

Growth rescue of iron-deficient yeast with small molecules on agar plates

Growth rescue in yeast was performed similar to previously reported[48] on low iron SD-agar plates in 50 mM MES/Tris buffer at pH=7.0 containing 2% agar, 10 μM $FeCl_3$, and 10 μM hinokitiol (from 40X stock in DMSO). Wild type and fet3Δftr1Δ or fet3Δarn1-4Δ controls treated with vehicle (DMSO) were performed under identical conditions using the same low iron SD media containing 10 μM $FeCl_3$ in the absence of hinokitiol. Yeast were grown overnight in YPD media and diluted to an optical density at 600 nM (OD_{600}) of 1.0 in low iron SD media before 10-fold serial dilution and inoculation of these yeast suspensions (10 μL per dot) onto the low iron SD-agar plates described above containing either DMSO vehicle or hinokitiol (10 μM from 40X DMSO stock).

For disc diffusion assays, yeast were grown overnight in YPD media and diluted to an OD_{600} = 0.1 in low iron SD media and streaked onto low iron SD-agar plates containing 10 μM $FeCl_3$. Disc diffusion assays were performed using ≥10 mM stock solutions (in DMSO) of hinokitiol, tropolone (Sigma T89702), α-dolabrin (Specs Compound Handling AN-584/43416897), maltol (Sigma H43407), deferiprone (DFP, Sigma 379409), pyridoxal isonicotinoyl hydrazone (PIH, Santa Cruz sc-204192), salicylaldehyde isonicotinoyl hydrazone (SIH, see synthesis and characterization below), comenic acid (COMA, kindly donated by Obiter Research, LLC), amphotericin B (AK Scientific L970), nonactin (Sigma N2286), calcimycin (Sigma C7522), or prodigiosin (Santa Cruz sc-202298) (10 μL per paper disc) on low iron SD-agar plates containing 10 μM $FeCl_3$ streaked with the appropriate yeast strain (from OD_{600} = 0.1 in low iron SD media). Growth restoration under non-fermentable conditions was performed using 3% glycerol instead of 2% dextrose. Images were taken 48-72 hours after inoculation and incubation at 30 °C unless otherwise noted.

Growth rescue of fet3Δftr1Δ yeast with small molecules in liquid media

Growth rescue in yeast was performed similar to previously reported[48] using 10 μM hinokitiol in low iron SD liquid media containing 10 μM $FeCl_3$ in a 96-well plate unless otherwise noted. Wild type and fet3Δftr1Δ controls treated with vehicle (DMSO) were performed under identical conditions using the same low iron SD media containing 10 μM $FeCl_3$ in the absence of hinokitiol. Yeast were grown overnight in YPD media and diluted at an OD_{600} of 0.1 in SD media, diluted 10-fold, and incubated at 30 °C with continuous shaking (200 rpm). The OD_{600} was obtained 24-48 hours after inoculation unless otherwise noted.

Small molecule dose-response with hinokitiol and C2-deoxy hinokitiol (C2deOHino, see synthesis below) was determined by addition of the small molecule (40X stock solution in DMSO) to give the indicated final concentrations.

Iron dose-response studies were performed in the same low iron SD media without $FeCl_3$ containing 10 μM hinokitiol (from a 40X stock solution in DMSO). $FeCl_3$ (40X stock solution in water) was added to the give the indicated final concentrations up to 10 μM $FeCl_3$.

For dose-dependent hinokitiol-promoted rescue at increasing dosages of $FeCl_3$, SD media was made containing either 10, 25, 50, or 100 μM $FeCl_3$ from a 10 mM $FeCl_3$ stock before adding hinokitiol (40X stock solution in DMSO) to give the indicated final concentrations.

Sustainability assay

Sustainable hinokitiol-promoted growth restoration of fet3Δftr1Δ yeast was performed similar to previously reported[48] by inoculation of hinokitiol-rescued yeast from low iron SD-agar plates containing 10 μM hinokitiol and 10 μM $FeCl_3$ into low iron SD liquid media containing 10 μM hinokitiol and 10 μM $FeCl_3$, then streaking of the yeast suspension (diluted to OD_{600} of

0.1) onto agar plates. This process was repeated for >100 days. Continued reliance of fet3Δftr1Δ yeast growth on hinokitiol was observed, as removal of hinokitiol from the SD-agar plates led to no fet3Δftr1Δ yeast cell growth.

Doubling time of fet3Δftr1Δ yeast treated with hinokitiol

Doubling times of wild type and hinokitiol-rescued fet3Δftr1Δ yeast were determined similar to previously reported[48] by tracking the OD_{600} every hour over 48 hours in the same low iron SD media containing 10 μM $FeCl_3$ and DMSO or 10 μM hinokitiol (from 40X stock in DMSO) and applying the equation $T_d = (t_2-t_1) \times [\log(2)/\log(q_2/q_1)]$ during exponential phase.

$^{55}Fe^{3+}$ uptake assay in yeast

Iron (III) uptake into wild type and fet3Δftr1Δ yeast was adapted from Kosman and coworkers[46]. Overnight yeast cultures were repeatedly centrifuged and rinsed with water. The cell pellet was resuspended in MilliQ water, and diluted in SD media without $FeCl_3$. The cells were incubated at 30 °C for 3 hours, centrifuged and rinsed with water twice. The cells were then suspended to $3x10^7$ cells/mL in SD media containing 50 mM sodium citrate and 2% glucose. Hinokitiol or C2deOHino (from 40X stocks in DMSO) was added to a final concentration of 100 μM before $^{55}FeCl_3$ (1.1 μCi) was added to the yeast suspensions. The suspension was continuously homogenized before aliquots were taken and diluted with 10 mL of room temperature water. Cells were then collected via vacuum filtration through a 0.45 μm nitrocellulose filter (Millipore HAWP), and rinsed with room temperature water (x5 of 100mL). The filters were then transferred to a scintillation vial containing 3 mL of scintillation cocktail for measuring radioactivity using a liquid scintillation counter. Hinokitiol showed a dose-

dependent increase in ^{55}Fe uptake from 5 to 100 μM while C2deOHino showed no uptake up to 100 μM.

Lipophilicity determination for small molecule iron chelates

Octanol-water partition coefficients were obtained as previously reported[49,50] with 100 μM small molecule and 33 μM $FeCl_3$, (50 μM $FeCl_3$ for PIH as it forms a 2:1 complex) using equal volumes of equilibrated pH=5 water and octanol. Concentrations of small molecule in water were determined via UV-Vis spectroscopy compared to known initial standards.

Hexane-water partition was obtained similar to above with 500 μM small molecule and 50 μM $FeCl_3$ using equal volumes of 50 mM Mes-Tris buffer at pH=7.0 and hexanes.

Titration of hinokitiol with iron (III)

An iron (III) titration study was performed by addition of 50 μM hinokitiol and increasing equivalents of $FeCl_3$ (0, 1, 5, 10, 12.5, 15, 16.67, 17.5, 20, 25, 30, 35, 37.5, 40, and 50 μM) in 10 mM MES/Tris buffer at pH=7.0. No precipitate was observed in all cases, and the solution changed to a brown colored solution with increasing equivalents of iron (III). As the amount of iron was increased, the λ_{max} shifted from ~240 to 250 nm and the absorbance at 420 nm increased up to ~3:1 Hino:Fe.

Crystal structure of $Fe(Hino)_3$

An x-ray quality crystal of synthesized $Fe(Hino)_3$ was obtained from a recrystallization of $Fe(Hino)_3$ (10 mg) in acetone (2 mL) and benzene (0.2 mL) in an uncapped 1 mL vial by

allowing the solvent to slowly evaporate undisturbed overnight. X-Ray single crystal analysis was performed by the University of Illinois X-Ray facility.

Determination of iron efflux from liposomes using ferrozine

Iron (III) efflux from POPC liposomes was determined similar to previously reported[51]. POPC liposomes were prepared as similarly reported[52] using 30 mM $FeCl_3$, 62.5 mM citrate at pH=7.0 in 25 mM Mes/Tris buffer. External iron was removed by size exclusion chromatography using Sephadex G-50 and eluting with external buffer. External buffer consisted of 62.5 mM ascorbate at pH=7.0 in 25 mM Mes/Tris buffer. The liposomes were diluted to 1 mM phosphorus in this buffer. Ferrozine (Sigma 160601) was added (100X stock in external buffer) to a final concentration of 500 μM. Liposomal suspension was then transferred to a 96-well plate, and either DMSO or 5 μM hinokitiol, C2deOHino, deferiprone, or PIH (40X stock solution in DMSO) were added to initiate the experiment. The OD_{562} was determined every minute over the course of 2 hours using a plate-reader with continuous shaking at 30 °C to detect the relative amounts of external ferrozine-iron chelate at the indicated times. After 2 hours, liposomes were lysed with Triton-X to give 100% iron efflux. Hinokitiol dose- and temperature-dependently promoted iron (III) efflux from POPC liposomes while C2deOHino showed no efflux up to 100 μM.

Iron (II) efflux was performed as described above, however, the internal buffer alternatively consisted of 30 mM $FeSO_4$, 62.5 mM ascorbate at pH=7.0 in 25 mM Mes/Tris buffer and Triton-X lysis was performed after 1 hour.

The rates of iron efflux with increasing concentrations of intraliposomal iron and/or hinokitiol were determined as described above using the indicated concentration of iron and

hinokitiol. For the varying concentrations of iron, hinokitiol (10 μM) was added to the POPC liposomes, and the change in absorbance at 562 nm was determined over 2 hours. For the varying concentrations of hinokitiol, 30 mM intraliposomal iron was used as described above. The concentration of iron outside of liposomes was determined using the extinction coefficient for ferrozine-iron (27,900 $M^{-1}cm^{-1}$)[53]. This was used to determine the amount of iron released from liposomes at the indicated times using the total volume for each experiment. Rates of iron efflux were determined after one hour of hinokitiol treatment.

Determination of metal efflux from liposomes using PhenGreen

Hinokitiol-promoted release of different divalent metals from POPC liposomes was performed by tracking the quenching of PhenGreen (Fisher P14312) similar to previously reported[54,55]. Liposomes were prepared as described above with an internal buffer consisting of either 10 mM ascorbate in a 5 mM MES/Tris buffer at pH=7.0 (for Fe^{2+}), 10 mM citrate in a 5 mM MES/Tris buffer at pH=7.0 (for Cu^{2+}), or a 5 mM MES/Tris buffer at pH=7.0 (for Mn^{2+}, Co^{2+}, Ni^{2+}, and Zn^{2+}). In all cases, liposomes were prepared using 5 mM of either $FeCl_2$, $MnCl_2$, $CoCl_2$, $NiCl_2$, $ZnCl_2$, or $CuCl_2$ added to the internal buffer. The external buffer was a 5 mM MES/Tris buffer at pH=7.0 containing 10 μM PhenGreen (from 1000X stock in DMSO). The liposome suspension was diluted to 1 mM of phosphorus. The liposome suspension was transferred to a 96-well plate, and either DMSO or 2 μM hinokitiol (from a 40X stock in DMSO) was added at t = 2min. The fluorescence was monitored with excitation at 500 nm and emission at 530 nm over 1 hour. After one hour, the liposomes were lysed with Triton-X and the fluorescence was recorded. In all cases, quenching of fluorescence was observed in the DMSO-treated liposomes after lysis, which reached similar levels to that for hinokitiol-treated liposomes

before lysis (except for Mn^{2+} where no efflux was observed in Hino-treated liposomes; fluorescence quenching was observed after lysis for Mn^{2+}). The DMSO-treated and hinokitiol-treated liposomes had similar fluorescence quenching levels after lysis. The total amount of metal efflux was determined using standard curves of fluorescence quenching in external buffer with 10 μM PhenGreen and known concentrations of each metal. The $t_{1/2}$ values were calculated using an asymptotic fit in OriginPro. The $t_{1/2}$ values indicate the time required to reach half of the maximum metal efflux for each metal.

Transfection of Caco-2 cells and MEL cells against DMT1

Caco-2 cells were transfected as previously reported[18] using lipofectamine LTX (Invitrogen 15338-100) and Plus reagent (Invitrogen 11514-015) with 10 μg/well of either non-targeting control shRNA or four other shRNA constructs targeting human DMT1 (Qiagen KH05760N) 24 hours after seeding $2x10^5$ cells/well in 6-well plates (~30% confluent). The transfection agents were removed, and the cells were allowed to recover for 24 hours before treatment with Caco-2 Complete media containing 0.8 g/L G418. Cells were incubated in G418 media for ~2 weeks to promote selection of transfected cells while complete cell death was observed with non-transfected cells. Non-targeting control construct = 5'-GGAATCTCATTCGATGCATAC-3'; shDMT1 construct (Clone 4) = 5'-AACCTATTCTGGCCAGTTTGT-3'.

MEL cells were transfected by electroporation (0.28 kV, 975 μF pulse) in 0.4 cm cuvette (Biorad 1652081) containing 400 μL of serum-free DMEM with 30 mM NaCl at $2x10^7$ cells/mL with 50 μg of either non-targeting control shRNA (Sigma, 5'-CAACAAGATGAAGAGCACCAA-3' using a CMV-neo vector) or five shRNA constructs

targeting mouse DMT1 (Sigma, Clone 1-5: TRCN0000332748, TRCN0000306610, TRCN0000079533, TRCN0000079535, and TRCN0000079536). After transfection, cells were transferred to T25 flasks containing 10 mL of MEL Complete media, and allowed to grow for 6 days with re-seeding every 2 days at 10:1 dilution in fresh MEL Complete media. After this, cells were re-seeded at $1x10^5$ cells/mL in MEL Complete media containing 1 g/L G418, and cells were selected over the course of 2 weeks by re-seeding at 10:1 dilution into fresh G418 media every ~2 days until no cells were observed in T25 flasks originally containing non-electroporated wild type (DS19) MEL cells.

Mfrn1-deficient MEL cell lines were developed using CRISPR/Cas9 genome editing as previously described[56–58]. Exons 2 and 4 of the Mfrn1 locus were targeted. The exon 2 targeting sequence was: 5'-GATGCTTGTATACCGGGCTT-3'; the exon 4 targeting sequence was: 5'-GAAGAACTCATAAACGGACC-3'. The primers used for documenting intragenic deletion of the Mfrn1 mouse locus were the following: Exon 4 (Fwd) 5'-GTTTGCCTCTGCGGTGTGATC-3'; Exon 2 (Fwd) 5'-GGAGGACGCTGTGGGGGGGGG-3'; Exon 2 (Rev) 5'-GTCCATCTTTTCTACAAGCC-3'.

qRT-PCR conditions

Dmt1 mRNA levels were determined via qRT-PCR using SYBR Green (Agilent 600825) following manufacturer protocols after undergoing treatment as described below. For determination of *Dmt1* mRNA levels in differentiated Caco-2 monolayers (21-28 days post seeding), mRNA was isolated using RNeasy Mini Kit (Qiagen 74104) according to manufacturer instructions. The threshold cycle (C_t) values of *Dmt1* were normalized to internal control *actin*

using primers against *Dmt1* (Origene HP200584) and *actin* (Origene HP204660) using the Pfaffl Method and were then normalized to shControl levels.

For determination of relative *Dmt1* mRNA levels in MEL clones, mRNA was isolated from MEL clones differentiated with 2% DMSO and 10 μM iron (III) citrate for 3 days using RNeasy Mini Kit (Qiagen 74104) according to manufacturer instructions. The C_t values of *Dmt1* were normalized to internal control *Hprt1* using primers against *Dmt1* (Origene MP215650) and *Hprt1* (Origene MP206455) using the Pfaffl Method and were then normalized to shControl levels.

Relative *Mfrn1* mRNA levels were determined via qRT-PCR using TaqMan probes (Applied Biosystems) as previously described[59].

Western blotting conditions

Caco-2 monolayers, differentiated MEL cells, or J774 cells underwent treatment as described in rescue experiments before lysis with RIPA buffer (Thermo 89901) containing protease inhibitors (Thermo 88266). Protein concentrations were determined by a BCA kit (Thermo 23225) and diluted to 2 mg/mL in the same RIPA buffer. Relative protein levels were then determined through western blotting of 10 or 20 μg of protein lysate blocking for 2 hours at room temperature with 5% BSA and using primary antibodies consisting of either human anti-DMT1 (1:3,000 dilution, Santa Cruz sc-30120), mouse anti-DMT1 (1:1,000 dilution, Santa Cruz sc-166884), in 5% BSA overnight at 5 °C before rinsing thoroughly with TBST and incubation (if non-HRP conjugated) with secondary antibody consisting of either goat anti-rabbit IgG HRP conjugate (1:5,000 dilution – DMT1, Cell Signaling 7074, in 5% milk), goat anti-mouse IgG_1 HRP conjugate (1:1,000 dilution – PCBP1, 1:5,000 dilution – IRP2, 1:3,000 dilution – DMT1,

Santa Cruz sc-2060, in 5% BSA), donkey anti-goat IgG HRP conjugate (1:1,000 dilution – IRP1, Santa Cruz sc-2020, in 5% BSA), or goat anti-mouse IgG_{2a} HRP conjugate (1:10,000 dilution – FTL1, Santa Cruz sc-2061, in 5% BSA) at room temperature for two hours. Blots were thoroughly rinsed with TBST and imaged after addition of Femto Chemluminescence solution according to manufacturer instructions (Thermo Fisher 34095).

^{55}Fe uptake and transport in differentiated Caco-2 monolayers

Media from differentiated Caco-2 monolayers (P25-50, 21-28 days post seeding) grown on PET inserts in 6-well plates was aspirated, and monolayers were rinsed with PBS. 2 mL of basolateral fluid (serum-free DMEM at pH = 7.4 in 10 mM HEPES buffer) was added to the basolateral side, and 1 mL of apical fluid (serum-free DMEM at pH = 5.5 in 10 mM MES buffer) containing 200 nM $^{55}FeCl_3$ or the indicated concentration of $FeCl_3$ and either DMSO vehicle, hinokitiol, C2deOHino, deferiprone, PIH, SIH, or deferoxamine mesylate (Sigma D9533) (500 nM Hino/C2deOHino for DMT1-deficiency, 1 μM Hino/C2deOHino for FPN1-deficiency, or indicated concentration of small molecule from a 1000X stock in DMSO) was added to the apical side via addition on the wall of the membrane insert without disrupting the cell monolayer. The monolayers were then incubated for four hours at 37 °C unless otherwise noted. A 100 μL aliquot of the basolateral fluid was removed, diluted in scintillation cocktail, and radioactivity was determined on a liquid scintillation counter to quantify relative amounts of ^{55}Fe transport. To determine intracellular ^{55}Fe, the basolateral and apical media was removed, and the monolayer was rinsed with PBS (x2). The cells were then lysed with 500 μL of 200 mM NaOH with nutator mixing overnight, and radioactivity was determined on a liquid scintillation counter after diluting the cell lysate in scintillation cocktail. All values were normalized to shControl monolayers unless otherwise noted. Absolute iron levels were determined through calibration of ^{55}Fe

radioactivity levels with known standards and average mg of protein per membrane was determined by protein lysis with RIPA buffer containing protease inhibitors and quantified through a BCA kit according to manufacturer instructions.

Determination of ^{55}Fe transport as a function of pH used the protocol described above except for the use of apical fluid containing either 10 mM PIPES (pH=6.5) or 10 mM HEPES (pH=7.4) in DMEM.

Determination of ^{55}Fe transport after FPN1 knockdown was determined as described above using 200 nM $^{55}FeCl_3$ after incubation of quercetin to knockdown FPN1[29] as described below.

TEER determination in Caco-2 monolayers

To determine Caco-2 membrane integrity, transport studies were performed as described above, except for the use of non-radioactive iron instead of $^{55}FeCl_3$. At the indicated time points, the transepithelial electrical resistance (TEER) was determined with an epithelial voltohmmeter and compared to the TEER of the membrane at the beginning of the experiment.

WST-8 toxicity in cell lines

Determination of small molecule-mediated toxicity in Caco-2, MEL, and/or J774 cells was performed according to manufacturer instructions using a WST-8 kit (Cayman Chemical 10010199) similar to previously reported[60] using a 1000X stock of the indicated small molecule in DMSO to give the indicated final concentration.

Differentiation of MEL cells with DMSO

To perform differentiation experiments with MEL cells[24]f, the indicated MEL cells were diluted to $1x10^5$ cells/mL in MEL Complete media containing 10 μM iron (III) citrate and 2% DMSO in the absence or presence of 1 μM hinokitiol or C2deOHino (added from 1000X stock in DMSO) in 12-well plates. Cells were then incubated at 37 °C for 72 hours unless otherwise noted. Control experiments were performed under identical conditions in the absence of DMSO, and it was found that no differentiation was observed by *o*-dianisidine staining as described below.

Staining of induced MEL cells with dianisidine

Hemoglobinized MEL cells were quantified three days after DMSO induction through *o*-dianisidine staining similar to previously reported[58]. Cells were centrifuged three days after induction and rinsed with PBS. The cells were then suspended in a solution containing 7.5 mM *o*-dianisidine, 900 mM H_2O_2, and 150 mM acetic acid in water at ~$1x10^6$ cells/mL. Cells were then imaged on an AXIO Zoom V16 microscope to obtain color images. The number of stained cells were then quantified via ImageJ analysis and compared to the number of total cells in each image. To determine that hinokitiol requires DMSO induction for hemoglobinization, 2% DMSO was not added at the beginning of the experiment before a 72-hour incubation and *o*-dianisidine staining.

^{55}Fe heme incorporation in MEL cells

MEL cells were induced for differentiation as described above and incubated at 37°C for 64 hours before addition of a saturated $^{55}Fe_2Tf$ solution (250 nM final concentration from a 10 μM $^{55}Fe_2Tf$ stock). The cells were incubated for an additional eight hours. After completion, the

cells were counted with a hemocytometer, the media was removed after centrifugation, and the cells were rinsed with PBS (x3). The cells were then lysed with RIPA buffer, diluted with water, and heme was extracted using a 3:1 ethyl acetate:acetic acid solution. An aliquot of the organic extract was diluted in scintillation cocktail and radioactivity was determined. Radioactive levels were normalized per cell (counted by hemocytometer) relative to wild type (DS19) levels.

Knockdown of FPN1 in Caco-2 cells and J774 cells

To knockdown FPN1 levels in wild type Caco-2 cells, the differentiated epithelial monolayers were incubated with 150 μM quercetin (Sigma 337951) for 18 hours in Caco-2 Complete media containing G418 similar to previously described[29]. To knockdown FPN1 levels in shControl and shDMT1 Caco-2 monolayers, incubation was performed as above except with 250 μM quercetin. After completion of the incubation, the apical and basolateral fluid was aspirated and rinsed with PBS before ^{55}Fe transport and uptake were determined as described above.

To knockdown FPN1 levels in wild type J774 cells, the cells were incubated with 2 μg/mL mouse hepcidin (Peptides International PLP-3773-PI) for 1 hour in J774 Complete media similar to previously described[35] before ^{55}Fe was loaded into J774 cells and ^{55}Fe release was determined.

^{55}Fe release from J774 macrophages

J774 cells were grown in 12-well plates to ~80% confluency. The cells were then treated with vehicle or hepcidin in fresh J774 Complete media (1 mL) and incubated at 37 °C for 1 hour. After incubation, the media was aspirated, and then a $^{55}Fe_2$Tf (50 nM) solution in J774 Complete

media (1 mL) containing vehicle or hepcidin was added. The cells were incubated at 37 °C for 10 minutes, and the media was removed. The cells were rinsed with PBS (x2), and then rinsed with J774 Complete media (1 mL) for 10 minutes at 37 °C. The media was aspirated, and J774 Complete media (1 mL) containing DMSO or small molecule (5 μM unless otherwise noted, 1000X dilution) was then added in the presence or absence of hepcidin. At the indicated times, aliquots (≤ 100 μL) of the media were removed, diluted in scintillation cocktail, and radioactivity was determined by liquid scintillation counting. After completion of the experiment, the media was removed, the cells were rinsed with PBS, and the cells were lysed with 500 μL of 200 mM NaOH at 37 °C for 2 hours with continuous shaking (50 rpm). The cell lysate was diluted in scintillation cocktail and intracellular ^{55}Fe levels were determined by liquid scintillation counting. The % ^{55}Fe release was determined by the ratio of extracellular ^{55}Fe to total (intracellular + extracellular) ^{55}Fe at the indicated times.

^{55}Fe uptake into J774 macrophages

J774 cells were grown in 12-well plates to ~80% confluency. The cells were then treated with vehicle or hepcidin in serum-free DMEM media at pH=7.4 in 10 mM HEPES buffer (1 mL) containing 50 μM $FeCl_3$ (100:1 ^{56}Fe:^{55}Fe). After four hours of incubation at 37 °C, the cells were rinsed with PBS (x2), and lysed with 500 μL RIPA buffer containing protease inhibitors. The cell lysate was diluted in scintillation cocktail and intracellular ^{55}Fe was determined by liquid scintillation counting and normalized to the total protein in each well.

Hinokitiol-promoted iron uptake as a function of extracellular iron was performed similar to described above in wild type J774 macrophages using 1 μM hinokitiol (from 1000X stock in DMSO) and the indicated final concentration of $FeCl_3$ (20:1 ^{56}Fe:^{55}Fe). At the indicated time,

cells were rinsed with PBS (x2), and lysed with 200 mM NaOH. The cell lysate was diluted in scintillation cocktail and intracellular ^{55}Fe was determined by liquid scintillation counting and normalized to the total protein in each well.

^{59}Fe gut absorption

To characterize the effects of hinokitiol on the gastrointestinal absorption of iron in healthy (+/+) and *ffe*/+ mice, food was withheld for 4 hours (8am to 12pm) prior to intragastric gavage. The mice were anesthetized with up to 2% isoflurane, and $^{59}FeCl_3$ was administered using a 20-gauge, 1.5-inch gavage needle. $^{59}FeCl_3$ (200 μCi/kg body weight) was diluted in Tris-buffered saline containing 10 mM ascorbic acid in the presence or absence of 6 mM hinokitiol. Final volume administered was 1.5 mL/kg for each mouse, correcting for individual body weight. Blood was collected at 60, 120, and 240 min after administration to determine ^{59}Fe levels. Mice were humanely sacrificed by isoflurane overdose after 6 hours and blood was collected by cardiac puncture. Radioactivity was quantified by gamma counting and calculated as the percentage of gavaged dose (± SEM). Experiments were performed with 4 genotyped-matched mice/day; preliminary analysis determined there were no gender effects on uptake of ^{59}Fe after intragastric gavage; mixed genders were used in the experiments shown.

^{59}Fe gastrointestinal absorption of iron in 3-5-month-old *b*/*b* rats was characterized similar to the procedure described above in the presence of either 6 mM hinokitiol or 6 mM C2deOHino. To compare with the rate of normal iron uptake, age-matched sibling control (+/+ or +/*b*) Belgrade rats were tested by the same procedure except that ^{59}Fe was administered without small molecule. Blood (50 μL) was taken from the tail vein at 15, 30, 60, 120, 180, 240, and 360 minutes post administration. Radioactivity was quantified by gamma counting and

calculated as the percentage of gavaged dose (± SEM). Animals were humanely euthanized at 6 hours.

Knockdown in morphant zebrafish

The morpholinos (MOs) were purchased from GeneTools, LLC (Philomath, OR). The sequences of the MO used were as follows: *dmt1* MO: 5'-GAGTGTGAAACGTGACGCACCCCTT-3'; *mfrn1* MO: 5'-TAAGTTGCATTACCTTGACTGAATC-3'. Zebrafish embryos at the 1-cell stage were injected with MOs as previously described[56,61]. *o*-dianisidine staining for hemoglobinized cells in embryos was as previously described[62]. Quantification by flow cytometry using fluorescently labeled erythrocytes from the transgenic *Tg(globinLCR:eGFP)* line[43] was performed as previously described[56,59]. Semi-quantitative RT-PCR of *dmt1* mRNA in morphants was performed using custom designed probes as previously described[63]. The sequences of the *dmt1* primers are as follows: 5'-CTGAACCTGCGCTGGTCCC-3' (Fwd); 5'-TCCGTTAGCGAAGTCGTGCATG-3' (Rev). The sequences of the control *actb* primers were as follows: 5'-GTTGGTATGGGACAGAAAGACAG-3' (Fwd); 5'-ACCAGAGGCATACAGGGACAG-3' (Rev).

Restored hemoglobinization in transporter-deficient zebrafish

Either mutant or morphant embryos were allowed to develop to >24 hours post fertilization (hpf), then dechorionated with pronase as previously described[64]. The dechorionated embryos or morphants were then incubated in the presence of 1 μM hinokitiol (or vehicle) and 10 μM iron (III) citrate for an additional forty-eight hours. Vehicle treated embryos were

exposed to 0.01 mM DMSO. C2deOHino (1 μM) with iron (III) citrate (10 μM) was used as a negative control. Control and either mutant or morphant embryos at ~72 hpf were either (a) directly stained by *o*-dianisidine[62]a or (b) mechanically homogenized as previously described for flow cytometry[59,61].

Genotyping and imaging of mutant zebrafish from heterozygous cross

Genotyping of the hinokitiol-rescued *frs*^{tq223} embryos were performed as previously described[42].

Synthesis and Characterization of Small Molecules

Materials

Commercial reagents were purchased from Sigma-Aldrich and were used without further purification unless otherwise noted. Solvents were purified via passage through packed columns as described by Pangborn and coworkers[65]. All water was deionized prior to use.

General experimental procedures

Unless otherwise noted, reactions were performed in flame-dried round-bottomed or modified Schlenk flasks fitted with rubber septa under a positive pressure of argon. Organic solutions were concentrated via rotary evaporation under reduced pressure with a bath temperature of 20-35 °C unless otherwise noted. Reactions were monitored by analytical thin layer chromatography (TLC) using the indicated solvent on E. Merck silica gel 60 F254 plates (0.25 mm). Compounds were visualized by exposure to a UV lamp (λ = 254 nm or 366 nm), and/or a solution of $KMnO_4$ stain, followed by heating using a Varitemp heat gun. Flash column

chromatography was performed using Merck silica gel grade 9385 60Å (230-240 mesh). Preparative HPLC purification was performed using an Agilent 1260 Infinity series preparative HPLC with a SunFire 5 μm C18 column (Waters Corporation).

Structural analysis

^{1}H NMR, ^{13}C NMR, and ^{19}F NMR were recorded at 20 °C on Unity Inova 500NB, Varian XR500, or Unity 500 instruments. Chemical shifts (δ) are reported in parts per million (ppm) downfield from tetramethylsilane and referenced to residual protium in the NMR solvent ($CHCl_3$, δ=7.26; DMSO-d_6, δ=2.50). Data are reported as follows: chemical shift, multiplicity (s=singlet, d=doublet, t=triplet, m=multiplet, app=apparent), coupling constant (*J*) in Hertz (Hz), and integration. ^{13}C NMR are referenced to carbon resonances in the NMR solvent ($CDCl_3$, δ=77.16; DMSO-d_6, δ=39.52). ^{19}F NMR are referenced to fluorine resonance in an external standard ($CFCl_3$, δ=0.00) High resolution mass spectra (HRMS) were performed at the University of Illinois, School of Chemical Sciences Mass Spectrometry Laboratory. Elemental analysis was performed at the University of Illinois Microanalysis Laboratory. HPLC characterization was performed using an Agilent 1260 Infinity series analytical HPLC with a 5 μm C18 column (Agilent Technologies).

Iron (III) hinokitiol complex

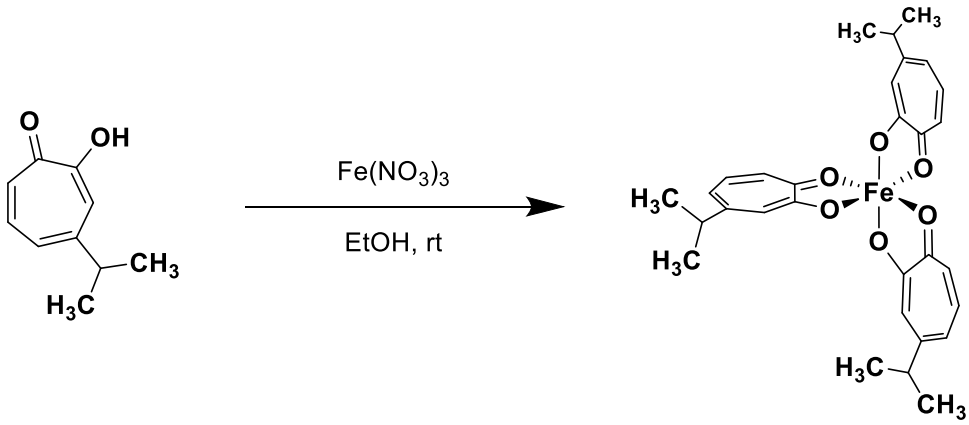

To a flame-dried 20-mL vial equipped with a stir bar was added iron (III) nitrate nonahydrate (819.8 mg, 2.03 mmol) followed by hinokitiol (1.0092 g, 6.15 mmol). Then ethanol (10 mL) was added. The reaction was vigorously stirred for 2 hours to give a purple colored suspension. The product was collected via filtration and recrystallized in acetone to yield the product as a purple solid (959.9 mg, 1.76 mmol, 86.7% yield).

HRMS (ESI+)

Calculated for $C_{30}H_{34}O_6Fe$ $(M+H)^+$: 546.1705

Observed : 546.1703

Elemental Analysis

Calculated [C] : 66.06%	Observed [C] : 65.88%
Calculated [H] : 6.10%	Observed [H] : 6.21%
Calculated [Fe] : 10.24%	Observed [Fe] : 10.19%

Triflation of hinokitiol

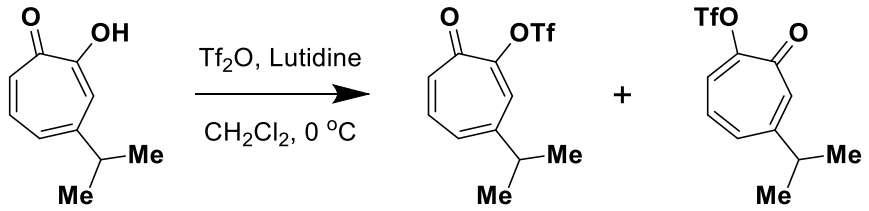

To an oven-dried 300 mL round-bottomed flask equipped with a stir bar was added hinokitiol (3.014 g, 18.27 mmol) followed by anhydrous CH_2Cl_2 (200 mL). The system was put under nitrogen, and freshly distilled lutidine (2.54 mL, 21.92 mmol) was added via syringe. The system was cooled to 0 °C in an ice/water bath before triflic anhydride (3.38 mL, 20.10 mmol) was added dropwise via syringe. The solution was stirred for 15 minutes at 0 °C, then allowed to warm to room temperature and stirred for an additional 3 hours. After completion, the reaction was quenched with a saturated aqueous NH_4Cl solution. The product was extracted in CH_2Cl_2, washed with $CuSO_4$, washed with brine, and dried over anhydrous $MgSO_4$. The product was filtered and solvent removed by rotary evaporation. The product was then purified as an inseparable mixture of the C-2 and C-7 isomers by flash column chromatography (3:1 Hexane:EtOAc) to yield a slightly colored oil (4.819 g, 16.27 mmol, 88.6% yield as a 53:47 mixture of the C-2 and C-7 isomers).

TLC (1:1 Hex:EtOAc)

R_f = 0.68, visualized by UV (254 nm) and $KMnO_4$ stain

H NMR (500 MHz, $CDCl_3$)

δ 7.34-7.24 (m, 5H), 7.14 (dt, *J* = 11.5, 0.7 Hz, 1H), 7.08 (dt, *J* = 8.6, 0.6 Hz, 1H), 6.99 (dd, *J* = 11.4, 9.4 Hz, 1H), 2.91-2.80 (app. m, 2H), 1.26 (d, *J* = 6.8 Hz, 6H), 1.26 (d, *J* = 6.8 Hz, 6H)

^{13}C NMR (126 MHz, $CDCl_3$)

δ 178.0, 177.7, 158.7, 155.9, 152.3, 139.0, 138.2, 137.9, 137.8, 131.9, 129.9, 129.3, 127.6, 38.8, 38.2, 22.9, 2.8

^{19}F NMR (470.2 MHz, $CDCl_3$)

δ -74.76, -74.84

HRMS (ESI+)

Calculated for $C_{11}H_{12}F_3O_4S$ $(M+H)^+$: 297.0408

Observed : 297.0408

Hydrogenolysis of hinokitiol-triflate

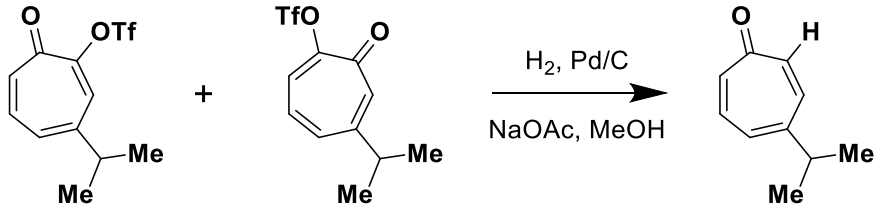

Sodium acetate (1.11 g, 13.4 mmol), the triflated hinokitiol (2.00 g, 6.76 mmol), 10 wt% palladium on carbon (71.8 mg) and methanol (75 mL) were added to a flame-dried 200 mL round-bottomed flask containing a stir bar. The suspension was degassed with N_2, then put under a H_2 atmosphere without bubbling H_2 through the solution. The reaction was stirred and analyzed by TLC (Et_2O) for 30 minutes. After completion, N_2 was bubbled through the system, and the black suspension was filtered over celite. The methanol was removed by rotary evaporation, and the product was extracted in diethyl ether and washed with brine. After drying with anhydrous

$MgSO_4$, the solvent was removed by rotary evaporation to yield a slightly colored oil. The product was purified by preparative HPLC (283 nm, 20% MeCN in H_2O) to yield C2-deoxyhinokitiol and C7-deoxyhinokitiol as clear oils (C2deOHino: 325 mg, 2.21 mmol, 32.4% yield; C7deOHino: 204 mg, 1.38 mmol, 20.4% yield).

TLC (Et_2O)

R_f = 0.49, visualized by UV (254 nm) and $KMnO_4$ stain

^1H NMR (500 MHz, $CDCl_3$)

δ C2: 7.10-6.97 (m, 3H), 6.91 (ddd, *J* = 12.0, 2.6, 0.8 Hz, 1H), 6.81 (ddd, *J* = 8.7, 1.5, 0.7 Hz, 1H), 2.73 (heptet, *J* = 6.8 Hz, 1H), 1.19 (d, *J* = 6.9 Hz, 6H)

δ C7: 7.09-7.01 (m, 3H), 6.93-6.92 (m, 2H), 2.74 (heptet, *J* = 6.8 Hz, 1H), 1.21 (d, *J* = 6.9 Hz, 6H)

^{13}C NMR (126 MHz, $CDCl_3$)

δ C2: 188.0, 156.2, 141.9, 140.1, 138.1, 137.2, 130.5, 38.1, 23.0

δ C7: 188.0, 157.4, 141.9, 138.7, 137.1, 136.1, 133.8, 38.4, 22.9

HRMS (ESI+)

Calculated for $C_{10}H_{13}O$ $(M+H)^+$: 149.0966

Observed : 149.0973

2.9 REFERENCES

1. Sohn, Y. S., Breuer, W., Munnich, A. & Cabantchik, Z. I. Redistribution of accumulated cell iron: A modality of chelation with therapeutic implications. *Blood* **111**, 1690–1699 (2008).
2. Poňka, P., Borová, J., Neuwirt, J. & Fuchs, O. Mobilization of iron from reticulocytes. Identification of pyridoxal isonicotinoyl hydrazone as a new iron chelating agent. *FEBS Lett.* **97**, 317–321 (1979).
3. Garrick, L. M. *et al.* Ferric-salicylaldehyde isonicotinoyl hydrazone, a synthetic iron chelate, alleviates defective iron utilization by reticulocytes of the belgrade rat. *J. Cell. Physiol.* **146**, 460–465 (1991).
4. Horackova, M., Ponka, P. & Byczko, Z. The antioxidant effects of a novel iron chelator salicylaldehyde isonicotinoyl hydrazone in the prevention of H2O2 injury in adult cardiomyocytes. *Cardiovasc. Res.* **47**, 529–536 (2000).
5. Bleackley, M. R. & MacGillivray, R. T. A. Transition metal homeostasis: From yeast to human disease. *BioMetals* **24**, 785–809 (2011).
6. Garrick, M. D. *et al.* DMT1: A mammalian transporter for multiple metals. *BioMetals* **16**, 41–54 (2003).
7. Trinder, D., Oates, P. S., Thomas, C., Sadleir, J. & Morgan, E. H. Localisation of divalent metal transporter 1 (DMT1) to the microvillus membrane of rat duodenal enterocytes in iron deficiency, but to hepatocytes in iron overload. *Gut* **46**, 270–276 (2000).
8. Mims, M. P. *et al.* Identification of a human mutation of DMT1 in a patient with microcytic anemia and iron overload. *Blood* **105**, 1337–1342 (2005).
9. Canonne-Hergaux, F., Zhang, A. S., Ponka, P. & Gros, P. Characterization of the iron

transporter DMT1 (NRAMP2/DCT1) in red blood cells of normal and anemic mk/mk mice. *Blood* **98**, 3823–3830 (2001).

10. Blanco, E., Kannengiesser, C., Grandchamp, B., Tasso, M. & Beaumont, C. Not all DMT1 mutations lead to iron overload. *Blood Cells, Mol. Dis.* **43**, 199–201 (2009).
11. Beaumont, C. *et al.* Two new human DMT1 gene mutations in a patient with microcytic anemia, low ferritinemia, and liver iron overload. *Blood* **107**, 4168–4170 (2006).
12. Iolascon, A. & De Falco, L. Mutations in the Gene Encoding DMT1: Clinical Presentation and Treatment. *Semin. Hematol.* **46**, 358–370 (2009).
13. Iolascon, A. *et al.* Natural History of Recessive Inheritance of DMT1 Mutations. *J. Pediatr.* **152**, 136–139 (2008).
14. Garrick, M. D. Human iron transporters. *Genes Nutr.* **6**, 45–54 (2011).
15. Iolascon, A. *et al.* Microcytic anemia and hepatic iron overload in a child with compound heterozygous mutations in DMT1 (SCL11A2). *Blood* **107**, 349–354 (2006).
16. Lolascon, A., De Falco, L. & Beaumont, C. Molecular basis of inherited microcytic anemia due to defects in iron acquisitionor heme synthesis. *Haematologica* **94**, 395–408 (2009).
17. Abouhamed, M., Wolff, N. A., Lee, W.-K., Smith, C. P. & Thevenod, F. Knockdown of endosomal/lysosomal divalent metal transporter 1 by RNA interference prevents cadmium-metallothionein-1 cytotoxicity in renal proximal tubule cells. *AJP Ren. Physiol.* **293**, F705–F712 (2007).
18. Espinoza, A. *et al.* Iron, copper, and zinc transport: Inhibition of divalent metal transporter 1 (DMT1) and human copper transporter 1 (hCTR1) by shRNA. *Biol. Trace Elem. Res.* **146**, 281–286 (2012).

19. Donovan, A. *et al.* The zebrafish mutant gene chardonnay (cdy) encodes divalent metal transporter 1 (DMT1). *Blood* **100**, 4655–4659 (2002).

20. Garrick, M. D. & Garrick, L. M. Cellular iron transport. *Biochim. Biophys. Acta - Gen. Subj.* **1790**, 309–325 (2009).

21. Hentze, M. W., Muckenthaler, M. U., Galy, B. & Camaschella, C. Two to Tango: Regulation of Mammalian Iron Metabolism. *Cell* **142**, 24–38 (2010).

22. Andrews, N. C. Iron homeostasis: Insights from genetics and animal models. *Nat. Rev. Genet.* **1**, 208–217 (2000).

23. Tabuchi, M., Yoshimori, T., Yamaguchi, K., Yoshida, T. & Kishi, F. Human NRAMP2/DMT1, which mediates iron transport across endosomal membranes, is localized to late endosomes and lysosomes in HEp-2 cells. *J. Biol. Chem.* **275**, 22220–22228 (2000).

24. Friend, C., Scher, W., Holland, J. G. & Sato, T. Hemoglobin synthesis in murine virus-induced leukemic cells in vitro: stimulation of erythroid differentiation by dimethyl sulfoxide. *Proc. Natl. Acad. Sci. U. S. A.* **68**, 378–82 (1971).

25. Johnson, E. E., Sandgren, A., Cherayil, B. J., Murray, M. & Wessling-Resnick, M. Role of ferroportin in macrophage-mediated immunity. *Infect. Immun.* **78**, 5099–5106 (2010).

26. Mackenzie, E. L., Iwasaki, K. & Tsuji, Y. Intracellular Iron Transport and Storage: From Molecular Mechanisms to Health Implications. *Antioxid. Redox Signal.* **10**, 997–1030 (2008).

27. Pietrangelo, A. The ferroportin disease. *Blood Cells, Mol. Dis.* **32**, 131–138 (2004).

28. Mayr, R. *et al.* Ferroportin disease: A systematic meta-analysis of clinical and molecular findings. *J. Hepatol.* **53**, 941–949 (2010).

29. Lesjak, M. *et al.* Quercetin inhibits intestinal iron absorption and ferroportin transporter expression in vivo and in vitro. *PLoS One* **9**, 1–10 (2014).

30. McKie, A. T. *et al.* A Novel Duodenal Iron-Regulated Transporter, IREG1, Implicated in the Basolateral Transfer of Iron to the Circulation. *Mol. Cell* **5**, 299–309 (2000).

31. Oates, P. S. The role of hepcidin and ferroportin in iron absorption. *Histol. Histopathol.* **22**, 791–804 (2007).

32. Loréal, O. *et al.* Iron, hepcidin, and the metal connection. *Front. Pharmacol.* **5 JUN**, 1–10 (2014).

33. Ludwiczek, S., Theurl, I., Artner-Dworzak, E., Chorney, M. & Weiss, G. Duodenal HFE expression and hepcidin levels determine body iron homeostasis: Modulation by genetic diversity and dietary iron availability. *J. Mol. Med.* **82**, 373–382 (2004).

34. Yamaji, S., Sharp, P., Ramesh, B. & Srai, S. K. Inhibition of iron transport across human intestinal epithelial cells by hepcidin. *Blood* **104**, 2178–2180 (2004).

35. Knutson, M. D., Oukka, M., Koss, L. M., Aydemir, F. & Wessling-Resnick, M. Iron release from macrophages after erythrophagocytosis is up-regulated by ferroportin 1 overexpression and down-regulated by hepcidin. *Proc. Natl. Acad. Sci.* **102**, 1324–1328 (2005).

36. Donovan, A. *et al.* Positional cloning of zebrafish ferroportin1 identifies a conserved vertebrate iron exporter. *Nature* **403**, 776–781 (2000).

37. Veuthey, T. & Wessling-Resnick, M. Pathophysiology of the Belgrade rat. *Front. Pharmacol.* **5 APR**, 1–13 (2014).

38. Imai, N. *et al.* Lack of hinokitiol (beta-thujaplicin) carcinogenicity in F334/DuCrj rats. *J. Toxicol. Sci.* **31**, 357–370 (2006).

39. Seo, Y. A., Elkhader, J. A. & Wessling-Resnick, M. Distribution of manganese and other biometals in flatiron mice. *BioMetals* **29**, 147–155 (2016).

40. Seo, Y. A. & Wessling-Resnick, M. Ferroportin deficiency impairs manganese metabolism in flatiron mice. *FASEB J.* **29**, 2726–2733 (2015).

41. Avagyan, S. & Zon, L. I. Fish to Learn: Insights into Blood Development and Blood Disorders from Zebrafish Hematopoiesis. *Hum. Gene Ther.* **27**, 287–294 (2016).

42. Shaw, G. C. *et al.* Mitoferrin is essential for erythroid iron assimilation. *Nature* **440**, 96–100 (2006).

43. Ganis, J. J. *et al.* Zebrafish globin switching occurs in two developmental stages and is controlled by the LCR. *Dev. Biol.* **366**, 185–194 (2012).

44. Chung, J. *et al.* Iron regulatory protein-1 protects against mitoferrin-1-deficient porphyria. *J. Biol. Chem.* **289**, 7835–7843 (2014).

45. Brownlie, A. *et al.* Positional cloning of the zebrafish sauternes gene: A model for congenital sideroblastic anaemia. *Nat. Genet.* **20**, 244–250 (1998).

46. Kwok, E. Y., Severance, S. & Kosman, D. J. Evidence for iron channeling in the Fet3p-Ftr1p high-affinity iron uptake complex in the yeast plasma membrane. *Biochemistry* **45**, 6317–6327 (2006).

47. Yun, C. W., Tiedeman, J. S., Moore, R. E. & Philpott, C. C. Siderophore-iron uptake in Saccharomyces cerevisiae: Identification of ferrichrome and fusarinine transporters. *J. Biol. Chem.* **275**, 16354–16359 (2000).

48. Cioffi, A. G., Hou, J., Grillo, A. S., Diaz, K. A. & Burke, M. D. Restored physiology in protein-deficient yeast by a small molecule channel. *J. Am. Chem. Soc.* **137**, 10096–10099 (2015).

49. Dearden, J. C. & Bresnen, G. M. The Measurement of Partition Coefficients. *Quant. Struct. Relationships* **7**, 133–144 (1988).

50. Andrés, A. *et al.* Setup and validation of shake-flask procedures for the determination of partition coefficients (log D) from low drug amounts. *Eur. J. Pharm. Sci.* **76**, 181–191 (2015).

51. Li, C. Y., Watkins, J. A. & Glass, J. The H+-ATPase from reticulocyte endosomes reconstituted into liposomes acts as an iron transporter. *J. Biol. Chem.* **269**, 10242–10246 (1994).

52. Davis, S. A. *et al.* C3-OH of Amphotericin B Plays an Important Role in Ion Conductance. *J. Am. Chem. Soc.* **137**, 15102–15104 (2015).

53. Berlett, B. S., Levine, R. L., Chock, P. B., Chevion, M. & Stadtman, E. R. Antioxidant activity of Ferrozine-iron-amino acid complexes. *Proc. Natl. Acad. Sci. U. S. A.* **98**, 451–6 (2001).

54. Illing, A. C., Shawki, A., Cunningham, C. L. & Mackenzie, B. Substrate profile and metal-ion selectivity of human divalent metal-ion transporter-1. *J. Biol. Chem.* **287**, 30485–30496 (2012).

55. Ehrnstorfer, I. A., Geertsma, E. R., Pardon, E., Steyaert, J. & Dutzler, R. Crystal structure of a SLC11 (NRAMP) transporter reveals the basis for transition-metal ion transport. *Nat. Struct. Mol. Biol.* **21**, 990–996 (2014).

56. Chung, J. *et al.* The mTORC1/4E-BP pathway coordinates hemoglobin production with L-leucine availability. *Sci Signal* **8**, ra34 (2015).

57. Canver, M. C. *et al.* Characterization of genomic deletion efficiency mediated by clustered regularly interspaced palindromic repeats (CRISPR)/cas9 nuclease system in mammalian

cells. *J. Biol. Chem.* **289**, 21312–21324 (2014).

58. Yien, Y. Y. *et al.* TMEM14C is required for erythroid mitochondrial heme metabolism. *J. Clin. Invest.* **124**, 4294–304 (2014).

59. Hildick-Smith, G. J. *et al.* Macrocytic anemia and mitochondriopathy resulting from a defect in sideroflexin 4. *Am. J. Hum. Genet.* **93**, 906–914 (2013).

60. Wilcock, B. C., Endo, M. M., Uno, B. E. & Burke, M. D. C2′-OH of amphotericin B plays an important role in binding the primary sterol of human cells but not yeast cells. *J. Am. Chem. Soc.* **135**, 8488–8491 (2013).

61. Cooney, J. D. *et al.* Teleost growth factor independence (gfi) genes differentially regulate successive waves of hematopoiesis. *Dev. Biol.* **373**, 431–441 (2013).

62. Amigo, J. D. *et al.* The role and regulation of friend of GATA-1 (FOG-1) during blood development in the zebrafish. *Blood* **114**, 4654–4663 (2009).

63. Nilsson, R. *et al.* Discovery of Genes Essential for Heme Biosynthesis through Large-Scale Gene Expression Analysis. *Cell Metab.* **10**, 119–130 (2009).

64. Kardon, J. R. *et al.* Mitochondrial ClpX activates a key enzyme for heme biosynthesis and erythropoiesis. *Cell* **161**, 858–867 (2015).

65. Pangborn, A. B., Giardello, M. A., Grubbs, R. H., Rosen, R. K. & Timmers, F. J. Safe and convenient procedure for solvent purification. *Organometallics* **15**, 1518–1520 (1996).

CHAPTER 3

HINOKITIOL HARNESSES IRON GRADITENTS THAT ACCUMULATE IN IRON TRANSPORTER DEFICIENT SYSTEMS

3.1 INTRODUCTION

In the previous chapters I have demonstrated that hinokitiol, a lipophilic, iron binding small molecule can transport iron across lipid membranes as well as mobilize iron into, within and out of living cells thus restoring physiology in iron transporter deficient cellular and animal models. With all of the phenomenological data in hand we next wanted to understand how an imperfect small molecule that has no inherent direction specificity on its own was restoring iron movement in site- and direction-specific ways. Hinokitiol did not appear to be moving iron or other metals out of cellular compartments when it was unhelpful or even pathological, as evidence by the lack of toxicity in most cell lines as well as animal models. We thus hypothesized that in the absence of an iron transporting protein a build up of iron would occur upstream of the missing protein because all of the other drivers of iron transport, iron transporters as well as other ion pumps and channels would be active. We hypothesized that these pumps and channels would be upregulated in order to compensate for the missing iron transporter[1,2], therefore priming the system for unidirectional iron movement. If logic followed these gradients would then allow a relatively non-selective small molecule, such as hinokitiol, to simply act as a shuttle, moving the iron down the gradient according to diffusion and Le Chatelier's principle.

Portions of the work presented in this chapter were preformed with aid from my colleagues Dr. Anthony Grillo, Dr. Alexander Cioffi. Portions of this chapter have been adapted from Grillo, A. S.; SantaMaria A. M.; Kafina M. D.; Cioffi A.G.; Huston N. C.; Han M.; Seo Y. A.; Yien Y.Y.; Nardone C.; Menon A. V.; Fan J.; Svoboda D. C.; Anderson J. B.; Hong J.D.;

Nicolau B. G.; Subedi K.; Gewirth A. A.; Wessling-Resnick M.; Kim J.; Paw B. H.; Burke M. D. "Restored iron transport by a small molecule promotes absorption and hemoglobinization in animals" *Science.* **2017**, *356*, 608-616. Reprinted with permission from AAAS.

3.2 SITE- AND DIRECTION-SELECTIVE BUILDUP OF IRON GRADIENTS AND RELEASE WITH HINOKITIOL

We hypothesized that there was a site- and direction-selective build up in iron transporter deficient cells, upstream of the missing protein (**Figure 1.5**). Further, we hypothesized that this gradient is what was allowing hinokitiol to restore iron movement into, within and out our multiple models of iron transporter deficiency (**Figure 1.6**). Therefore we set out to test this hypothesis.

In order to see where the iron was located in our cells in real time we chose to use temporal, confocal, fluorescent microscopy with iron binding dyes that localized to specific locations within the cell. In the DMT1 deficient MEL cells the iron gradient we predicted was expected to be in the endosome making DMT1 deficient cells a great candidate for study. Because the gradients as well as their target location are all housed within the cell, we could watch were the iron was going within a cell with different treatment groups (**Figure 3.1 A and B**). In order to visualize the iron pools within the DMT1-deficient MEL cells we chose fluorescent dyes that localized to specific cellular locations (**Figure 3.2 A-C**)[3–5]. We chose to use an oxyburst green-

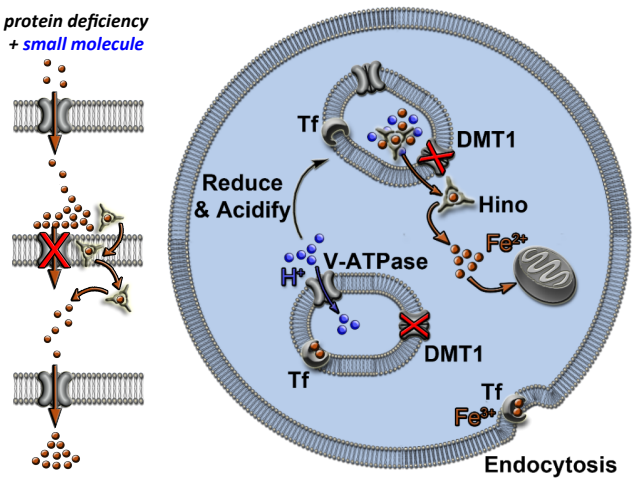

Figure 3.1 shDMT1 MEL cells with an iron gradient in their late endosome being released by hinokitiol

BSA conjugate that localizes to endosomes and fluoresces upon iron-mediated oxidation (**Figure 3.2 C**), and fluorescence emissions from the turn-off probes calcein green (**Figure 3.2 A**) which localizes to the cytosol and is quenched when iron binds and RPA (**Figure 3.2 B**) which localizes to the mitochondria and is likewise quenched upon iron binding.

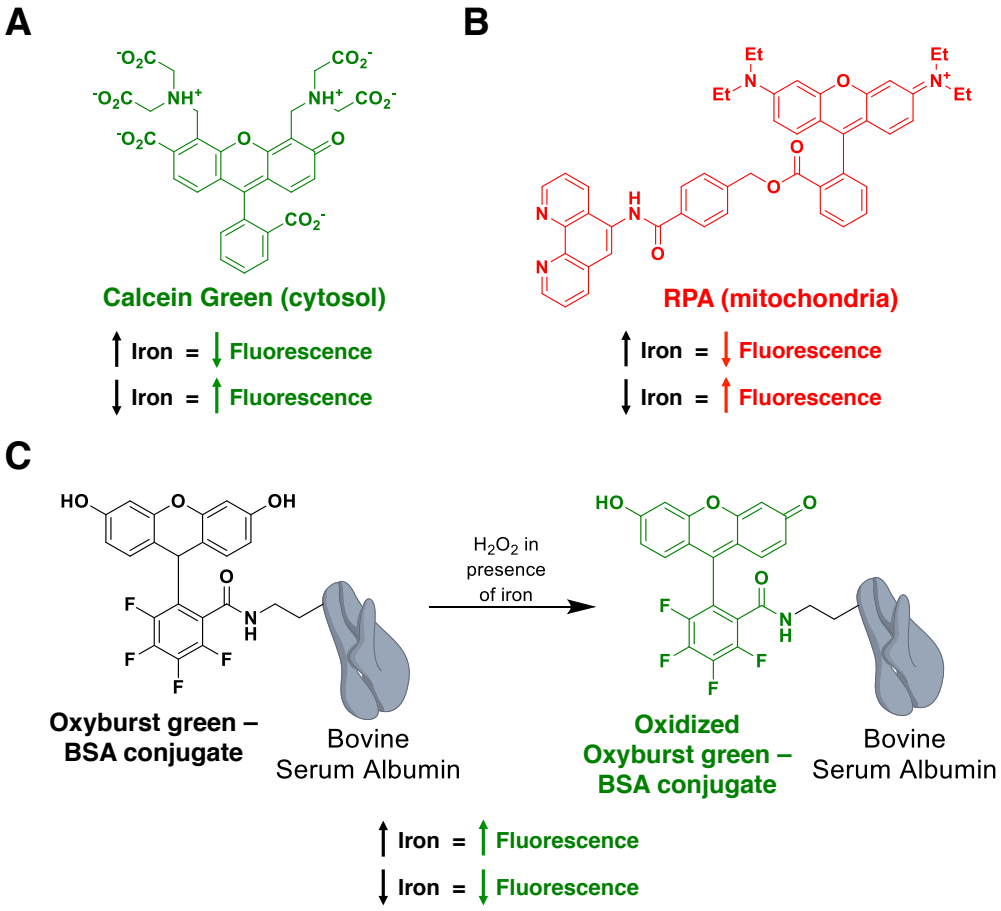

Figure 3.2 Use of iron-sensitive fluorescent dyes to visualize intracellular iron levels. (**A and B**) Structures of turn-off probes (**A**) Calcein Green used to visualize cytosolic labile iron levels and (**B**) RPA used to visualize mitochondrial labile iron levels, respectively. Fluorescence quenching is observed after iron binding. (**C**) BSA-conjugated Oxyburst Green fluoresces afteroxidation with H2O2 and labile Fe in the endosome**.**

Relatively low endosomal, high cytosolic, and high mitochondrial iron levels were observed in induced shControl MEL cells (**Figure 3.3 A-D**) We observed 2-fold increases in iron-promoted oxyburst green fluorescence in DMT1-deficient MEL cells indicating that there is

a large amount of iron in the endosomes of DMT1 deficient MEL cells compared to control (**Figure 3.3 A and B**). Interestingly this corresponded with reduced cytosolic iron, indicating that the iron the MEL cells were taking up via the phagocytosis of transferrin bound iron was not making it out of the late endosome (**Figure 3.3 A and C**). As expected mitochondrial iron was also very low in the DMT1 deficient MEL cells (**Figure 3.3 A and D**). Hinokitiol treatment decreased oxyburst green fluorescence 2.1-fold, indicating that the endosome had around the same amount of iron in it as control DMT1 replete cells; concomitantly calcein green and RPA fluorescence was quenched indicating that the iron that was in the endosome was being released into the cytosol and eventually making its way into the mitochondria (**Figure 3.3 A-D**). These data support hinokitiol-mediated release of built-up pools of endosomal iron into the cytosol and subsequent mitochondrial uptake.

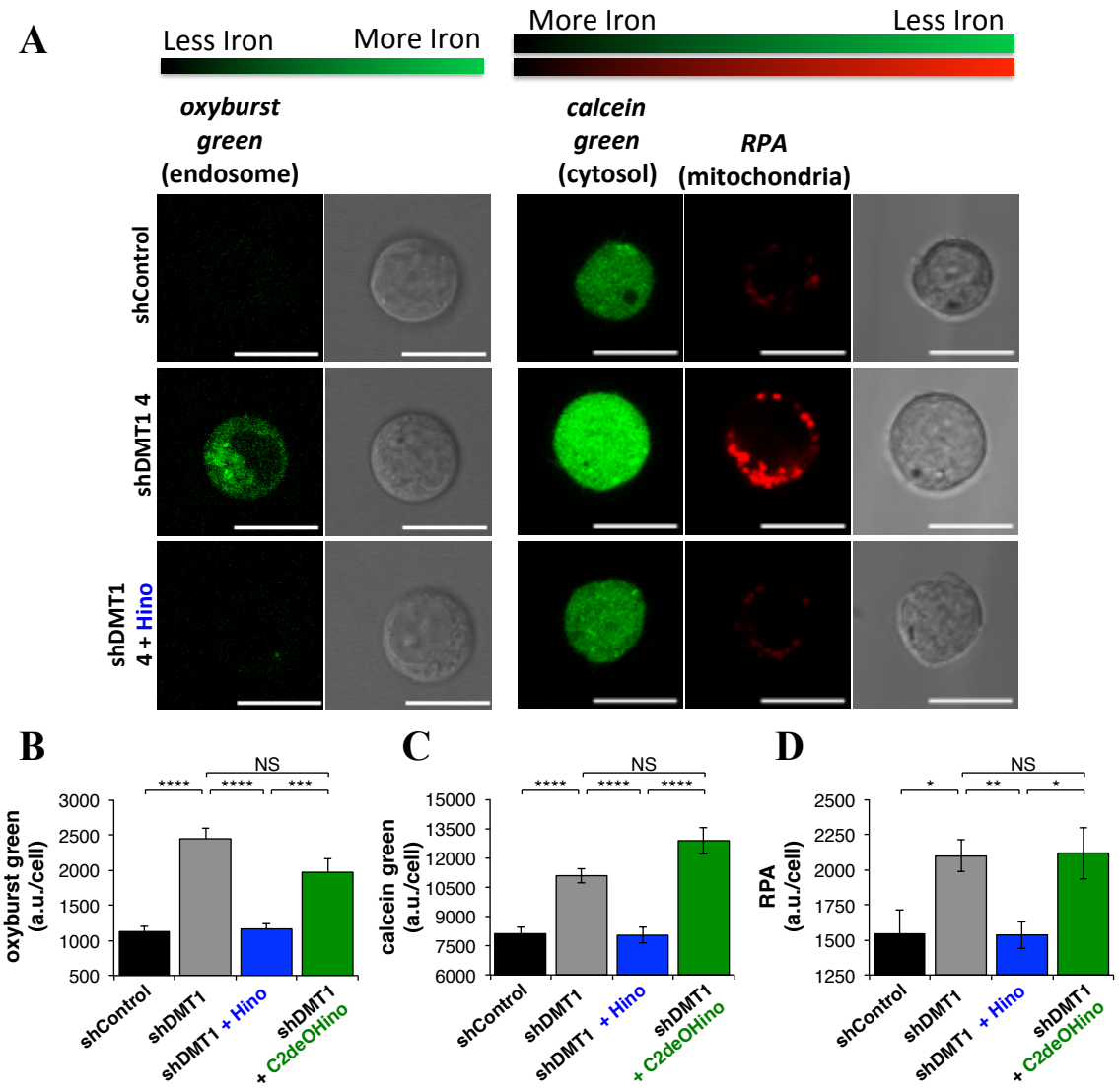

Figure 3.3 Hinokitiol releases iron gradients in shDMT1 MEL cells. (**A**) Representative
fluorescence images of differentiated shControl and DMT1-deficient MEL cells in the absence or presence of hinokitiol (1 μM), using OxyBURST Green, calcein green, and RPA to detect relative endosomal, cytosolic, and mitochondrial iron levels, respectively. A buildup of labile iron was observed in endosomes of DMT1-deficient cells, which was released after hinokitiol treatment. (**B**) ImageJ quantification of endosomal oxyburst green ($N \geq 40$), (**C**) cytosolic calcein green (N=23-67) and (**D**) mitochondrial RPA (N=23-67) fluorescence.

We next used calcein green and ^{55}Fe to determine if FPN1 deficiency in J774 macrophagess causes a similar buildup of iron, in this case inside of the cell, because ferroportin is unable to efflux it. When J774 cells were incubated with hepcidin, followed by incubation with $FeSO_4$ the hepcidin treated, and therefore FPN1 deficient cells, accumulated more labile iron in their cytosol over a one hour time frame than their wild type counterparts (**Figure 3.4 A and B**). Additionally when a similar assay was run with ^{55}Fe, a buildup of total iron was observed in the FPN1 deficient cells (**Figure 3.4 C**).

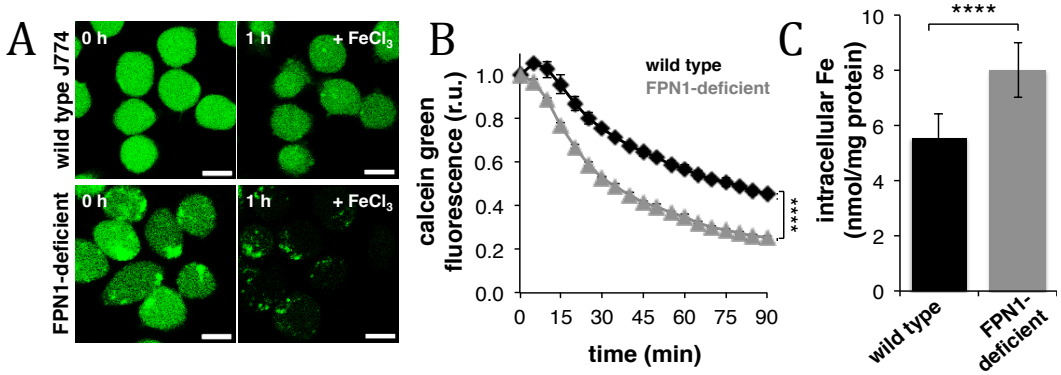

Figure 3.4 FPN1 deficient J774 Macrophages have more intracellular iron than their wild type counterparts. (**A and B**) A buildup of intracellular labile iron was observed in FPN1-deficient J774 macrophages treated with 200 μM $FeSO_4$ by quenching of calcein green fluorescence (n = 3). (**D**) Iron(III) uptake into J774 macrophages treated with 50 μM $FeCl_3$ similarly revealed a buildup of total intracellular iron in FPN1-deficient cells after 4 hours, as observed using ^{55}Fe as a radiotracer (n = 8).

3.3 ARTIFICIAL MANIPULATION OF IRON GRADIENTS REVERSES HINOKITIOL'S DIRECTION OF IRON MOBILIZATION

In order to determine if the gradients were the main cause of hinokitiol's directionality, we artificially manipulated them in a wild type system. We loaded iron into J774 macrophages, rinsed the cells to remove extracellular iron, and stained with calcein green (**Figure 3.5 A Left**).

Hinokitiol addition (t = 5 min) rapidly increased calcein green fluorescence, indicating iron efflux from the cells, whereas vehicle and C2deOHino had no effect (**Figure 3.5 A-C**). We then reversed the gradient in the same cells via external addition of a large bolus of $FeCl_3$ (t = 12 min) (**Figure 3.5 Right**). In DMSO and C2deOHino treated cells there was no significant effect (**Figure 3.5 A-C**), whereas quenching of calcein green fluorescence was observed with hinokitiol treatment (**Figure 3.5 A-C**). These results are consistent with an initial hinokitiol-mediated release of iron from J774 macrophages when intracellular iron levels are high, followed by hinokitiol-mediated uptake of iron into these macrophages when this transmembrane gradient is reversed by addition of extracellular iron (**Figure 3.5 A**). These studies support the hypothesis that hinokitiol is merely releasing iron from gradients formed when a protein iron transporter is not functioning properly. Collectively they allow us insight into how a simple small molecule like hinokitiol, which unlike a protein has no direction bias built in, is able to site- and direction-selectively restore iron movement within an iron transporter deficient system to restore normal physiology. It also explains why little to no effect is seen when wild type systems are treated with hinokitiol (data not shown, refer to A. S. Grillo, A. M. SantaMaria *et al.* Science. 2017[6]). This implies that there may be a generalizable approach to treating disorders caused by missing ion channels by simply by leveraging the gradient of the ion that has built up in the absence of the necessary protein transporter.

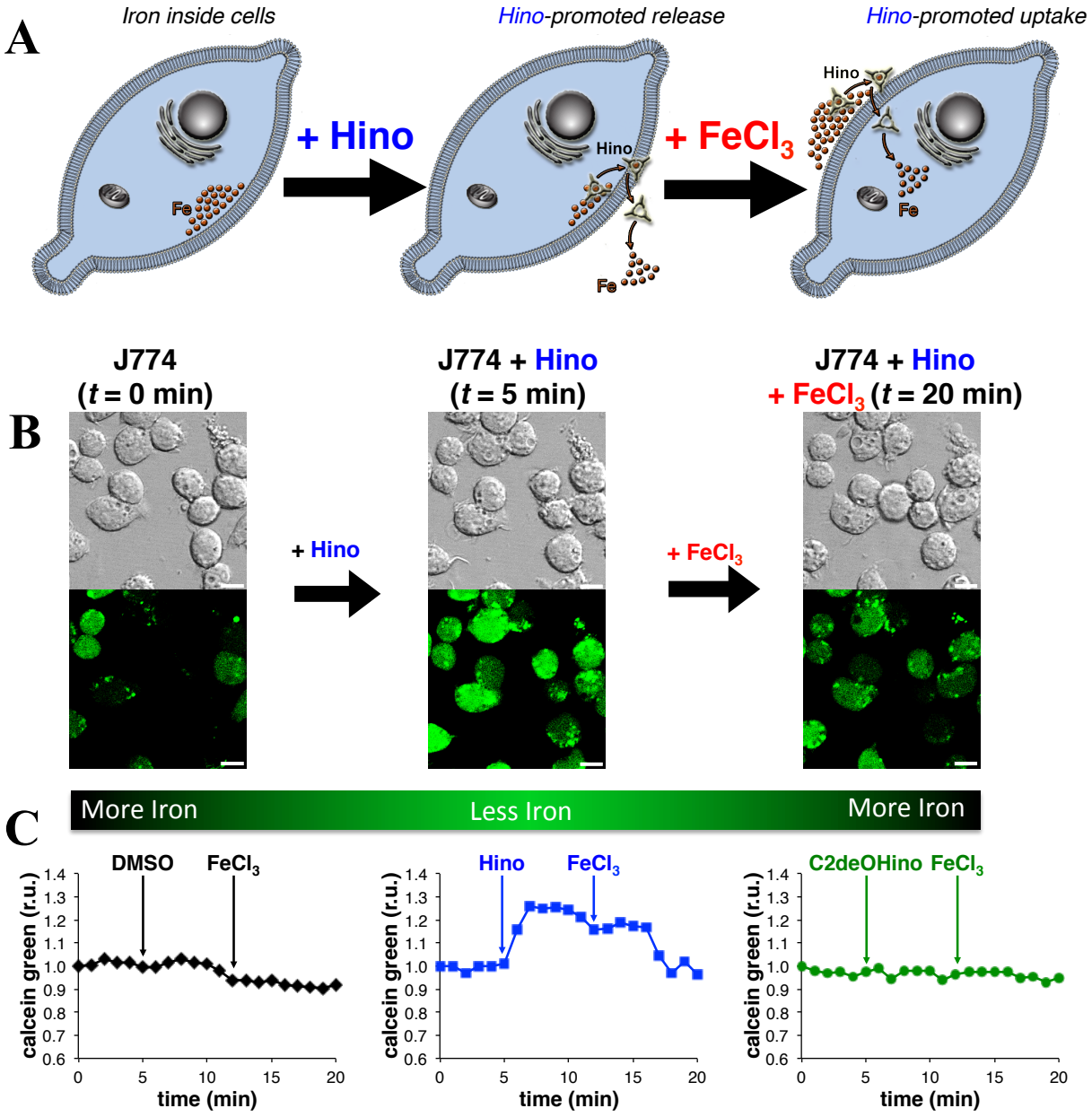

Figure 3.5 Hinokitiol mediated iron transport can be reversed by artificially manipulating the iron gradient (**A**) Schematic of hinokitiol-promoted direction-selective iron transport across J774 memebranes using artificial gradients. $FeSO_4$ (200 μM) is first loaded into J774 cells, the extracellular fluid is replaced with a low iron media (<500 nM), then hinokitiol (100 μM) is added at t = 5 min. Hinokitiol releases iron to the extracellular fluid. When the gradient is then reversed by addition of extracellular FeCl3 (100 μM) at t = 12 min. hinokitiol promotes iron uptake, consistent with direction-selective transport depending on the direction of the iron gradient. (**B**) Fluorescence imaging of cytosolic iron with calcein green, using artificially created iron gradients in opposite directions in J774 macrophages. (**C**) Representative ImageJ quantification of calcein green fluorescence in iron-loaded J774 cells with addition of DMSO, hinokitiol, or C2deOHino at t = 5 min and FeCl3 at t = 12 min.

3.4 METHODS

Materials

MEL cells were grown in suspension in T25 flasks until ~$1x10^6$ cells/mL and re-seeding into a new T25 flask at $1x10^5$ cells/mL in MEL Complete media with or without G418. Every month of culturing, new backstocks of MEL cells were used.

J774 cells (passage 20-80) were grown in T25 flasks to ≥90% confluency before scraping and re-seeding at 5:1 dilution in J774 Complete media. Media was changed every 1-2 days.

Live cell fluorescence imaging of MEL cells

To visualize cytosolic and mitochondrial iron, confocal imaging of calcein green and RPA fluorescence was performed, respectively. MEL cells were induced for differentiation as described above. After 70 hours of incubation, iron (III) citrate (10 μM final concentration) was added. The cells were incubated for an additional 2 hours, and then were centrifuged and rinsed with PBS. The cells were then re-suspended in PBS containing 1 μM calcein green-AM (Thermo Fisher C34852) and 1 μM RPA (Axxora SQX-RPA.1). The cells were then incubated at 37 °C for 15 minutes. The cells were centrifuged, rinsed with PBS, and re-suspended in DMEM containing 10 μM Fe_2Tf. The cells were then imaged within 10 minutes on a LSM710 microscope. Relative calcein green and RPA fluorescence per cell was determined by ImageJ analysis using >100 cells per experiment.

To visualize endosomal iron levels, confocal imaging of an oxyburst green-BSA conjugate (Thermo Fisher O13291) was performed. MEL cells were induced for differentiation as described above. After 70 hours, iron (III) citrate (10 μM final concentration) and an oxyburst green-BSA conjugate (200 μg/mL) were added. The cells were incubated for an additional 2

hours, and then were centrifuged and rinsed with PBS. The cells were then re-suspended in DMEM-HEPES buffer, and H_2O_2 (50 mM final concentration) was added. The cells were incubated at room temperature, and the oxyburst green fluorescence was then determined 10 minutes after addition of H_2O_2 on a LSM710 microscope. Relative oxyburst green fluorescence per cell was determined by ImageJ analysis using >100 cells per experiment.

^{55}Fe uptake into J774 macrophages (Fig. 4D, E)

J774 cells were grown in 12-well plates to ~80% confluency. The cells were then treated with vehicle or hepcidin in serum-free DMEM media at pH=7.4 in 10 mM HEPES buffer (1 mL) containing 50 μM $FeCl_3$ (100:1 ^{56}Fe:^{55}Fe). After four hours of incubation at 37 °C, the cells were rinsed with PBS (x2), and lysed with 500 μL RIPA buffer containing protease inhibitors. The cell lysate was diluted in scintillation cocktail and intracellular ^{55}Fe was determined by liquid scintillation counting and normalized to the total protein in each well.

Hinokitiol-promoted iron uptake as a function of extracellular iron was performed similar to described above in wild type J774 macrophages using 1 μM hinokitiol (from 1000X stock in DMSO) and the indicated final concentration of $FeCl_3$ (20:1 ^{56}Fe:^{55}Fe). At the indicated time, cells were rin sed with PBS (x2), and lysed with 200 mM NaOH. The cell lysate was diluted in scintillation cocktail and intracellular ^{55}Fe was determined by liquid scintillation counting and normalized to the total protein in each well.

Temporal imaging of cytosolic iron levels in J774 macrophages

To assess for the capacity for hinokitiol to reversibly and autonomously transport iron across the plasma membrane through the creation of artificial iron gradients, J774 macrophages

were grown in Ibidi dishes (Ibidi NC0723624) to ~80% confluency before incubation with J774 Complete media containing 5 mM ascorbic acid and 200 μM $FeSO_4$. The cells were incubated for 1.5 hours, media was aspirated, and the cells were rinsed with PBS. The cells were then incubated with calcein green-AM (1 μM) in DMEM for 20 minutes at 37 °C. The media was aspirated and cells were rinsed (x2) with PBS before DMEM (pH=7.4 in 10 mM HEPES) and 1 mM probenecid (Sigma P8761) was added. Calcein green fluorescence was then imaged on a LSM880 microscope at 37 °C with 5% CO_2 at the indicated time points for 30 minutes. Hinokitiol (100 μM final concentration), C2deOHino (100 μM final concentration), or DMSO (all from 1000X stocks in 50 μL DMEM) were added at 5 minutes, and a solution of $FeCl_3$ (100 μM final concentration, in 50 μL DMEM) was added at 12 minutes. Fluorescence in each image at each time point was analyzed by ImageJ analysis then normalized to the fluorescence at $t = 0$ for each image using >100 cells per experiment.

Temporal live cell imaging of iron uptake in wild type and FPN1-deficient J774 cells was performed after staining of cells with calcein green as described above. The cells were then rinsed with PBS (x2), and incubated in J774 Complete media containing 200 μM $FeSO_4$, 5 mM ascorbic acid, and 5 mM probenecid in the presence or absence of hepcidin. Calcein green fluorescence was obtained at the indicated time points, and fluorescence in each image at each time point was quantified by ImageJ analysis then normalized to the fluorescence at $t = 0$ for each image using >100 cells per experiment.

3.5 REFERENCES

1. Andrews, N. C. Iron homeostasis: Insights from genetics and animal models. *Nat. Rev. Genet.* **1**, 208–217 (2000).

2. Muckenthaler, M. U., Galy, B. & Hentze, M. W. Systemic Iron Homeostasis and the Iron-Responsive Element/Iron-Regulatory Protein (IRE/IRP) Regulatory Network. *Annu. Rev. Nutr.* **28**, 197–213 (2008).

3. Espósito, B. P., Breuer, W. & Cabantchik, Z. I. Design and applications of methods for fluorescence detection of iron in biological systems. *Biochem. Soc. Trans.* **30**, 729–732 (2002).

4. Espósito, B. P., Epsztejn, S., Breuer, W. & Cabantchik, Z. I. A review of fluorescence methods for assessing labile iron in cells and biological fluids. *Anal. Biochem.* **304**, 1–18 (2002).

5. Sohn, Y. S. *et al.* The role of endocytic pathways in cellular uptake of plasma non-transferrin iron. *Haematologica* **97**, 670–678 (2012).

6. Grillo, A. S. *et al.* Restored iron transport by a small molecule promotes absorption and hemoglobinization in animals. *Science (80-.).* **356**, 608–616 (2017).

CHAPTER 4

HINOKITIOL INTERFACES WITH THE ENDOGENOUS IRON REGULATORY SYSTEM IN ORDER TO RESTORE PHYSIOLOGY

4.1 INTRODUCTION

With the collective phenomenological and mechanistic data from chapters 1 and 2, hinokitiol was beginning to look like a very promising candidate for development as a molecular prosthetic to treat human diseases of iron homeostasis. That being said, we wanted to get a better understanding of how the natural, endogenous system was interacting with hinokitiol itself, as well as the iron that it was mobilizing into, within or out of cells and tissues. We had already observed that hinokitiol was not causing an upregulation of the proteins we had knocked down in our functional complementation assays (**Figures 2.7, 2.12, 2.14)**; however we wanted to probe what else was happening in the cells and tissues when they were treated with hinokitiol. Therefore we next asked whether hinokitiol was autonomously carrying iron through the entire cell (**Figure 4.1 A)**, or if it was handing the iron off in the cytosol and therefore allowing the natural system to take over (**Figure 4.1 B**). Importantly, if hinokitiol hands the iron off in the cytoplasm the endogenous system would be able to interact with the iron brought in by hinokitiol. We thus hypothesized that this would allow the cell's endogenous iron regulatory system to adapt to the hinokitiol mediated iron influx, making the down stream affects of hinokitiol mediated iron movement a regulated phenomena. This is especially important in gut enterocytes, which are crucial in maintaining iron homeostasis. If hinokitiol is able to completely bypass the endogenous checks and balances the cell has in place to maintain iron homeostasis, the risk of systemic iron overload with hinokitiol treatment would be far greater. We therefore set out to probe how much, if at all, hinokitiol was interacting with the endogenous system.

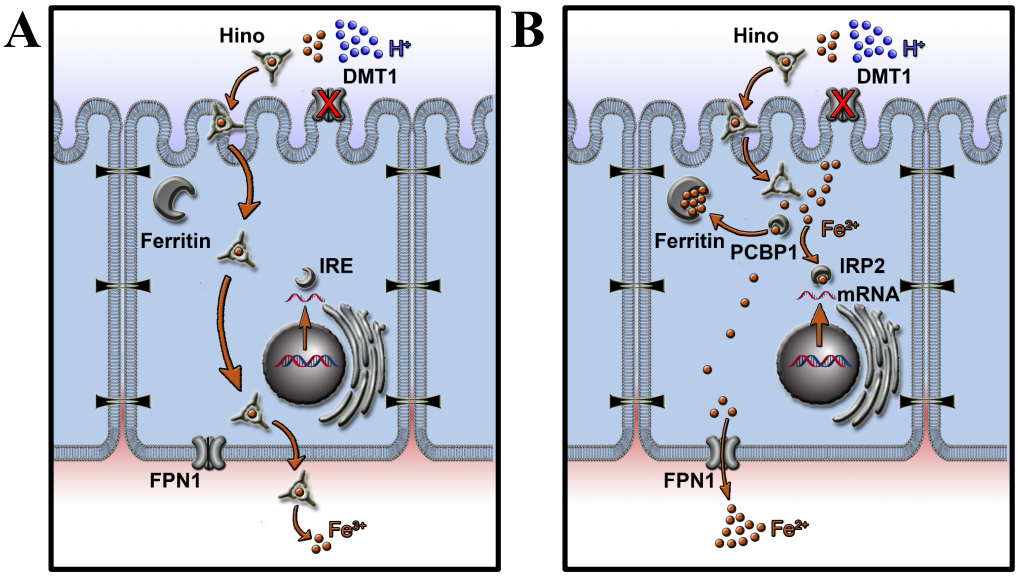

Figure 4.1 Does hinokitiol move iron through cells (A) Autonomously or (B) in collaboration with the endogenous system?

Portions of the work presented in this chapter were preformed with aid from my colleagues Dr. Anthony Grillo and Dr. Alexander Cioffi, our undergrads Dillon Svoboda, Chris Nardone, and James Fan. Portions of this chapter have been adapted from Grillo, A. S.; SantaMaria A. M.; Kafina M. D.; Cioffi A.G.; Huston N. C.; Han M.; Seo Y. A.; Yien Y.Y.; Nardone C.; Menon A. V.; Fan J.; Svoboda D. C.; Anderson J. B.; Hong J.D.; Nicolau B. G.; Subedi K.; Gewirth A. A.; Wessling-Resnick M.; Kim J.; Paw B. H.; Burke M. D. "Restored iron transport by a small molecule promotes absorption and hemoglobinization in animals" *Science.* **2017**, *356*, 608-616. Reprinted with permission from AAAS.

4.2 ENDOGENOUS PROTEIN ION TRANSPORTERS HELP DRIVE HINOKITIOL-MEDIATED GROWTH RESCUE IN YEAST

We thus asked whether endogenous networks of other ion-transport proteins and regulators[1] in iron transporter-deficient cells were collaborating with the small molecule,

hinokitiol, to help promote restoration of site- and direction-selective iron transport while still maintaining iron homeostasis. In yeast, the intracellular movement and storage of iron is dependent on a proton gradient known as the proton motive force, which is generated by the ATP-dependent active ion-transport proteins Pma1 and V-ATPase in the plasma and vacuolar membranes, respectively[2,3]. To test if hinokitiol mediated iron transport depended on the proton motive force created by Pma1 and V-ATPase we perfromed a chemical inhibition study where we chemically blocked the function of Pma1 and V-ATPase as well as an off target cell process, cell wall biosynthesis. We utilized ebselen to block Pma1 activity, bafilomycin to block V-ATPase activity, and Casponfungin to block cell wall biosynthesis. We treated both the wild type and the fet3Δftr1Δ yeast with hinokitiol to rule out any combinatorial effects of treatment with two small molecules at the same time. As expected, we observed that hinokitiol-rescued fet3Δftr1Δ and wild type yeast are equisensative to caspofungin with an EC_{50} of 7.9 μM and 7.1 μM respectively. In contrast hinokitiol-rescued fet3Δftr1Δ are exceptionally sensitive to chemical inhibition of Pma1 compared to wild type yeast with an EC_{50} of 0.4 μM and 2.1 μM respectively. Hinokitiol-rescued fet3Δftr1Δ are also exceptionally sensitive to chemical inhibition of V-ATPase compared to wild type with an EC_{50} of 24.4 μM and 29.2 μM respectively. These reulsts are consistent with the dependence of hinokitiol-mediated iron transport on the proton gradient created by Pma1 and V-ATPase.

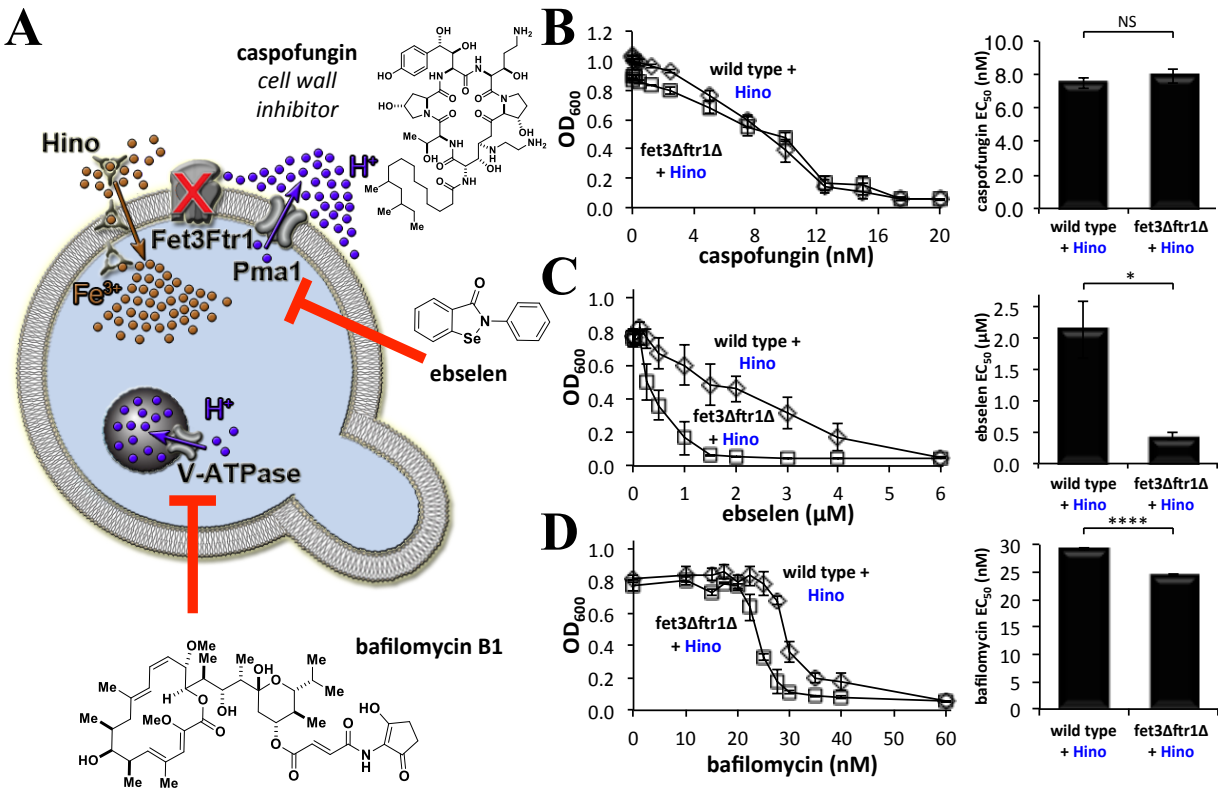

Figure 4.2 Hinokitiol collaborates with the endogenous proton pumps in yeast in order to restore physiology. (**A**) Schematic of fet3Δftr1Δ with ebselen and bafilomycin chemically inhibiting the active proton transporters Pma1 and V-ATPase. (**B**) As expected, wild type and fet3Δftr1Δ yeast grown in the presence of hinokitiol (10 μM) are equisensitive to an inhibitor of cell wall biosynthesis, caspofungin, which is off-pathway of iron uptake. N = 3. Inhibition of the proton-motive force generating pumps, (**C**) Pma1 with ebselen and (**D**) V-ATPase with bafilomycin, lead to increased sensitivity of hinokitiol-rescued fet3Δftr1Δ yeast relative to hinokitiol-treated wild type yeast. This suggests these proteins play a role in hinokitiol-mediated restoration of yeast cell growth. N = 3.

4.3 HINOKITIOL INTERFACES WITH ENDOGENOUS PROTEINS IN MAMMALIAN CELLS TO RESTORE PHYSIOLOGY

In intestinal epithelia, iron-transport proteins are transcriptionally and translationally regulated to maintain pysiological systemic iron levels while avoiding overload[1,4,5]. Specifically, levels of the apical H^+/Fe^{2+} symporter Divalent Metal Transporter 1 (DMT1), the iron sequestration protein ferritin (heavy, FTH1 and light, FTL1 chains), the basolateral efflux protein ferroprotin (FPN1), and the iron uptake mediator transferrin receptor 1 (TfR1) are translationally regulated through short hairpin iron response elements (IREs) located at the 5'- and 3'-untranslated regions of the corresponding mRNA transcripts (**Figure 4.3**)[1,5–7]. Iron-sensing iron response proteins (IRP1 and IRP2) bind to these IREs to block translation (5'-IRE, *Fth1*, *Ftl1*, *Fpn1*) or stabilize mRNA (3'-IRE, *Dmt1*, *TfR1*) under iron starvation (**Figure 4.3 A**). Upon iron stimulation and binding, the IRPs dissociate from the mRNAs, reversing their described effects. Transcriptional regulation is achieved through the transcriptional activator, hypoxia-inducible factor 2-alpha (Hif2α), which is degraded after O_2 and iron-mediated proline hydroxylation (**Figure 4.3 B**)[1]. Interestingly, Hif2α activates transcription of an isoform of *Fpn1* in order to evade IRE-mediated translational repression under iron deprivation conditions[1,5].

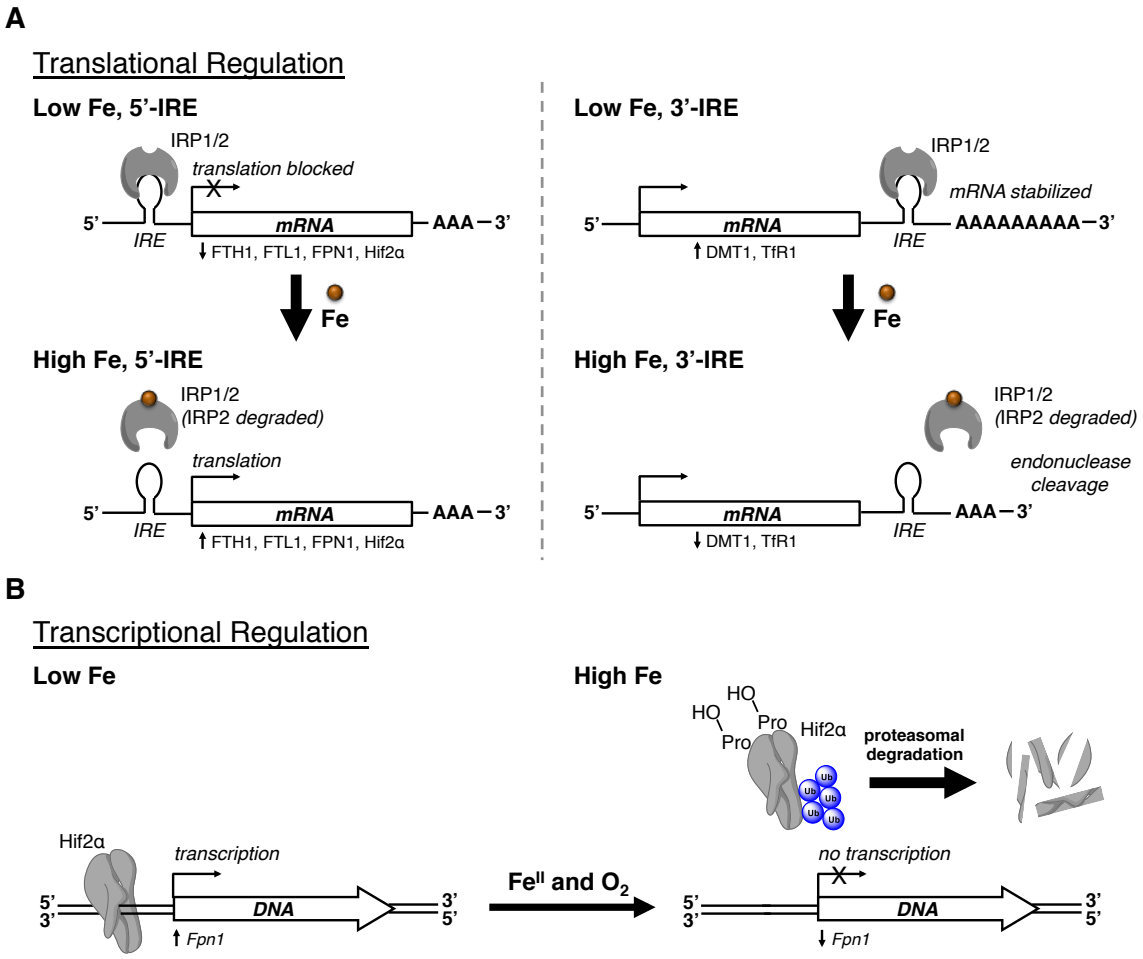

Figure 4.3 Simplified schematics for translational and transcriptional regulation of iron related proteins. (**A**) Translational regulation in duodenal enterocytes is mediated through iron response elements (IREs) located on the 5' or 3' ends of mRNA of several iron-related proteins. In the absence of iron, iron response proteins (IRP1 and IRP2) bind to the 5'- or 3'-IRE to block translation or stabilize mRNA, respectively. Upon iron binding, IRP1/2 dissociate from IRE (and IRP2 is degraded) and translation occurs (5'-IRE) or mRNA degrades (3'-IRE) to allow for ironsensitive regulation of proteins involved in iron uptake and transport. (**B**) Transcriptional regulation of FPN1 via Hif2α occurs to evade translational repression of FPN1. Hif2α activates Fpn1 transcription under iron-deplete conditions, however, in the presence of iron and O2, Hif2α is degraded, thus decreasing FPN1 protein levels.

Consistent with the iron homeostatic mechanisms mentioned above, an anemic state[8] is initially observed in DMT1-deficient Caco-2 monolayers, with decreased levels of ferritin and increased levels of FPN1, TfR1, and IRP2 (**Figure 4.4 A-E**), and as expected no significant change observed with PCBP1, IRP1, Hif1α, Hif2α. Collectively these protein levels provide a

favorable cellular environment for small molecule-mediated iron transport. This "priming" of the system toward unidirectional iron transport is likely critical for hinokitiol mediated iron mobilization into, within and out of cells.

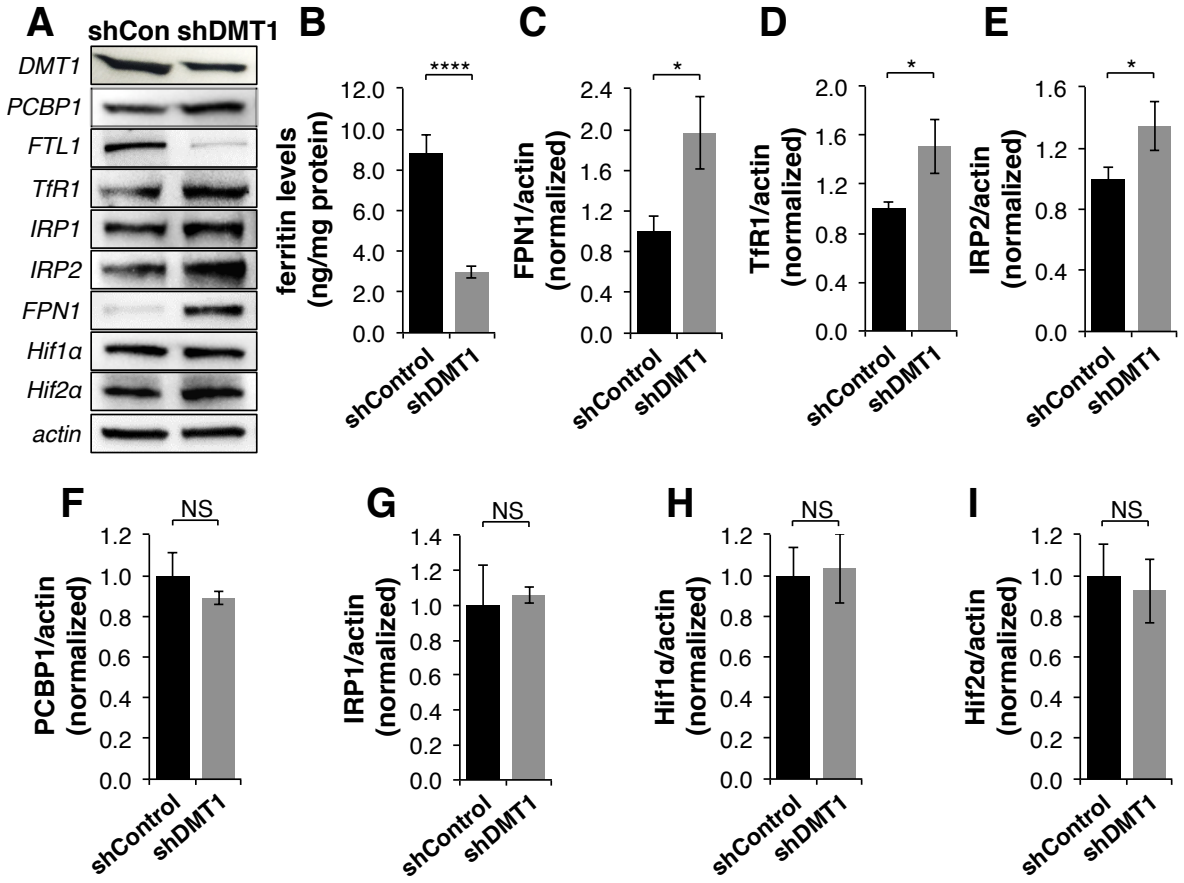

Figure 4.4 DMT1 deficient Caco-2 monolayers are in an anemic state. (A) Representative Western blot images of proteins involved in iron absorption and regulation indicate an anemic state in shDMT1 Caco-2 monolayers to promote maximal iron absorption. **(B-I)** Western blot or ELISA quantification of protein levels of iron-related proteins in shDMT1 Caco-2 monolayers indicate other proteins respond via transcriptional and translational feedback mechanisms to changes in cellular iron status. Importantly, (**B**) decreased ferritin and (**C**) increased FPN1 levels were observed, presumably creating an environment favorable for small molecule-mediated iron transport. N = 3-16.

Providing support for functional collaboration with these endogenous proteins, hinokitiol-mediated iron uptake and transport across DMT1-deficient Caco-2 monolayers is unidirectional (**Figure 4.5 A and B**). When both hinokiitol and iron are added to the basolateral side, hinokitiol is unable to allow for the flux of iron to go through the basolateral membrane, against the flow of

iron the cell has established. Therefore iron does not accumulate and show up as increased uptake in the assay. It is possible however, that hinokitiol is indeed moving iron across the basolateral membrane, however because of the proximity to high levels of FPN1, which is being upregulated in response to the anemic state, the hinokitiol mediated iron influx is merely effluxed back into the basolateral fluid. In either case, this leads to no inrease in uptake or transport to the apical side.

Apical treatment with this low dose of hinokitiol (500 nM) allows for ^{55}Fe incorporation into ferritin (**Figure 4.5 C**), this increase incorporation of ^{55}Fe into ferritin in hinokitiol treated shDMT1 cells is strong evidence that hinokitiol is either deilvering the iron directly to ferritin, releasing it into the cytosol, or handing it off to the high affinity iron chaperone Poly (rC)-binding protein 1 (PCBP1). PCBP1 is known to shuttle excess iron in the cytosol to ferritin where it is stored in order to abate the toxic effects seen with large amounts of excess, labile iron[1,9–11]. Finally, quercetin-mediated knockdown of FPN1[12] antagonizes hinokitiol-mediated transmembrane transport without affecting apical uptake, indicating that at the concentration of hinokitiol that is efficatious in the DMT1 deficient Caco-2 cells, the basolateral efflux is ferroportin mediated (**Figure 4.5 D-G**). This is another strong piece of evidence that hinokitiol is releasing iron into the cytosol and allowing for the endogenous iron transporting system and regulatory network to take over. Interestingly, if hinokitiol is added to the basolateral side and ^{55}Fe is added to the apical side iron transport is observed, although it is slightly delayed compared to apically added hinokitiol. This suggests that hinokitiol is going into the Caco-2 monolayer from the basolateral side, going through the cell and the apical membrane and then grabbing iron from the apical side and allowing it to get into the cell where it is then transported through to the basolateral fluid (data not shown).

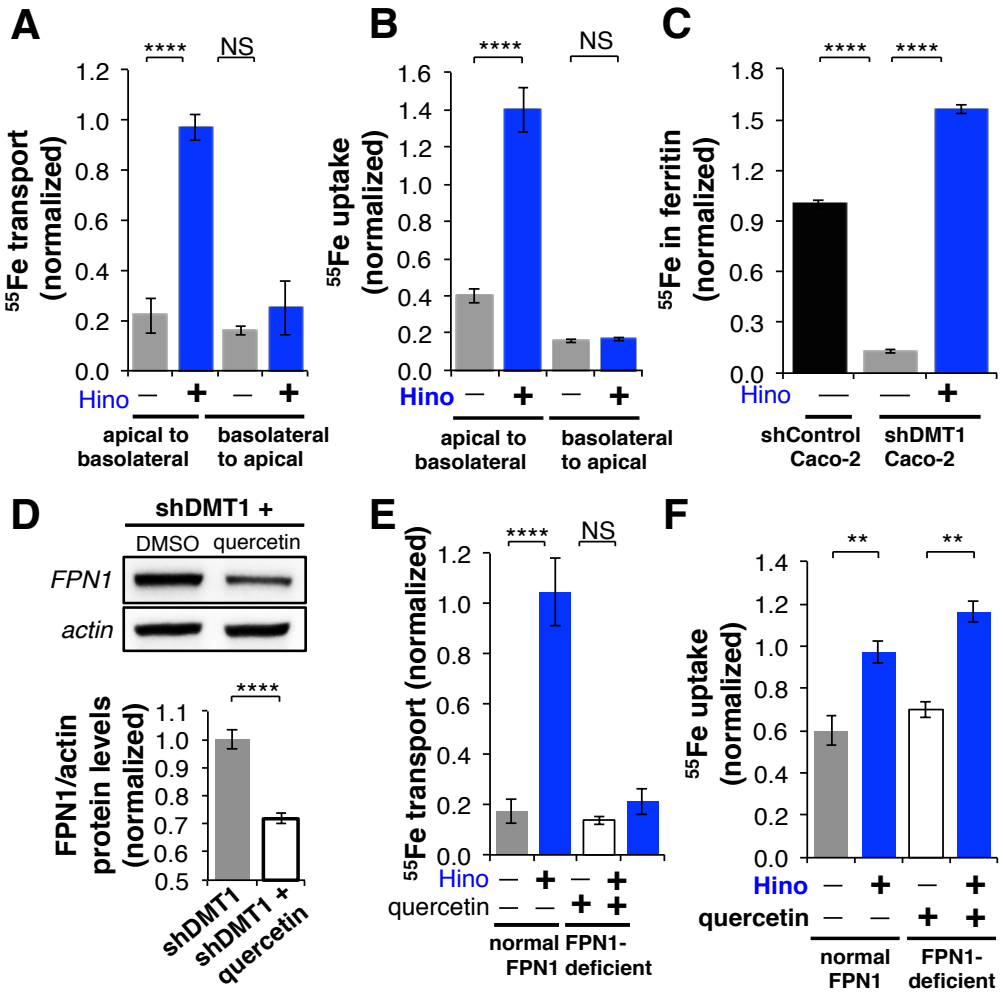

Figure 4.5 The endogenous network of iron regulators is involved in hinoktiol mediated Caco-2 iron transport. (A and B) Unidirectional hinokitiol-mediated (**A**) transport and (**B**) uptake in shDMT1 Caco-2 monolayers observed with apical or basolateral addition of hinokitiol (500 nM) and 55Fe radiotracer (n = 3). (**C**) Determination of ^{55}Fe levels in immunoprecipitated ferritin in Caco-2 monolayers (n = 3). (**D**) Quercetin (250 µM) treatment for 18 hours decreased FPN1 levels in shDMT1 Caco-2 monolayers by western blotting analysis. N = 16 (**E**) Knockdown of FPN1 in shDMT1 Caco-2 monolayers with quercetin abrogates hinokitiol-mediated transport (n = 3). (**F**) Quercetin-mediated knockdown of FPN1 in Caco-2 monolayers did not affect iron uptake into these cells in the presence and absence of hinokitiol (1 µM). N = 3.

Collectively these studies demonstrate that hinokitiol is interacting with the endogenous iron transport and regulatory systems and is therefore not supassing all of the checks and balances estabilished by the cell. This is encouraging because it has great implications for the use

of hinokitiol as a theraputic as well as the potential for other diseases cause by missing ion transporters to be treated in a similar, regulated way. Because hinokitiol is effective at such low doses, we wanted to explore what would happen at higher doses in the same systems, Chapter 5 goes into those effects in detail.

4.4 METHODS

Materials

Wild type (DEY1457) and isogenic fet3Δftr1Δ *S. cerevisiae* were obtained from D. Kosman[13]. Wild type (YPH499) and isogenic fet3Δarn1-4Δ *S. cerevisiae* were obtained from C. Philpott[14]. Yeast were maintained on standard YPD media containing 10 g/L yeast extract, 20 g/L peptone, and 20 g/L dextrose without (liquid media) or with (solid media) 20 g/L agar. Unless otherwise indicated, growth-restoration assays in yeast used a low iron SD media consisting of 1.91 g/L iron-free YNB-$FeCl_3$ (ForMedium CYN 1201), 0.79 g/L Complete Supplement Mixture (Sunrise Science Products 1001-010), 5 g/L ammonium sulfate (Sigma A4418), 20 g/L dextrose, 10 μM $FeCl_3$ (Sigma 451649), and 10 μM hinokitiol (β-Thujaplicin, Sigma 469521) in 50 mM MES/Tris buffer at pH=7.0 without (liquid media) or with (solid media) 20 g/L agar. Dextrose, hinokitiol, and $FeCl_3$ were added after autoclave sterilization from a filter-sterilized 40% w/v dextrose solution in water, from a freshly prepared sterile 10 mM hinokitiol stock in DMSO, and from a freshly prepared 10 mM $FeCl_3$ stock in sterile water, respectively. Non-fermentable growth restoration used the same synthetic medium except for the use of 30 g/L glycerol instead of dextrose.

Human Caco-2 cells (HTB-37) and mouse macrophages (J774A.1) were obtained from ATCC and cultured with DMEM (Gibco 10313-021) containing 10% HI FBS (Gibco 16000-

036), 4 mM glutamine (Lonza BE17-605E), 100 µg/mL PEN-STREP (Lonza DE17-602E), and 1% MEM NEAA (Fisher 11140-050). Transfected Caco-2 cell lines were maintained on this media containing 800 mg/L G418 (Santa Cruz sc-29065B). Friend mouse erythroleukemia cells (MEL, DS19 subclone) were obtained from Arthur Skoultchi (Albert Einstein College of Medicine, Bronx, NY) and cultured with DMEM containing 10% HI FBS, 2 mM glutamine, 100 µg/mL PEN-STREP, and 1% MEM NEAA. Transfected shControl and shDMT1 MEL cell lines were maintained on this media containing 1 g/L G418.

Caco-2 cells (passage 18-50) were grown in T75 flasks to ≥90% confluency before trypsinization with 0.25% trypsin-EDTA (Fisher 25200-056) and passaging at 10:1 dilution in Caco-2 media without (wild type) or with G418 (transfected). Monolayers were grown by seeding Caco-2 cells (passage 20-50) onto 0.4 µm PET cell culture inserts (Fisher 08-771) in 6-well companion plates (Fisher 08-771-24) at $2x10^5$ cells/well and allowed to fully differentiate for 21-28 days before experiments were performed with changing of media every 3-4 days.

MEL cells were grown in suspension in T25 flasks until ~$1x10^6$ cells/mL and re-seeding into a new T25 flask at $1x10^5$ cells/mL in MEL Complete media with or without G418. Every month of culturing, new backstocks of MEL cells were used.

J774 cells (passage 20-80) were grown in T25 flasks to ≥90% confluency before scraping and re-seeding at 5:1 dilution in J774 Complete media. Media was changed every 1-2 days.

Statistics

All data depicts the means or weighted mean ± SEM with a minimum of 3 biological replicates unless otherwise noted. Statistical analysis represents P values obtained from student t-test or one- or two-way analysis of variance (ANOVA) with post-hoc TUKEY test where

appropriate. NS, not significant; * $P < 0.05$; ** $P \leq 0.01$; *** $P \leq 0.001$; **** $P \leq 0.0001$ unless otherwise noted.

Growth rescue of fet3Δftr1Δ yeast with small molecules in liquid media

Growth rescue in yeast was performed similar to previously reported[15] using 10 μM hinokitiol in low iron SD liquid media containing 10 μM $FeCl_3$ in a 96-well plate unless otherwise noted. Wild type and fet3Δftr1Δ controls treated with vehicle (DMSO) were performed under identical conditions using the same low iron SD media containing 10 μM $FeCl_3$ in the absence of hinokitiol. Yeast were grown overnight in YPD media and diluted at an OD_{600} of 0.1 in SD media, diluted 10-fold, and incubated at 30 °C with continuous shaking (200 rpm). The OD_{600} was obtained 24-48 hours after inoculation unless otherwise noted.

Small molecule dose-response with hinokitiol and C2-deoxy hinokitiol (C2deOHino, see synthesis below) was determined by addition of the small molecule (40X stock solution in DMSO) to give the indicated final concentrations.

Chemical inhibition of yeast cell growth with inhibitors of Pma1, V-ATPase

Chemical inhibition of hinokitiol-treated wild type and hinokitiol-rescued fet3Δftr1Δ yeast cell growth was performed as previously reported[15] in low iron SD media containing 10 μM $FeCl_3$ and 10 μM hinokitiol. Increasing dosages of caspofungin (Sigma SML0425), ebselen (Sigma 70530), or bafilomycin B1 (Santa Cruz sc-202072) (40X stocks in DMSO) were added to a yeast suspension (10-fold dilution from $OD_{600} = 0.1$) to give the indicated final dose. EC_{50} values were calculated from fitting of yeast growth curves using GraphPad PRISM.

Western blotting conditions

Caco-2 monolayers, differentiated MEL cells, or J774 cells underwent treatment as described in rescue experiments before lysis with RIPA buffer (Thermo 89901) containing protease inhibitors (Thermo 88266). Protein concentrations were determined by a BCA kit (Thermo 23225) and diluted to 2 mg/mL in the same RIPA buffer. Relative protein levels were then determined through western blotting of 10 or 20 μg of protein lysate blocking for 2 hours at room temperature with 5% BSA and using primary antibodies consisting of either human anti-DMT1 (1:3,000 dilution, Santa Cruz sc-30120), mouse anti-DMT1 (1:1,000 dilution, Santa Cruz sc-166884), human anti-FTL1 (1:1,000 dilution, Santa Cruz sc-74513), human anti-FPN1 HRP conjugate (1:10,000 dilution, Novus Biologicals NBP1-21502H), mouse anti-globin α HRP conjugate (not heated at 100 °C, 1:10,000 dilution, Lifespan Biosciences LS-C212172), human anti-TfR1 HRP conjugate (1:10,000 dilution, Abcam ab10250), human anti-IRP1 (1:1,000 dilution, Santa Cruz sc-14216), human anti-IRP2 (1:1,000 dilution, Santa Cruz sc-33682), human anti-Hif1α HRP conjugate (1:1,000 dilution, Novus Biologicals NB100-105H), human anti-Hif2α HRP conjugate (1:1,000 dilution, Novus Biologicals NB100-122H), human anti-PCBP1 (1:1,000 dilution, Santa Cruz sc-393076), or human anti-actin HRP conjugate (1:10,000 dilution, Cell Signaling 5125S) in 5% BSA overnight at 5 °C before rinsing thoroughly with TBST and incubation (if non-HRP conjugated) with secondary antibody consisting of either goat anti-rabbit IgG HRP conjugate (1:5,000 dilution – DMT1, Cell Signaling 7074, in 5% milk), goat anti-mouse IgG_1 HRP conjugate (1:1,000 dilution – PCBP1, 1:5,000 dilution – IRP2, 1:3,000 dilution – DMT1, Santa Cruz sc-2060, in 5% BSA), donkey anti-goat IgG HRP conjugate (1:1,000 dilution – IRP1, Santa Cruz sc-2020, in 5% BSA), or goat anti-mouse IgG_{2a} HRP conjugate (1:10,000 dilution – FTL1, Santa Cruz sc-2061, in 5% BSA) at room temperature for two hours.

Blots were thoroughly rinsed with TBST and imaged after addition of Femto Chemluminescence solution according to manufacturer instructions (Thermo Fisher 34095).

Determination of ferritin levels by ELISA

Absolute ferritin protein levels in shControl and shDMT1 Caco-2 monolayer lysates were determined using a commercial sandwich ELISA kit (Abcam ab108837) according to manufacturer instructions.

For results found in fig. S14E, protein lysate was isolated after treatment with 500 nM $FeCl_3$ as described below.

^{55}Fe uptake and transport in differentiated Caco-2 monolayers

Media from differentiated Caco-2 monolayers (P25-50, 21-28 days post seeding) grown on PET inserts in 6-well plates was aspirated, and monolayers were rinsed with PBS. 2 mL of basolateral fluid (serum-free DMEM at pH = 7.4 in 10 mM HEPES buffer) was added to the basolateral side, and 1 mL of apical fluid (serum-free DMEM at pH = 5.5 in 10 mM MES buffer) containing 200 nM $^{55}FeCl_3$ or the indicated concentration of $FeCl_3$ and either DMSO vehicle, hinokitiol, C2deOHino, deferiprone, PIH, SIH, or deferoxamine mesylate (Sigma D9533) (500 nM Hino/C2deOHino for DMT1-deficiency, 1 μM Hino/C2deOHino for FPN1-deficiency, or indicated concentration of small molecule from a 1000X stock in DMSO) was added to the apical side via addition on the wall of the membrane insert without disrupting the cell monolayer. The monolayers were then incubated for four hours at 37 °C unless otherwise noted. A 100 μL aliquot of the basolateral fluid was removed, diluted in scintillation cocktail, and radioactivity was determined on a liquid scintillation counter to quantify relative amounts of ^{55}Fe transport. To determine intracellular ^{55}Fe, the basolateral and apical media was removed, and the monolayer

was rinsed with PBS (x2). The cells were then lysed with 500 µL of 200 mM NaOH with nutator mixing overnight, and radioactivity was determined on a liquid scintillation counter after diluting the cell lysate in scintillation cocktail. All values were normalized to shControl monolayers unless otherwise noted. Absolute iron levels were determined through calibration of ^{55}Fe radioactivity levels with known standards and average mg of protein per membrane was determined by protein lysis with RIPA buffer containing protease inhibitors and quantified through a BCA kit according to manufacturer instructions.

Determination of unidirectional uptake and transport was determined as described above except for basolateral addition of $^{55}FeCl_3$ (200 nM) and basolateral addition of DMSO or hinokitiol (500 nM). An aliquot of the apical fluid was then taken to determine the basolateral to apical transport. Intracellular ^{55}Fe was determined as described above.

Determination of ^{55}Fe transport after FPN1 knockdown was determined as described above using 200 nM $^{55}FeCl_3$ after incubation of quercetin to knockdown FPN1[12] as described below.

^{55}Fe immunoprecipitation of ferritin in Caco-2 monolayers

Immunoprecipitation of ferritin was performed using human anti-FTL1 (Santa Cruz sc-74513) and Protein G PLUS-Agarose beads (Santa Cruz sc-2002). Cell lysate was obtained from shControl and shDMT1 Caco-2 monolayers after apical treatment with 200 nM $FeCl_3$ for four hours as described above. Cell lysate was incubated with primary antibody (1:100 dilution) at room temperature for 1 hour, then with the secondary antibody (1:10 dilution) at room temperature for 1 hour with constant mixing. Repeated centrifugations and PBS rinses were performed, and the radioactive levels in the agarose pellet were determined by dilution in scintillation fluid.

Knockdown of FPN1 in Caco-2 cells

To knockdown FPN1 levels in wild type Caco-2 cells, the differentiated epithelial monolayers were incubated with 150 μM quercetin (Sigma 337951) for 18 hours in Caco-2 Complete media containing G418 similar to previously described[12]. To knockdown FPN1 levels in shControl and shDMT1 Caco-2 monolayers, incubation was performed as above except with 250 μM quercetin. After completion of the incubation, the apical and basolateral fluid was aspirated and rinsed with PBS before ^{55}Fe transport and uptake were determined as described above.

Live cell fluorescence imaging of MEL cells

To visualize cytosolic and mitochondrial iron, confocal imaging of calcein green and RPA fluorescence was performed, respectively. MEL cells were induced for differentiation as described above. After 70 hours of incubation, iron (III) citrate (10 μM final concentration) was added. The cells were incubated for an additional 2 hours, and then were centrifuged and rinsed with PBS. The cells were then re-suspended in PBS containing 1 μM calcein green-AM (Thermo Fisher C34852) and 1 μM RPA (Axxora SQX-RPA.1). The cells were then incubated at 37 °C for 15 minutes. The cells were centrifuged, rinsed with PBS, and re-suspended in DMEM containing 10 μM Fe_2Tf. The cells were then imaged within 10 minutes on a LSM710 microscope. Relative calcein green and RPA fluorescence per cell was determined by ImageJ analysis using >100 cells per experiment.

To visualize endosomal iron levels, confocal imaging of an oxyburst green-BSA conjugate (Thermo Fisher O13291) was performed. MEL cells were induced for differentiation as described above. After 70 hours, iron (III) citrate (10 μM final concentration) and an oxyburst

green-BSA conjugate (200 μg/mL) were added. The cells were incubated for an additional 2 hours, and then were centrifuged and rinsed with PBS. The cells were then re-suspended in DMEM-HEPES buffer, and H_2O_2 (50 mM final concentration) was added. The cells were incubated at room temperature, and the oxyburst green fluorescence was then determined 10 minutes after addition of H_2O_2 on a LSM710 microscope. Relative oxyburst green fluorescence per cell was determined by ImageJ analysis using >100 cells per experiment.

Temporal imaging of cytosolic iron levels in J774 macrophages

To assess for the capacity for hinokitiol to reversibly and autonomously transport iron across the plasma membrane through the creation of artificial iron gradients, J774 macrophages were grown in Ibidi dishes (Ibidi NC0723624) to ~80% confluency before incubation with J774 Complete media containing 5 mM ascorbic acid and 200 μM $FeSO_4$. The cells were incubated for 1.5 hours, media was aspirated, and the cells were rinsed with PBS. The cells were then incubated with calcein green-AM (1 μM) in DMEM for 20 minutes at 37 °C. The media was aspirated and cells were rinsed (x2) with PBS before DMEM (pH=7.4 in 10 mM HEPES) and 1 mM probenecid (Sigma P8761) was added. Calcein green fluorescence was then imaged on a LSM880 microscope at 37 °C with 5% CO_2 at the indicated time points for 30 minutes. Hinokitiol (100 μM final concentration), C2deOHino (100 μM final concentration), or DMSO (all from 1000X stocks in 50 μL DMEM) were added at 5 minutes, and a solution of $FeCl_3$ (100 μM final concentration, in 50 μL DMEM) was added at 12 minutes. Fluorescence in each image at each time point was analyzed by ImageJ analysis then normalized to the fluorescence at $t = 0$ for each image using >100 cells per experiment.

Temporal live cell imaging of iron uptake in wild type and FPN1-deficient J774 cells was performed after staining of cells with calcein green as described above. The cells were then rinsed with PBS (x2), and incubated in J774 Complete media containing 200 μM $FeSO_4$, 5 mM ascorbic acid, and 5 mM probenecid in the presence or absence of hepcidin. Calcein green fluorescence was obtained at the indicated time points, and fluorescence in each image at each time point was quantified by ImageJ analysis then normalized to the fluorescence at $t = 0$ for each image using >100 cells per experiment.

4.5 REFERENCES

1. Hentze, M. W., Muckenthaler, M. U., Galy, B. & Camaschella, C. Two to Tango: Regulation of Mammalian Iron Metabolism. *Cell* **142**, 24–38 (2010).
2. Bleackley, M. R. & MacGillivray, R. T. A. Transition metal homeostasis: From yeast to human disease. *BioMetals* **24**, 785–809 (2011).
3. Cyert, M. S. & Philpott, C. C. Regulation of cation balance in Saccharomyces cerevisiae. *Genetics* **193**, 677–713 (2013).
4. Arredondo, M., Orellana, A., Garate, M. A. & Nunez, M. T. Intracellular iron regulates iron absorption and IRP activity in intestinal epithelial (Caco-2) cells. *Am. J. Physiol. Liver Physiol.* **273**, G275–G280 (1997).
5. Muckenthaler, M. U., Galy, B. & Hentze, M. W. Systemic Iron Homeostasis and the Iron-Responsive Element/Iron-Regulatory Protein (IRE/IRP) Regulatory Network. *Annu. Rev. Nutr.* **28**, 197–213 (2008).
6. Andrews, N. C. Iron homeostasis: Insights from genetics and animal models. *Nat. Rev. Genet.* **1**, 208–217 (2000).

7. Pantopoulos, K. Iron Metabolism and the IRE/IRP Regulatory System: An Update. *Ann. N. Y. Acad. Sci.* **1012**, 1–13 (2004).

8. Zhang, D. L., Hughes, R. M., Ollivierre-Wilson, H., Ghosh, M. C. & Rouault, T. A. A Ferroportin Transcript that Lacks an Iron-Responsive Element Enables Duodenal and Erythroid Precursor Cells to Evade Translational Repression. *Cell Metab.* **9**, 461–473 (2009).

9. Shi, H., Bencze, K. Z., Stemmler, T. L. & Philpott, C. C. A cytosolic iron chaperone that delivers iron to ferritin. *Science (80-.).* **320**, 1207–1210 (2008).

10. Leidgens, S. *et al.* Each member of the poly-r(C)-binding protein 1 (PCBP) family exhibits iron chaperone activity toward ferritin. *J. Biol. Chem.* **288**, 17791–17802 (2013).

11. Yanatori, I., Yasui, Y., Tabuchi, M. & Kishi, F. Chaperone protein involved in transmembrane transport of iron. *Biochem. J.* **462**, 25–37 (2014).

12. Lesjak, M. *et al.* Quercetin inhibits intestinal iron absorption and ferroportin transporter expression in vivo and in vitro. *PLoS One* **9**, 1–10 (2014).

13. Kwok, E. Y., Severance, S. & Kosman, D. J. Evidence for iron channeling in the Fet3p-Ftr1p high-affinity iron uptake complex in the yeast plasma membrane. *Biochemistry* **45**, 6317–6327 (2006).

14. Yun, C. W., Tiedeman, J. S., Moore, R. E. & Philpott, C. C. Siderophore-iron uptake in *Saccharomyces cerevisiae*: Identification of ferrichrome and fusarinine transporters. *J. Biol. Chem.* **275**, 16354–16359 (2000).

15. Cioffi, A. G., Hou, J., Grillo, A. S., Diaz, K. A. & Burke, M. D. Restored physiology in protein-deficient yeast by a small molecule channel. *J. Am. Chem. Soc.* **137**, 10096–10099 (2015).

CHAPTER 5

AT HIGH CONENTRATIONS HINOKITIOL SEQUESTRS IRON INTRACELLULARLY

5.1 INTRODUCTION

In Chapter 4 I described the anemic markers of protein expression that we observed in the iron transporter deficient cells and the ability of hinokitiol to interface with the endogenous system of ion transporters and iron regulatory proteins and channels. Because hinokitiol is interfacing with the endogenous system we thus explored what would happen in protein transporter deficient systems with treatment of a range of concentrations of hinokitiol. We hypothesized that at intermediary concentrations of hinokitiol the influx of iron would cause the IRE controlled protein expression to revert from an anemic expression profile to that of a non-anemic or wild type protein expression profile. At high concentrations of hinokitiol we expected the treated cell's expression profile to look like a cell that is experiencing iron overload, specifically with high levels of ferritin, and low levels of TfR1, IRP2, FPN1, Hif1α, and Hif2α. With the change in expression of these proteins we also expected to see a rise and fall of the iron transport indicating that the natural system is regulating hinokitiol mediated iron transport. The studies in this chapter aim to understand how the natural system reacts to hinokitiol at high concentrations as well as causes for the potential loss of efficacy and/or toxicity.

Portions of the work presented in this chapter were preformed with aid from my colleagues Dr. Anthony Grillo and Dr. Alexander Cioffi, and our undergrads Chris Nardone, and James Fan. Portions of this chapter have been adapted from Grillo, A. S.; SantaMaria A. M.; Kafina M. D.; Cioffi A.G.; Huston N. C.; Han M.; Seo Y. A.; Yien Y.Y.; Nardone C.; Menon A. V.; Fan J.; Svoboda D. C.; Anderson J. B.; Hong J.D.; Nicolau B. G.; Subedi K.; Gewirth A. A.;

Wessling-Resnick M.; Kim J.; Paw B. H.; Burke M. D. "Restored iron transport by a small molecule promotes absorption and hemoglobinization in animals" *Science.* **2017**, *356*, 608-616. Reprinted with permission from AAAS.

5.2 HINOKITIOL BINDS MANY DIFFERENT DIVALENT METALS

Because the alpha hydroxyl ketone is a very common binding motif for many different divalent metals, and even trivalent metals, we first asked whether hinokitiol was causing toxicity via the mobilization and therefore disregulation of other off target metals with in the system. To get a more complete understanding we looked at hinokitiol's ability to bind and transport other divalent metals *in vitro*. Using modified partition assays, combined with ICP-MS, we extracted hinokitiol iron complexes from aqueous buffer and then quantified the concentration of metal in the organic layer. We found that hinokitiol acted as a broad spectrum metallophore and is capable of binding multiple divalent metals (**Figure 5.1 A and B and Table 5.1**). Specifically hinokitiol can bind Iron, Manganese, Cobalt, Nickel, Zinc and Copper (**Figure 5.1 A**). In order to determine hinokitiol's specificity for each of the divalent metals tested we performed a competition assay with stoichiometric amounts of hinokitiol and all of the metals listed above. Surprisingly, we found that hinokitiol competitively bound 10-fold more Cu^{II} than Fe^{II} (**Table 5.1**). We next looked at how well hinokitiol mobilized these metals out of liposomal systems. Once again we found that hinokitiol not only bound copper better than iron but also transported Cu^{II} 80-fold faster than Fe^{II} . When first encountering these numbers they can be quite daunting until the low accessibility of copper is considered. Specifically, the cytosolic labile copper pool is ten billion times lower than iron, which is the most abundant divalent metal in the body, by orders of magnitude (**Table 5.1**).

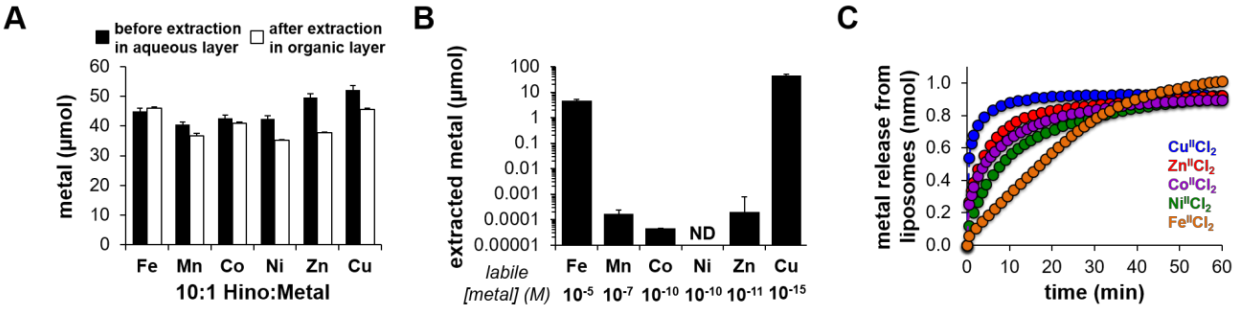

Figure 5.1. Selectivity of hinokitiol-mediated binding and transport with divalent cations. (A**)** Metal content in aqueous layer before extraction (black bars) and the organic layer after extraction with 1:1 Hexanes:Ethyl Acetate (white bars) using 10:1 Hino:Metal indicates hinokitiol forms organic soluble complexes with each individual metal. No metal was detected in the organic layer in the absence of hinokitiol. N = 3. (**B**) Stoichiometric competition experiments with 1 mM of each divalent metal and 1 mM hinokitiol in a 10 mM Mes/Tris buffer in 1:1 MeOH:H2O at pH=7.0. Hinokitiol binds many metals by ICP-MS quantification of extracted hinokitiol-bound metal. The metal in the organic layer was determined to be in the order of Cu > Fe > Mn ≈ Zn > Co > Ni. ND = Not detected. N = 6. (**C**) Hinokitiol (10 µM) rapidly promotes the efflux of multiple divalent metals from POPC liposomes as determined by a PhenGreen assay. In these studies, hinokitiol was unable to transport MnII to any observable degree. Quantification of metal release was done by comparison of fluorescence quenching to a standard curve for each metal. The reciprocal half-lives for efflux were determined to be in the order of Cu > Zn > Co > Ni > Fe >> Mn. The values for binding and transport, as well as the labile metal levels found inside of cells, can be found in **Table 5.1** N = 3.

Divalent Metal	Extracted Metal (µmol)		$t_{1/2}$ (s)	Labile [Metal] (M)‡
	10:1* Hino : Metals	1:1† Hino : Metals		
Fe^{II}	46 ± 0.4	4.66 ± 0.61	1054 ± 88	10^{-5}
Mn^{II}	37 ± 0.8	0.0003 ± 0.0001	ND	10^{-7}
Co^{II}	41 ± 0.3	0.001 ± 0.000	219 ± 3	10^{-10}
Ni^{II}	35 ± 0.3	ND	432 ± 64	10^{-10}
Zn^{II}	38 ± 0.2	0.0015 ± 0.0006	164 ± 1	10^{-11}
Cu^{II}	46 ± 0.2	45.15 ± 6.46	13 ± 13	10^{-15}

* 60 mM Hino and 1 mM of each metal in 10 mM Mes/Tris in 1:1 MeOH:H_2O at pH=7.0
† 1 mM Hino and 1 mM of each metal in 10 mM Mes/Tris in 1:1 MeOH:H_2O at pH=7.0
‡ Estimated cytosolic labile metal found inside of cells: Reference 33 and 34

Table 5.1 Selectivity of hinokitiol binding and transport. Hinokitiol binds and transports many divalent metals, as determined by ICP-MS analysis of organic-soluble hinokitiol:metal complexes after extraction and by determination of the rates of metal efflux from liposomes. The selectivity for binding and transport in biological systems is likely high for iron due to the high metallomic abundance of labile iron over other metals inside of cells. ND = Not Determined; Values represent means of at least three independent experiments.

We thus hypothesized that the low level of labile copper present would lead to high iron selectivity in vivo[1–3]. This is attributed to robust networks of transporters, chaperones, storage proteins, and regulators that bind Cu^{II} with exceptional affinities and selectivities thus sequestering the copper away from hinokitiol[3]. For example, the transcriptional activator Mac1, which is essential in regulating yeast copper homeostasis, binds copper with a KD of 9.7 x 10-20 M[3]. We thus hypothesized that in our systems hinokitiol would only cause a net movement of iron and not the other metal ions it is able to bind and transport, due to lack of gradients of the other metal ions, low labile pools, as well as other metal ion homeostasis mechanisms that would correct any aberrant metal ion movement to maintain homeostasis.

In order to test our hypothesis on a living system we turned to our fet3Δftr1Δ yeast model system. Upon treatment of fet3Δftr1Δ yeast with hinokitiol, lysis, digestion and ICP-MS quantification we found intracellular iron levels to increased relative to vehicle-treated controls, whereas levels of manganese, cobalt, nickel, zinc, and copper were unchanged (**Figure 5.2**). Other biologically relevant ions, such as Magnesium, Sodium, and Potassium also remained unchanged (data not shown).

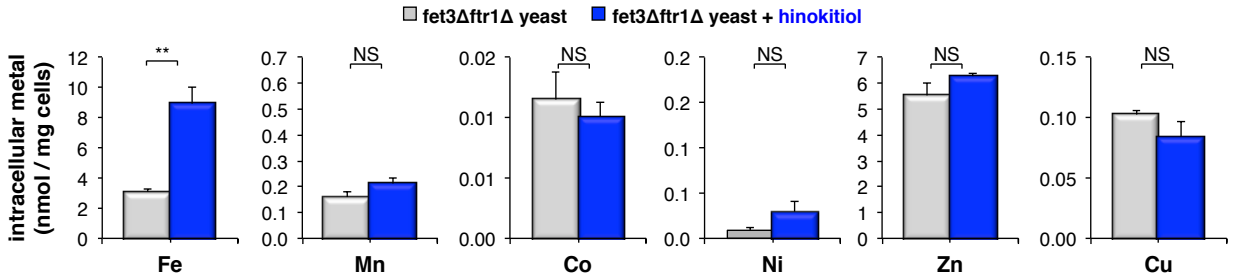

Figure 5.2 Hinokitiol only causes a net movement of iron in fet3Δftr1Δ yeast. Hinokitiol-mediated changes in intracellular metal levels were determined by growing treating fet3Δftr1Δ yeast with vehicle or hinokitiol (10 μM) for 2.5 h and the intracellular metal content was quantified by ICP-MS. Intracellular iron levels increased in hinokitiol-treated fet3Δftr1Δ yeast relative to vehicle-treated controls, whereas levels of manganese, cobalt, nickel, zinc, and copper were unchanged N = 3.

5.3 HINOKITIOL DOES NOT TAKE IRON AWAY FROM IRON BINDING PROTEINS

Another potential cause of toxicity is hinokitiol's ability to bind iron extremely tightly. Hinokitiol binds both ferrous and ferric iron very strongly with a $K_A = 5.1x10^{15}$ for ferrous iron and $K_A = 5.8x10^{25}$ for ferric iron, the latter of which is more than an order of magnitude stronger than deferiprone (**Figure 5.3 A and Table 5.2**). There is therefore a real concernt that hinokitiol could potentially take iron away from iron binding proteins and even disrupt iron-sulfur clusters, which are critical for many protein functions. In competition experiments, in a buffered system we found that hinokitiol can remove iron from iron-binding proteins such as transferrin and ferritin. However this was only possible when hinokitiol was in >1,000-fold excess relative to transferrin and >1,000,000-fold excess relative to ferritin (**Figure 5.3 B-D**). Concentrations of

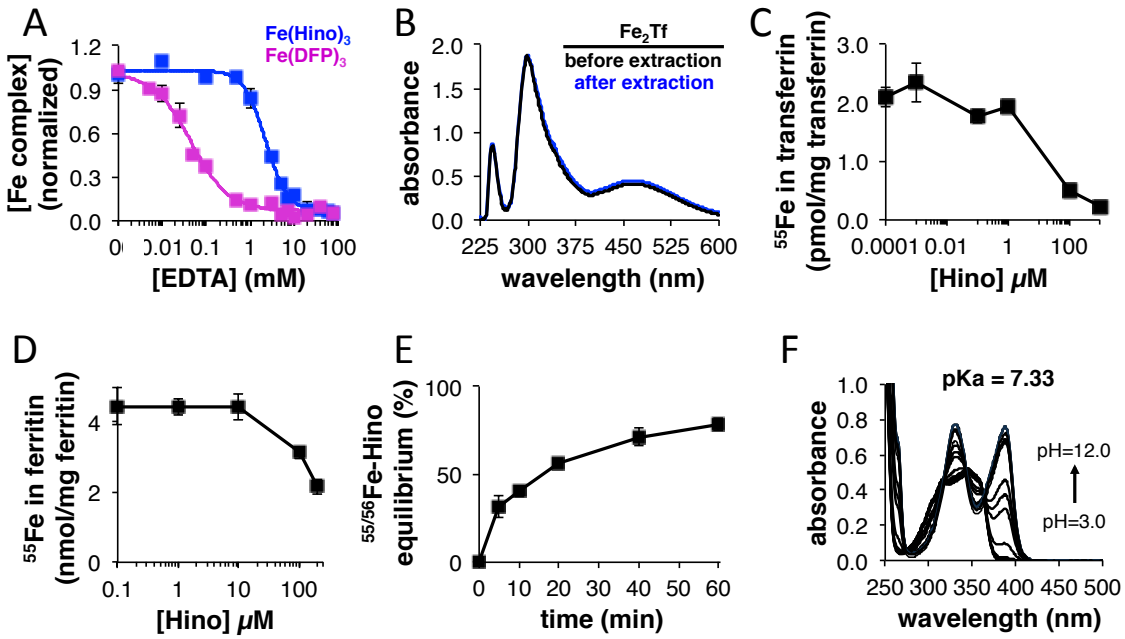

Figure 5.3 Biophysical studies on the binding of iron and hinokitiol. (**A**) Hinokitiol strongly binds iron (III) relative to deferiprone as determined by the EC50 values obtained from an EDTA competition study. N = 3. (**B**) Transferrin (100 μM) saturated with iron is not denatured after extraction with ethyl acetate. (**C and D**) Hinokitiol removes iron from (**C**) transferrin (1 nM) and (**D**) ferritin (2.5 ng ferritin/mL) in a dose-dependent fashion using ^{55}Fe as a radiotracer. N = 3. (**E**) Stoichiometric ionic ^{55}Fe was added to a solution containing a pre-formed ^{56}Fe-hinokitiol complex in 10 mM Mes/Tris buffer at pH=7.0. Equilibrium between the ^{55}Fe-hinokitiol complex and the ^{56}Fe-hinokitiol complex was achieved within one hour. N = 3. (**F**) Increased absorbance of the peak at 387 nm for hinokitiol increases with increasing pH. A clear isobestic point is observed (365 nm), indicating speciation between the protonated and deprotonated forms of hinokitiol. pKa was calculated through logistic fitting of the plot of Abs_{387}/Abs_{240} vs. pH on OriginPro (R^2 = 0.996).

that magnitude are not possible in a cellular system so we were confident that hinokitiol would not take iron away from most iron binding proteins. In fact, ^{56}Fe bound to hinokitiol readily exchanges with ^{55}Fe in solution. We found that the exchange rate between hinokitiol and iron to be incredibly rapid, with >20% exchange observed within 10 minutes (**Figure 5.3 E**). This is most likely facilitated by Hinokitiol's pKa. Hinokitiol has a pKa = 7.33 suggesting both the neutral and anionic states are accessible under physiological conditions (**Figure 5.3 F**).

Hinokitiol does not bind iron as strongly when the hydroxyl group is protinated, therefore it is likely that the pKa contributes to its ability to readily exchange with the proteins within the cell. Adding to this phenomena is the fact that hinokitiol does not bind ferrous iron as well as ferric. We hypothesize that once the iron is released in the cytoplasm the reducing nature of the intracellular environment will keep the iron as Fe^{II} and therefore the hinokitiol will have less of an affinity for it. Thus, the binding of iron by hinokitiol under physiological conditions is expected to be highly dynamic, which may be the key to allow for the facile release of iron from hinokitiol complexes to iron-binding proteins and its subsequent use in iron-related physiological processes. We therefore concluded that at the concentrations at which we are seeing efficaey, hinokitiol is not taking iron away from iron binding proteins.

Small Molecule	K_A for iron (II)	K_A for iron (III)	pFe^{III}	E^0 (mV vs. N.H.E.)		logP Fe^{III} Complex
				1:1 MeOH:H_2O	Aqueous	
Hinokitiol	$5.1x10^{15}$	$5.8x10^{25}$	23.7[†]	-211	-361[¶]	1.71
Deferiprone	$2.1x10^{15}$	$1.2x10^{24}$	22[†] (21)[§]	-410	-420 (-423)[#]	-1.32
Tropolone	$2.3x10^{15}$	$1.1x10^{24}$	22[†]	38	39 (0)[**]	-0.03
Maltol	$7.8x10^{13}$	$3.9x10^{17}$	15.4[‡] (15)[§]	8	41 (40)[***]	0.01
EDTA	$1.2x10^{15}$	$(1.7x10^{24})^{*}$	(22)[||]	139	181 (137)[****]	-

Literature values indicated in parenthesis
Literature values not run under identical conditions
[*] Reference 60
[†] Estimated from known pFe of EDTA (pFe = 22.2): Ref 104
[‡] Estimated from known pFe of Citrate (pFe = 14.8): Ref 105
[§] Reference 106
[||] Reference 104
[¶] Estimated from MeOH standard curve (see fig. S6H)
[#] Reference 107
[**] Reference 71
[***] Reference 108
[****] Reference 109

Table 5.2. Physical characteristics of iron chelators. Binding affinities and redox potentials of hinokitiol and other chelators was determined through competition assays and cyclic voltammetry, respectively. Hinokitiol binds iron (II) and iron (III) stronger than many other iron chelators, including deferiprone. The iron:hinokitiol complex is soluble in non-polar solvents as determined by its octanol-water partition coefficient. Values represent means.

5.4 HINOKITIOL CAUSES INTRACELLULAR IRON SEQUESTRATION AT HIGH CONCENTRATIONS

Hinokitiol is toxic to yeast at high concentrations; due to hinokitiol's ability to bind and transport iron Occam's razor would suggest that the associated toxicity is somehow connected with iron. We thus hypothesized that we could extend the theraputeic window in yeast just by adding in iron. Increasing concentrations of iron increased the minimum inhibitory concentration (MIC) in both wildtype and fet3Δftr1Δ yeast (**Figure 5.4**) but other divalent metals failed to have the same affect (Data not shown).

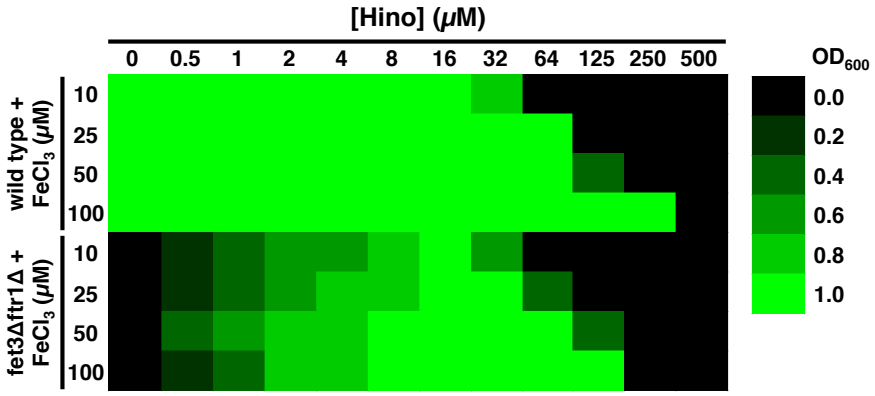

Figure 5.4 Increased iron in the media broadens hinokitiol's rescue window.

So far all of the data I have presented is evidence in support of the hypothesis that hinokitiol is interfacing with the endogenous system and therefore hinokitiol-mediated iron mobilization within cells is a regulated phenomena. We thus set out to test the hypothesis that with increasing concentrations of hinokitiol, the concomitant increase in cytosolic iron would cause the cell's protein expression profile to imitate an iron overload expression profile with high levels of ferritin, and low levels of TfR1, IRP2, FPN1, Hif1α, and Hif2α. We first probed what iron transport in DMT1 deficient caco-2 cells looks like at high hinokitiol and iron concentrations.

We first treated Caco-2 monolayers with increasing concentrations of hinokitiol. The increase in hinokitiol concentration caused and increase in the amount of iron taken into the cell, however the transport leveled off at 5 μM and and actually began to decrease at 25 μM. (**Figure 5.5**). To us this indicated that somehow hinokitiol mediated transport, even at concentrations orders of magnitutde over those that are efficatious, is a regulated phenomena.

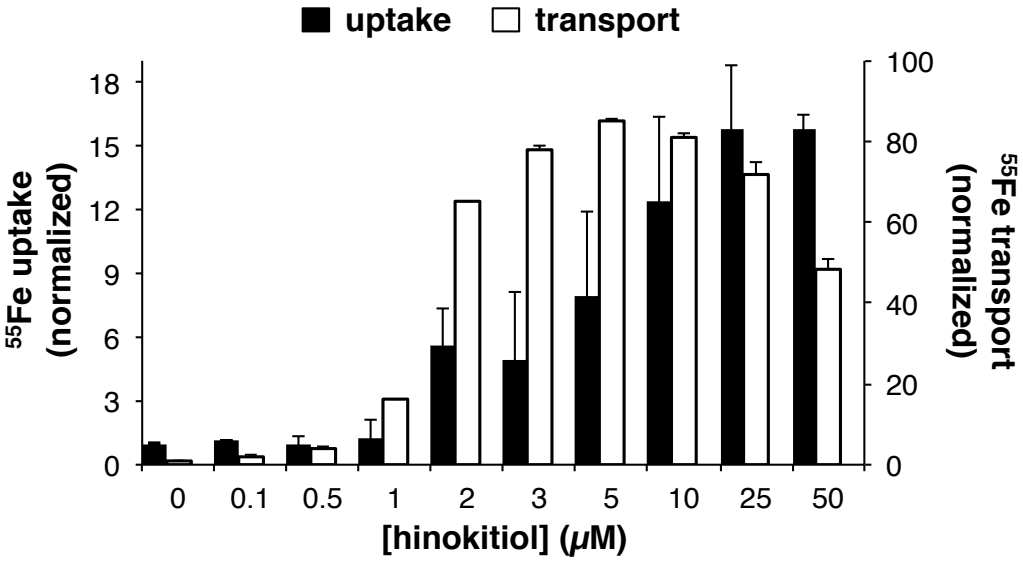

Figure 5.5 Increased doses of hinokitiol increase uptake into shDMT1 Caco-2 monolayers, a bimodal transport effect is observed.

With this interesting phenominological data in hand, we next asked how the endogenous system responds to the hinokitiol-mediated changes in cellular iron status in the presence of a persistent iron gradient. Consistent with IRP-mediated translational regulation, decreased IRP2, increased ferritin subunits (5'-IREs), and decreased TfR1 (3'-IRE) protein levels were observed as a function of hinokitiol concentrations up to 5 μM in the presence of a persistent iron gradient (**Figure 5.6 A-F**). The transcription factors Hif1α and Hif2α similarly decreased along with decreased *Fpn1* mRNA and protein levels (**Figure 5.6 A, G-J**). As expected, IRE-independent expression of the cytosolic iron chaperone PCBP1 and Hif2α-independent *Fth1* mRNA levels

did not change, and no changes in FPN1 were observed upon the addition of hinokitiol in the absence of iron (**Figure 5.6 A, L-O**). Most interestingly, a reversal of these effects was observed with higher concentrations of hinokitiol, even though by radioactive iron we know that the uptake of iron into the cells mediated by hinokitiol is steadily increasing (**Figure 5.6 A-O**). This indicates that while the iron within the cells is high the iron response proteins are unable to sense it. This points towards a situation where the cell has a lot of iron in it, but that iron is not "free" or labile. In the field this is called the chelatable iron pool[4].

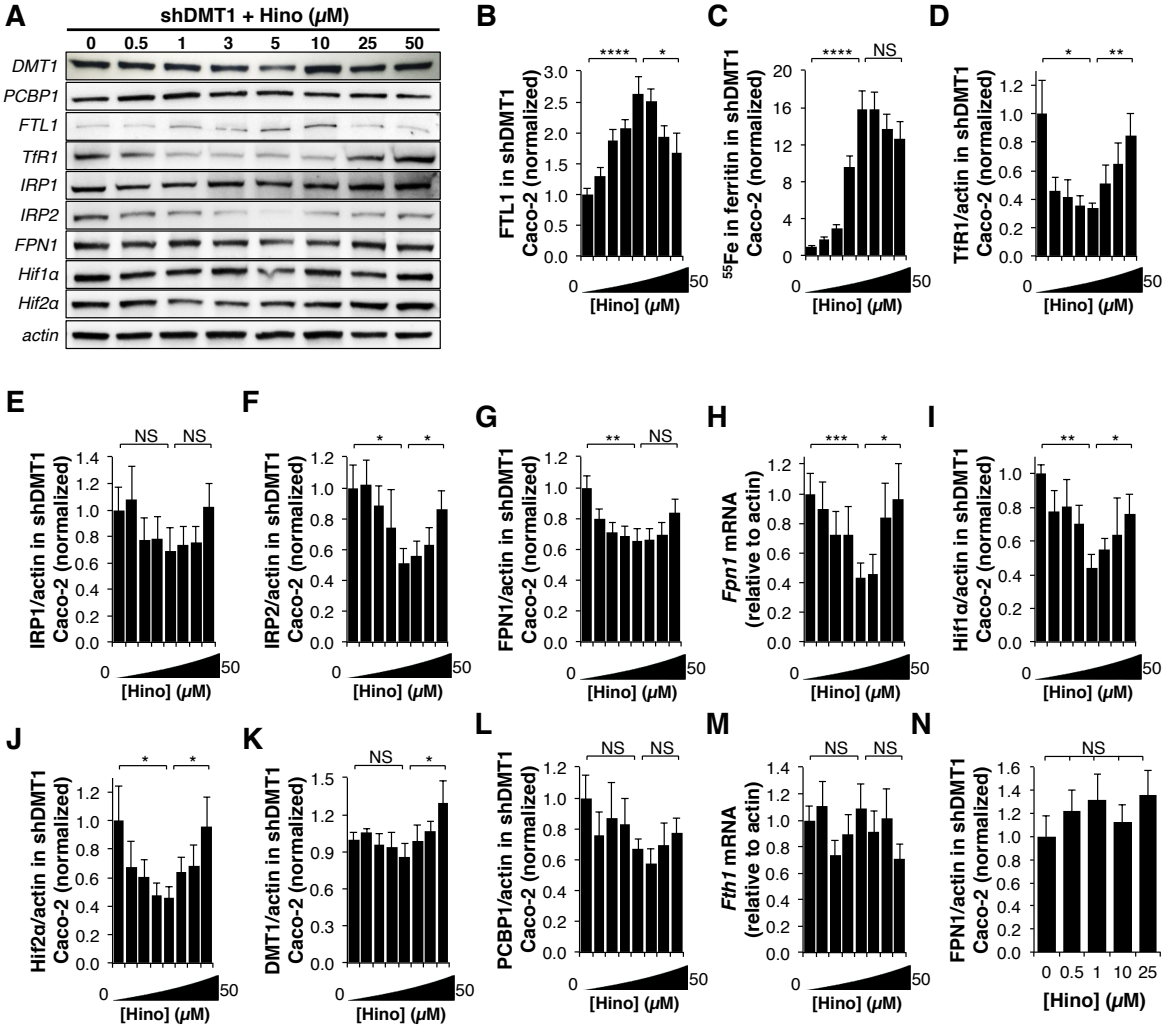

Figure 5.6 Bimodal effects in hinokitiol treated shDMT1 Caco-2 monolayers. (**A**) Representative Western blot images of proteins involved in iron absorption and regulation after treatment with increasing hinokitiol and 25 mM FeCl3. Bimodal effects were observed in protein

Figure 5.6 (cont.) levels involved in iron absorption and regulation. (**B)** Increased ferritin (5'-IRE) levels (N = 6-21) and (**C**) increased ^{55}Fe incorporation into immunoprecipitated ferritin was observed up to 5 μM hinokitiol. N = 11-15. (**D**) TfR1 (3'-IRE) levels decrease up to 5 μM hinokitiol N = 8. (**E and F**) As expected, (**E**) IRP1 levels did not change (N = 14) while (**F**) decreased IRP2 protein levels were observed, consistent with hinokitiol-mediated increases in labile iron levels leading to translational regulation of ferritin and TfR1. N = 12. (**G and H**) Consistent with Hif2α-mediated transcriptional regulation of FPN1, (**G**) decreased FPN1 protein (N = 16) and (**H**) decreased Fpn1 mRNA levels were observed upon hinokitiol treatment up to 5 μM. N = 9-12. (**I and J**) Hif1α and Hif2α levels respond to increases in labile iron up to 5 μM hinokitiol. N = 4-13. (**I**) Presumably due to shRNA targeting DMT1, no translational regulation of DMT1 was observed up to 5 μM hinokitiol. N = 6. (**B-I**) These effects were reversed upon treatment with higher doses of hinokitiol up to 50 μM, possibly due to competitive chelation of labile iron with high hinokitiol doses. (**K**) IRE-independent protein levels of the iron chaperone PCBP1 (N = 6) and (**L**) Hif2α-independent Fth1 mRNA levels did not change when treated with hinokitiol under identical conditions. N = 16. (**M and N**) No changes were observed in FPN1 levels treated with hinokitiol in the absence of added iron, supporting the conclusion that the changes observed were due to translational and transcriptional responses to dynamic cellular iron status. N = 6-8. (**A-L**) Experiments in shDMT1 Caco-2 monolayers used apical addition of hinokitiol (0, 0.5, 1, 3, 5, 10, 25, and 50 μM) in the presence of 25 μM apical FeCl3 for 4 hours in the pH=5.5 apical buffer and pH=7.4 basolateral buffer as described previously. (**M and N**) Experiments utilized identical conditions using 500 nM Fe.

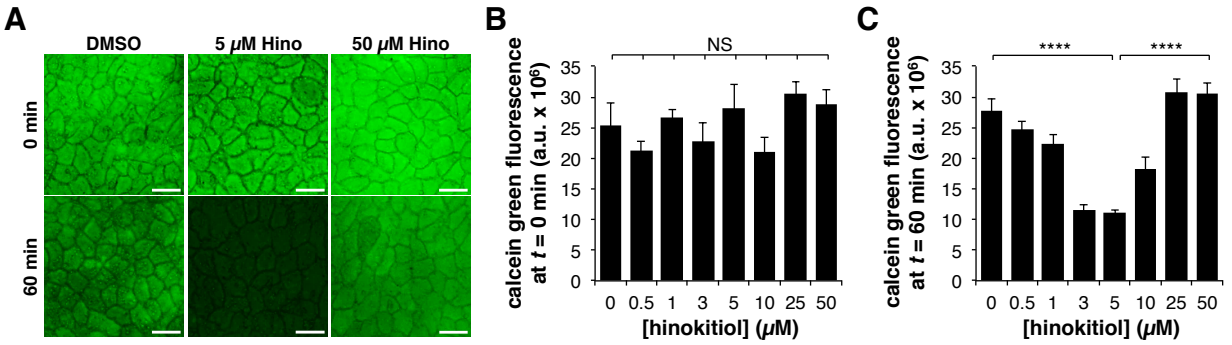

Figure 5.7 Despite large influxes of iron into cells with intermediate and high hinokitiol concentrations, the labile iron pool shows a bimodal effect. (**A***)* Intermediate concentrations of hinokitiol lead to significant calcein green quenching in shDMT1 monolayers treated with 25 μM $FeCl_3$ after 1 hour, consistent with increased labile iron. This effect was reversed at high doses of hinokitiol. Scale bar, 20 mM. (B and C) ImageJ quantification of calcein green fluorescence in these monolayers (n = 3 to 6).

We therefore chose to use calcein green, a fluorescent dye which only detects the labile iron within the cytosol and does not take into account the tightly bound iron. Visualization of cytosolic iron with calcein green indicated that incubation of DMT1-deficient Caco-2

monolayers with increasing hinokitiol led to increased labile iron up to 5 µM (**Figure 5.7 A-C**). Interestingly, further increases in hinokitiol concentration prevented fluorescence quenching, this means that while the total iron in the cell is high (**Figure 5.7 C**), the calcien cannot bind it and therefore it is not labile and the IREs are not recognizing it. One possibility is that the excess iron is being bound by ferritin, however ferritin protein levels go down above 5 µM and ^{55}Fe incorporation into ferritin also begins to trend downwards, although not statistically significantly. In order to determine if the hinokitiol concentration within the caco-2 cells was increased with increasing concentrations of hinokitiol I turned to tritiated hinokitiol to track where the hinokitiol was located during the experiment. I found that as the concentration of hinokitiol in the system increased, a disproportionate amount of hinokitiol, was located in the intracellular fraction, which makes up ~0.5% of the total volume of the system (**Figure 5.8**). Specifically, in cells treated with 10 uM Hinokitiol ~20% of the total trititated hinokitiol was

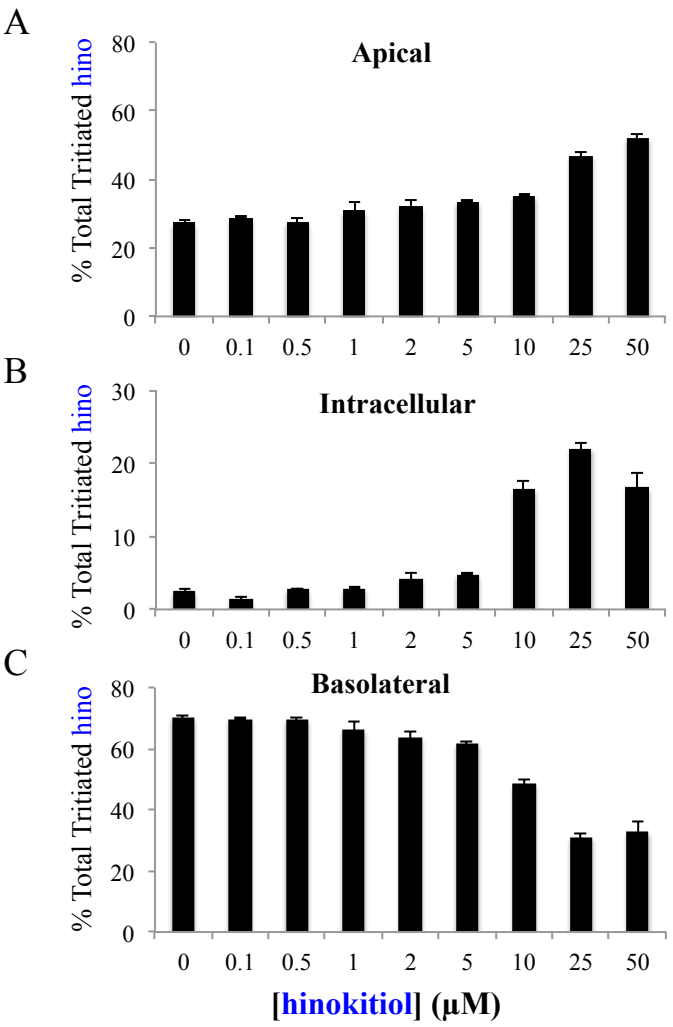

Figure 5.8 Hinokitiol builds up disproportionally intracellularly in shDMT1 Caco-2 cells treated with >10 µM hinokitiol. Percent of hinokitiol (**A**) apically (**B**) intracellularly (**C**) and basolaterally. At doses of hinokitiol >10 µM a disproportionate amount of hino was thus found to be localized intracellularly compared to apical and basolateral fractions.

found to be in the intracellular fraction (**Figure 5.8 B**). This data corresponds with the fluctuation point we see in the other experiments which occurs in the 10 uM treatment group. In combination, these results lead us to the hypotheis that hinokitiol is competitively chelating and sequestering iron in the labile iron pool inside of cells (**Figure 5.9**).

Some future work that is needed in further support of this hypothesis is needed. Looking in other systems, such as yeast, MELs, and J774 cells for intracellular aggregation with tritiated hinokitiol would help demonstrate that this is a general biophysical behavior of hinokitiol. Additionally exchange experiments, similar to the one in **Figure 5.3 D**, would be helpful to discover if high hinokitiol concentrations cause the iron exchange rate to be slower. A slower exchange rate could reduce iron assimilation into endogenous proteins and regulatory networks causing a lack of iron mobilization across the basolateral membrane. All together these data have shown that hionkitiol has unique biophysical properties that allow the restoration of regulated site- and direction-selective iron transport by harnessing gradients in ron transporter defiencent systems. This efficacy is lost at higher concentrations due to hinokitiol mediated intracellular sequestration of iron.

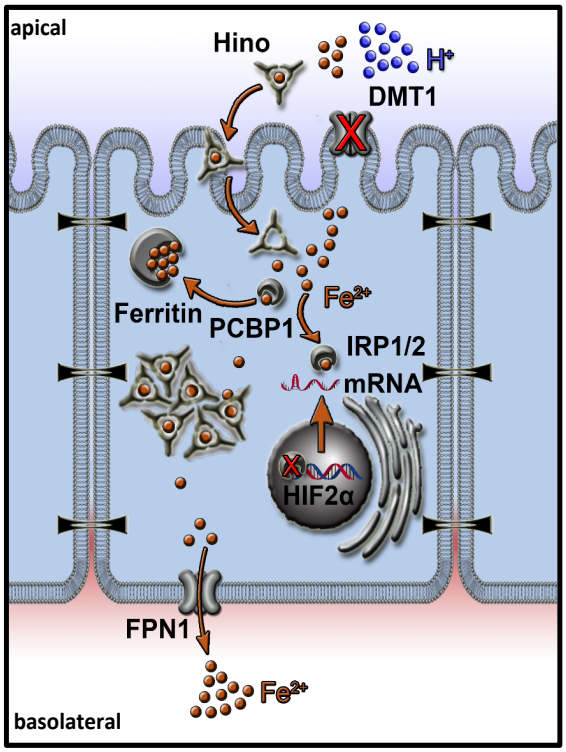

Figure 5.9 Hypothesized hinokitiol intracellular aggregate caused by high concentrations of hinokitiol cause intracellular iron sequestration.

5.5 METHODS

Materials

Wild type (DEY1457) and isogenic fet3Δftr1Δ S. cerevisiae were obtained from D. Kosman13. Wild type (YPH499) and isogenic fet3Δarn1-4Δ S. cerevisiae were obtained from C. Philpott14. Yeast were maintained on standard YPD media containing 10 g/L yeast extract, 20 g/L peptone, and 20 g/L dextrose without (liquid media) or with (solid media) 20 g/L agar. Unless otherwise indicated, growth-restoration assays in yeast used a low iron SD media consisting of 1.91 g/L iron-free YNB-FeCl3 (ForMedium CYN 1201), 0.79 g/L Complete Supplement Mixture (Sunrise Science Products 1001-010), 5 g/L ammonium sulfate (Sigma A4418), 20 g/L dextrose, 10 μM FeCl3 (Sigma 451649), and 10 μM hinokitiol (β-Thujaplicin, Sigma 469521) in 50 mM MES/Tris buffer at pH=7.0 without (liquid media) or with (solid media) 20 g/L agar. Dextrose, hinokitiol, and FeCl3 were added after autoclave sterilization from a filter-sterilized 40% w/v dextrose solution in water, from a freshly prepared sterile 10 mM hinokitiol stock in DMSO, and from a freshly prepared 10 mM FeCl3 stock in sterile water, respectively. Non-fermentable growth restoration used the same synthetic medium except for the use of 30 g/L glycerol instead of dextrose.

Human Caco-2 cells (HTB-37) and mouse macrophages (J774A.1) were obtained from ATCC and cultured with DMEM (Gibco 10313-021) containing 10% HI FBS (Gibco 16000-036), 4 mM glutamine (Lonza BE17-605E), 100 μg/mL PEN-STREP (Lonza DE17-602E), and 1% MEM NEAA (Fisher 11140-050). Transfected Caco-2 cell lines were maintained on this media containing 800 mg/L G418 (Santa Cruz sc-29065B). Friend mouse erythroleukemia cells (MEL, DS19 subclone) were obtained from Arthur Skoultchi (Albert Einstein College of Medicine, Bronx, NY) and cultured with DMEM containing 10% HI FBS, 2 mM glutamine, 100

μg/mL PEN-STREP, and 1% MEM NEAA. Transfected shControl and shDMT1 MEL cell lines were maintained on this media containing 1 g/L G418.

Caco-2 cells (passage 18-50) were grown in T75 flasks to ≥90% confluency before trypsinization with 0.25% trypsin-EDTA (Fisher 25200-056) and passaging at 10:1 dilution in Caco-2 media without (wild type) or with G418 (transfected). Monolayers were grown by seeding Caco-2 cells (passage 20-50) onto 0.4 μm PET cell culture inserts (Fisher 08-771) in 6-well companion plates (Fisher 08-771-24) at 2x105 cells/well and allowed to fully differentiate for 21-28 days before experiments were performed with changing of media every 3-4 days.

MEL cells were grown in suspension in T25 flasks until ~1x106 cells/mL and re-seeding into a new T25 flask at 1x105 cells/mL in MEL Complete media with or without G418. Every month of culturing, new backstocks of MEL cells were used.

J774 cells (passage 20-80) were grown in T25 flasks to ≥90% confluency before scraping and re-seeding at 5:1 dilution in J774 Complete media. Media was changed every 1-2 days.

Statistics

All data depicts the means or weighted mean ± SEM with a minimum of 3 biological replicates unless otherwise noted. Statistical analysis represents P values obtained from student t-test or one- or two-way analysis of variance (ANOVA) with post-hoc TUKEY test where appropriate. NS, not significant; * $P < 0.05$; ** $P \leq 0.01$; *** $P \leq 0.001$; **** $P \leq 0.0001$ unless otherwise noted.

Growth rescue of fet3Δftr1Δ yeast with small molecules in liquid media

Growth rescue in yeast was performed similar to previously reported15 using 10 μM hinokitiol in low iron SD liquid media containing 10 μM FeCl3 in a 96-well plate unless otherwise noted. Wild type and fet3Δftr1Δ controls treated with vehicle (DMSO) were performed under identical conditions using the same low iron SD media containing 10 μM FeCl3 in the absence of hinokitiol. Yeast were grown overnight in YPD media and diluted at an OD600 of 0.1 in SD media, diluted 10-fold, and incubated at 30 °C with continuous shaking (200 rpm). The OD600 was obtained 24-48 hours after inoculation unless otherwise noted.

Small molecule dose-response with hinokitiol and C2-deoxy hinokitiol (C2deOHino, see synthesis below) was determined by addition of the small molecule (40X stock solution in DMSO) to give the indicated final concentrations.

Determination of the pKa of hinokitiol

The pKa of hinokitiol was determined by spectrophotometric titration with varying pH. Hinokitiol (100 μM) was dissolved in a 0.1 M KCl solution in H_2O and acidified to pH = 3.0 (using 0.1 M HCl). The UV-Vis spectrum was repeatedly obtained upon sequential titration of 0.1 M KOH to obtain a range of pHs (3.0, 3.4, 3.9, 4.2, 4.6, 4.9, 6.0, 6.4, 7.0, 7.2, 7.6, 8.4, 9.3, 9.7, 10.4, 10.9, 11.7, 12.0). A clear isobestic point was observed at 365 nm, and a new λ_{max} was observed with decreasing pH at 387 nm. The pKa was then determined via plotting the Abs_{387} / Abs_{240} vs. pH and logistic fitting on OriginPro (R^2 = 0.996) to calculate the point of inflection (pKa = 7.33).

Determination of small molecule iron binding

Small molecule iron (III) binding was determined by UV-Vis spectroscopy of small molecules (30 μM) before and after addition of $FeCl_3$ (10 μM) or iron (III) citrate (10 μM, Sigma F3388) in 10 mM MES/Tris buffer at pH=7.0. Iron (II) binding was determined by UV-Vis spectroscopy of small molecules (30 μM) and $FeCl_2$ (10 μM) in a 25 mM MES/Tris buffer at pH=7.0 containing 62.5 mM sodium ascorbate.

Determination of iron (II) and iron (III) binding affinity with small molecules

The association constants of hinokitiol, deferiprone, tropolone, maltol, and/or EDTA with iron (II) or iron (III) were determined through competition studies similar to previously reported[5]. Specifically, the association constant for iron (II) was determined by a ferrozine competition assay (K_A of ferrozine = $3.65x10^{15}$)[6] $FeCl_2$ (25 μM) was pre-mixed with ferrozine (75 μM) in a 25 mM MES/Tris buffer at pH=7.0 containing 62.5 mM sodium ascorbate. Then increasing concentrations of small molecule (from 40X stocks in DMSO) were added to the indicated final concentrations. The solutions were allowed to equilibrate for 24 hours before reading of the absorbance at 562 nm. The association constants of hinokitiol, tropolone, and deferiprone for iron (III) was determined by an EDTA ($K_A = 1.7x10^{24}$) competition assay[5], and a citrate ($K_A = 1x10^{17}$) competition assay for maltol[7]. Each chelator was mixed with $FeCl_3$ in a 3:1 ratio in 50 mM MES/Tris buffer at pH=7.0 containing 0.1 M KCl to form the corresponding iron complex. The λ_{max} of the peak corresponding to the 3:1 chelator:iron complex was determined (~400-500 nm) for each complex. Then this $Fe(chelator)_3$ stock was added to a solution containing increasing concentrations of EDTA or citrate in 50 mM MES/Tris buffer at pH=7.0 containing 0.1 M KCl to give the indicated final concentrations of chelator (75 μM), $FeCl_3$ (25 μM), and the competitive chelator. The system was allowed to equilibrate overnight, and the

absorbance corresponding to the Fe(chelator)$_3$ complex was determined. The EC_{50} values for each chelator were calculated by a nonlinear curve fit (Hill1) on OriginPro by plotting the absorbance vs. concentration of titrant, and the K_A for each complex was determined from the equation: $K_{A,\ ligand} = (K_{A,\ competitor} * [EC_{50}]) / [ligand]$ where the ligand is the molecule originally bound to iron, and the competitor is the competing chelator.

Removal of ^{55}Fe from iron-binding proteins with hinokitiol

The capacity for hinokitiol to remove iron from transferrin was determined through a ^{55}Fe assay adapted from Cerami and coworkers[8]. ^{55}Fe was loaded onto transferrin (Tf) similar to previously described in PBS buffer[9]. Increasing hinokitiol doses (from 1000X stocks in DMSO) were added to a solution of $^{55}Fe_2Tf$ (1 nM) in PBS buffer to give the final indicated concentrations. The solution was incubated at 37 °C for 3 hours. After incubation, any ^{55}Fe bound to hinokitiol was isolated by extraction of iron:hinokitiol complexes with EtOAc. The radioactive levels in the organic layer were determined after dilution in scintillation cocktail. No extraction of ^{55}Fe was observed in the absence of hinokitiol, and transferrin was not denatured from the extraction process as determined by UV-Vis spectroscopy of holo-transferrin before and after EtOAc extraction in PBS buffer.

Ferritin was loaded with ^{55}Fe by incubation of wild type Caco-2 monolayers and isolation of ferritin through immunoprecipitation as described below. The immunoprecipitated ferritin was diluted to 2.5 ng ferritin/mL (determined by ELISA as described below) in 50 mM MES/Tris buffer at pH=7.0, and increasing concentrations of hinokitiol were added (from 1000X stock in DMSO) to give the final indicated concentrations. The suspension was mixed at room temperature for 2 hours. After incubation, repeated centrifugations and rinses with PBS were

performed to remove any ^{55}Fe not bound to ferritin, and the radioactive levels remaining in the agar pellet were determined after dilution in scintillation cocktail and liquid scintillation counting.

Determination of hinokitiol binding selectivity by ICP-MS

The binding selectivity for hinokitiol with multiple divalent metals was determined similar to previously described[10]. Specifically, a 2 mM solution of hinokitiol in 10 mM MES/Tris buffer in 1:1 H_2O:MeOH at pH=7.0 was mixed in equal volume with a solution containing 2 mM $FeCl_2$, 2 mM $MnCl_2$, 2 mM $CoCl_2$, 2 mM $NiCl_2$, 2 mM $ZnCl_2$, and 2 mM $CuCl_2$ in a 10 mM MES/Tris buffer in 1:1 H_2O:MeOH at pH=7.0 to give a final concentration of 1 mM for each divalent metal and hinokitiol. The colored solution was allowed to incubate for 4 hours at room temperature. The solution was diluted in buffer, and extracted (x3) using 1:1 Hexanes:Ethyl Acetate. The organic layer was collected, dried by $MgSO_4$, and filtered. The solvent was removed *in vacuo*, digested with 70% HNO_3, and metal content was determined by ICP-MS analysis through the University of Illinois SCS Microanalysis Facility.

Control experiments were performed similar to those described above but in the absence of hinokitiol. No metal was detected in the organic layer by ICP-MS. Control experiments were also performed similar to those described above but using 60 mM hinokitiol. Metal content after extraction was compared to the initial metal content in the aqueous solution before extraction, and it was determined that the metal:hinokitiol complexes are extracted into the organic layer.

Determination of metal selectivity in yeast

Hinokitiol-mediated changes in intracellular metal levels were determined using growth rescue conditions adapted from he Fe uptake study.. Specifically, wild type and fet3Δftr1Δ yeast

were grown in YPD media overnight, rinsed, and incubated in SD media without $FeCl_3$ at 30 °C for 3 hours. Yeast were then resuspended at an OD_{600} = 0.50 in SD media (50 mM MES/Tris, pH=7.0) containing 100 μM $FeCl_3$ and either DMSO vehicle or 10 μM hinokitiol. After 2.5 hours of incubation, cells were centrifuged at 5 °C, rinsed twice with cold 10 mM EDTA in 50 mM Tris/HCl buffer (pH = 6.5), and once with cold metal-free water. Cells were then lyophilized for 48 hours. The lyophilized cells were digested with a 5:1 mixture of HNO_3:HCl and then subjected to an automated sequential microwave digestion in a CEM Discover SP-D microwave digester. The resulting clear solution was diluted in metal-free water, and elemental analysis was performed by ICP-MS through the University of Illinois SCS Microanalysis Facility using a Perkin Elmer DRC-e instrument.

Exchangeability of ferric iron bound to hinokitiol

The reversible exchange of ferric iron bound to hinokitiol was determined similar to previously described[11]. Non-radioactive $FeCl_3$ (100 nM from a 1000X stock, referred to as ^{56}Fe) was added to hinokitiol (100 nM from a 1000X stock) in 10 mM MES/Tris buffer at pH=7.0. The solution was equilibrated for 1 hour at 37 °C, and then an equal amount of $^{55}FeCl_3$ (100 nM) was added. The solution was incubated at 37 °C, and at the indicated time points an aliquot was taken and added to water. The iron-hinokitiol complex was immediately separated from unbound iron through extraction with ethyl acetate and the radioactive counts were determined by scintillation counting. Less than 2% of iron was found in the ethyl acetate layer in the absence of hinokitiol. The percent equilibrium was then determined by normalizing the radioactive counts from the theoretical maximum ^{55}Fe found in the hinokitiol complex (1:1 ^{55}Fe:^{56}Fe at equilibrium).

Western blotting conditions

Caco-2 monolayers, differentiated MEL cells, or J774 cells underwent treatment as described in rescue experiments before lysis with RIPA buffer (Thermo 89901) containing protease inhibitors (Thermo 88266). Protein concentrations were determined by a BCA kit (Thermo 23225) and diluted to 2 mg/mL in the same RIPA buffer. Relative protein levels were then determined through western blotting of 10 or 20 μg of protein lysate blocking for 2 hours at room temperature with 5% BSA and using primary antibodies consisting of either human anti-DMT1 (1:3,000 dilution, Santa Cruz sc-30120), mouse anti-DMT1 (1:1,000 dilution, Santa Cruz sc-166884), human anti-FTL1 (1:1,000 dilution, Santa Cruz sc-74513), human anti-FPN1 HRP conjugate (1:10,000 dilution, Novus Biologicals NBP1-21502H), mouse anti-globin α HRP conjugate (not heated at 100 °C, 1:10,000 dilution, Lifespan Biosciences LS-C212172), human anti-TfR1 HRP conjugate (1:10,000 dilution, Abcam ab10250), human anti-IRP1 (1:1,000 dilution, Santa Cruz sc-14216), human anti-IRP2 (1:1,000 dilution, Santa Cruz sc-33682), human anti-Hif1α HRP conjugate (1:1,000 dilution, Novus Biologicals NB100-105H), human anti-Hif2α HRP conjugate (1:1,000 dilution, Novus Biologicals NB100-122H), human anti-PCBP1 (1:1,000 dilution, Santa Cruz sc-393076), or human anti-actin HRP conjugate (1:10,000 dilution, Cell Signaling 5125S) in 5% BSA overnight at 5 °C before rinsing thoroughly with TBST and incubation (if non-HRP conjugated) with secondary antibody consisting of either goat anti-rabbit IgG HRP conjugate (1:5,000 dilution – DMT1, Cell Signaling 7074, in 5% milk), goat anti-mouse IgG_1 HRP conjugate (1:1,000 dilution – PCBP1, 1:5,000 dilution – IRP2, 1:3,000 dilution – DMT1, Santa Cruz sc-2060, in 5% BSA), donkey anti-goat IgG HRP conjugate (1:1,000 dilution – IRP1, Santa Cruz sc-2020, in 5% BSA), or goat anti-mouse IgG_{2a} HRP conjugate (1:10,000 dilution – FTL1, Santa Cruz sc-2061, in 5% BSA) at room temperature for two hours.

Blots were thoroughly rinsed with TBST and imaged after addition of Femto Chemluminescence solution according to manufacturer instructions (Thermo Fisher 34095).

Determination of ferritin levels by ELISA

Absolute ferritin protein levels in shControl and shDMT1 Caco-2 monolayer lysates were determined using a commercial sandwich ELISA kit (Abcam ab108837) according to manufacturer instructions.

^{55}Fe uptake and transport in differentiated Caco-2 monolayers

Media from differentiated Caco-2 monolayers (P25-50, 21-28 days post seeding) grown on PET inserts in 6-well plates was aspirated, and monolayers were rinsed with PBS. 2 mL of basolateral fluid (serum-free DMEM at pH = 7.4 in 10 mM HEPES buffer) was added to the basolateral side, and 1 mL of apical fluid (serum-free DMEM at pH = 5.5 in 10 mM MES buffer) containing 200 nM $^{55}FeCl_3$ and 25 μM $FeCl_3$ and either DMSO vehicle, or hinokitiol at the indicated concentrations was added to the apical side via addition on the wall of the membrane insert without disrupting the cell monolayer. The monolayers were then incubated for four hours at 37 °C unless otherwise noted. A 100 μL aliquot of the basolateral fluid was removed, diluted in scintillation cocktail, and radioactivity was determined on a liquid scintillation counter to quantify relative amounts of ^{55}Fe transport. To determine intracellular ^{55}Fe, the remaining basolateral and apical fluid was removed, and the monolayer was rinsed with PBS (x2). The cells were then lysed with 500 μL of 200 mM NaOH with nutator mixing overnight, and radioactivity was determined on a liquid scintillation counter after diluting the cell lysate in scintillation cocktail. All values were normalized to shControl monolayers unless otherwise noted. Absolute

iron levels were determined through calibration of ^{55}Fe radioactivity levels with known standards and average mg of protein per membrane was determined by protein lysis with RIPA buffer containing protease inhibitors and quantified through a BCA kit according to manufacturer instructions.

^{55}Fe immunoprecipitation of ferritin in Caco-2 monolayers

Immunoprecipitation of ferritin was performed using human anti-FTL1 (Santa Cruz sc-74513) and Protein G PLUS-Agarose beads (Santa Cruz sc-2002). Cell lysate was obtained from shControl and shDMT1 Caco-2 monolayers after apical treatment with DMSO or hinokitiol (0, 0.5, 1, 3, 5, 10, 25, or 50 μM) and $FeCl_3$ (200 nM of ^{55}Fe for and 25 μM of 20:1 ^{56}Fe:^{55}Fe) for four hours as described above. Cell lysate was incubated with primary antibody (1:100 dilution) at room temperature for 1 hour, then with the secondary antibody (1:10 dilution) at room temperature for 1 hour with constant mixing. Repeated centrifugations and PBS rinses were performed, and the radioactive levels in the agarose pellet were determined by dilution in scintillation fluid.

Temporal imaging of cytosolic iron with calcein green in Caco-2 monolayers

Temporal live cell imaging of labile iron levels in shDMT1 Caco-2 monolayers was performed after staining of Caco-2 monolayers with calcein green-AM (5 μM) in the apical and basolateral liquid for 30 minutes in pH=7.4 DMEM. After rinsing with PBS (x2 apically and basolaterally), monolayers were treated similar to Caco-2 transport experiments with a pH=7.4 HEPES buffer in DMEM (basolateral) and an apical fluid (pH=5.5 MES buffer in DMEM) containing 25 μM $FeCl_3$ and either 0, 0.5, 1, 3, 5, 10, 25, or 50 μM hinokitiol (from 1000x stocks

in DMSO). Calcein green fluorescence was obtained at t = 0 min and t = 60 min, and the fluorescence in each image was quantified by ImageJ analysis.

Localization of Hinokitiol in the Caco-2 monolayer system using tritiated hinokitiol

Media from differentiated Caco-2 monolayers (P25-50, 21-28 days post seeding) grown on PET inserts in 6-well plates was aspirated, and monolayers were rinsed with PBS. 2 mL of basolateral fluid (serum-free DMEM at pH = 7.4 in 10 mM HEPES buffer) was added to the basolateral side, and 1 mL of apical fluid (serum-free DMEM at pH = 5.5 in 10 mM MES buffer) containing 25 μM $FeCl_3$, 4.6 nM tritiated hinokitiol and either DMSO vehicle, or indicated concentration hinokitiol from a 1000X stock in DMSO was added to the apical side via addition on the wall of the membrane insert without disrupting the cell monolayer. The monolayers were then incubated for four hours at 37 °C. A 100 μL aliquot of the apical and basolateral fluid was removed, diluted in scintillation cocktail, and radioactivity was determined on a liquid scintillation counter to quantify relative amounts of tritiated hinokitiol. To determine intracellular tritiated hinokitiol, the remaining basolateral and apical fluid was removed, and the monolayer was rinsed with PBS (x2). The cells were then lysed with 500 μL of 200 mM NaOH with nutator mixing overnight, and radioactivity was determined on a liquid scintillation counter after diluting the cell lysate in scintillation cocktail. All values are expressed as percent of the total tritiated hinokitiol in the system.

5.6 REFERENCES

1. Finney, L. A. Transition Metal Speciation in the Cell: Insights from the Chemistry of Metal Ion Receptors. *Science.* **300**, 931–936 (2003).

2. Ba, L. A., Doering, M., Burkholz, T. & Jacob, C. Metal trafficking: from maintaining the metal homeostasis to future drug design. *Metallomics* **1**, 292 (2009).

3. Cyert, M. S. & Philpott, C. C. Regulation of cation balance in *Saccharomyces cerevisiae*. *Genetics* **193**, 677–713 (2013).

4. Petrat, F., de Groot, H., Sustmann, R. & Rauen, U. The chelatable iron pool in living cells: A methodically defined quantity. *Biol. Chem.* **383**, 489–502 (2002).

5. Park, S. R. *et al.* Discovery of cahuitamycins as biofilm inhibitors derived from a convergent biosynthetic pathway. *Nat. Commun.* **7**, 1–11 (2016).

6. Gentry, L. E., Thacker, M. A., Doughty, R., Timkovich, R. & Busenlehner, L. S. His86 from the N-Terminus of Frataxin Coordinates Iron and Is Required for Fe–S Cluster Synthesis. *Biochemistry* **52**, 6085–6096 (2013).

7. Katoh, H., Hagino, N. & Ogawa, T. Iron-Binding Activity of FutA1 Subunit of an ABC-type Iron Transporter in the Cyanobacterium Synechocystis sp. Strain PCC 6803. *Plant Cell Physiol.* **42**, 823–827 (2001).

8. White, G. P., Jacobs, A., Grady, R. W. & Cerami, A. The effect of chelating agents on iron mobilization in Chang cell cultures. *Blood* **48**, 923–9 (1976).

9. Vyoral, D. & Petrák, J. Iron transport in K562 cells: a kinetic study using native gel electrophoresis and 59Fe autoradiography. *Biochim. Biophys. Acta - Mol. Cell Res.* **1403**, 179–188 (1998).

10. Ghssein, G. *et al.* Biosynthesis of a broad-spectrum nicotianamine-like metallophore in Staphylococcus aureus. *Science.* **352**, 1105–1109 (2016).

11. Lovenberg, W., Rabinowitz, J. C. & Buchanan, B. B. Studies On Chemical Nature of Clostridial Ferredoxin. *J. Biol. Chem.* **238(12)**, 3899–3905 (1963).

CHAPTER 6

SUMMARY AND OUTLOOK

These findings demonstrate that the small molecul hinokitiol can restore mobilization of iron into, within and out of cells deficient in many different iron transporters. Hinokitiol is the first small moecule, molecular prothetic to restore physiology downsttream of a missing iron transporter in a whole animal. The mobilization of iron by hinokitiol seems to be regulated via an interface of hinokitiol with the natural system. This is made possible by iron gradients which accumulate upstream of the missing iron transporters. It is intriguing to consider whether other ion transporter deficiencies create similar ion gradients, potentially making this a generalizable strategy to develop new therapies for diseases caused by missing ion transporters such as Cystic Fibrosis, Barter's syndrome, and Liddle syndrome. Therefore these studies provide a conceptual framework and proof-of-concept demonstration to support the pursuit of small molecule surrogates for missing or dysfunctional iron-transport proteins that underlie many human diseases.

The disorders outline herein are very rare with a few patients world wide. However, it has recently been recognized that acquired, rather than genetic germline, deficiencies of FPN1 underlie the anemia of chronic inflammation that frequently occurs in patients suffering from many common diseases, including rheumatoid arthritis, systemic lupus erythematosus, and inflammatory bowel disease[1–3]. Genetic or induced deficiencies of FPN1 underlie many other diseases, including hemochromatosis type IV (Ferroportin disease)[4], mentioned in this thesis, as well as iron-refractory iron deficiency anemia (IRIDA)[5] and Anemia of Inflammation (AI)[3,6–8]. AI decreases the quality of life in >10 million patients suffering from autoimmune disorders including rheumatoid arthritis, celiac disease, systemic lupus erythematosus, inflammatory bowel

disease, and ulcerative colitis.[8] Moreover, ~50,000 children with juvenile idiopathic arthritis suffer from anemia that leads to decreased energy, growth, and cognition during the critical early years of their development.[9–11] Current therapies fail to address the common underlying defect that duodenal enterocytes and reticuloendothelial macrophages are unable to mobilize iron across specific membranes. Effectively addressing AI typically requires intravenous iron therapy and/or trying to eliminate the source of inflammation, the former can lead to iron overload in select tissues such as the liver and the latter is, in many cases, challenging to achieve.[3,12,13]

Hinokitiol has the potential to treat disorders of aquired ferroportin deficiency due to its ability to autonomously perform transmembrane iron transport and leverage iron gradients which accumulate upstream of deficient iron transporters to restore site- and direction- selective iron transport and thus physiology. Further, this approach may have potential in promoting the rapid excretion of excess iron that builds up in tissues (e.g. liver or brain) in many diverse iron overload disorders such as hereditary hemochromatosis[14–17]. Because networks of active and passive ion-transport proteins similarly underlie the directional movement of many other ions in most living systems, including humans, these findings may also have even broader scientific and therapeutic implications for treating human diseases which are currently untreatable.

This project has started a world wide network of collaborators all rallying around hinokitiol as an interesting biological probe and potential therapuitc. I look forward to watching and potentially advising future studies and colaborators as hinokitiol is developed into a theraputic and highly useful biological probe.

6.1 REFERENCES

1. Poggiali, E., Migone De Amicis, M. & Motta, I. Anemia of chronic disease: A unique defect of iron recycling for many different chronic diseases. *Eur. J. Intern. Med.* **25**, 12–17 (2014).
2. Basseri, R. J. *et al.* Hepcidin is a key mediator of anemia of inflammation in Crohn's disease. *J. Crohn's Colitis* **7**, 1–2 (2013).
3. Gangat, N. & Wolanskyj, A. P. Anemia of chronic disease. *Semin. Hematol.* **50**, 232–238 (2013).
4. Pietrangelo, A. The ferroportin disease. *Blood Cells, Mol. Dis.* **32**, 131–138 (2004).
5. Finberg, K. E. *et al.* Mutations in TMPRSS6 cause iron-refractory iron deficiency anemia (IRIDA). *Nat. Genet.* **40**, 569–571 (2008).
6. Ganz, T. & Nemeth, E. Iron Sequestration and Anemia of Inflammation. *Semin. Hematol.* **46**, 387–393 (2009).
7. Rivera, S. & Ganz, T. Animal Models of Anemia of Inflammation. *Semin. Hematol.* **46**, 351–357 (2009).
8. Wessling-Resnick, M. Iron homeostasis and the inflammatory response. *Annu. Rev. Nutr.* **30**, 105–22 (2010).
9. Ravelli, A. & Martini, A. Juvenile idiopathic arthritis. *Lancet* **369**, 767–778 (2007).
10. Cazzola, M. *et al.* Defective iron supply for erythropoiesis and adequate endogenous erythropoietin production in the anemia associated with systemic-onset juvenile chronic arthritis. *Blood* **87**, 4824–4830 (1996).
11. Egorov, A. *et al.* Anemia in children with JIA: is it really driven by hepcidin level, or by a set of factors of a chronic disease. *Pediatr. Rheumatol.* **12**, P187 (2014).

12. Sun, C. C., Vaja, V., Babitt, J. L. & Lin, H. Y. Targeting the hepcidin-ferroportin axis to develop new treatment strategies for anemia of chronic disease and anemia of inflammation. *Am. J. Hematol.* **87**, 392–400 (2012).

13. Ganz, T. Hepcidin, a key regulator of iron metabolism and mediator of anemia of inflammation. *Blood* **102**, 783–788 (2003).

14. Pietrangelo, A. Hereditary Hemochromatosis — A New Look at an Old Disease. *N. Engl. J. Med.* **350**, 2383–2397 (2004).

15. Anderson, G. J. Ironing Out Disease: Inherited Disorders of Iron Homeostasis. *IUBMB Life (International Union Biochem. Mol. Biol. Life)* **51**, 11–17 (2001).

16. Brissot, P. *et al.* Current approach to hemochromatosis. *Blood Rev.* **22**, 195–210 (2008).

17. Montosi, G. *et al.* Wild-type HFE protein normalizes transferrin iron accumulation in macrophages from subjects with hereditary hemochromatosis. *Blood* **96**, 1125–1129 (2000).